Quantum Monte Carlo simulations within dynamical mean-field theory

Nils Blümer, Univ. Mainz

Outline

Motivation and Introduction

Efficiency of QMC DMFT solvers

Unbiased Green functions and spectra from HF-QMC

Multigrid Hirsch-Fye quantum Monte Carlo algorithm

Spectral weight transfer at the Mott transition

Breakdown of a Fermi liquid

Summary and outlook

Motivation: strong electronic correlations

Mott metal-insulator transition

Prototype example: V_2O_3 doped
with Cr/Ti and/or under pressure

Phase diagram

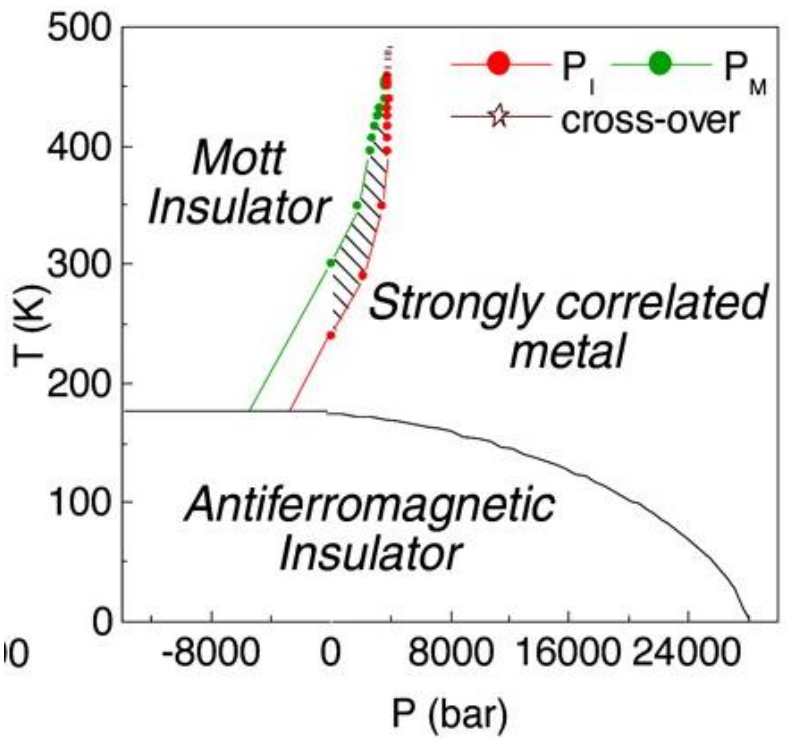

Motivation: strong electronic correlations

Mott metal-insulator transition

Prototype example: V_2O_3 doped with Cr/Ti and/or under pressure

Phase diagram

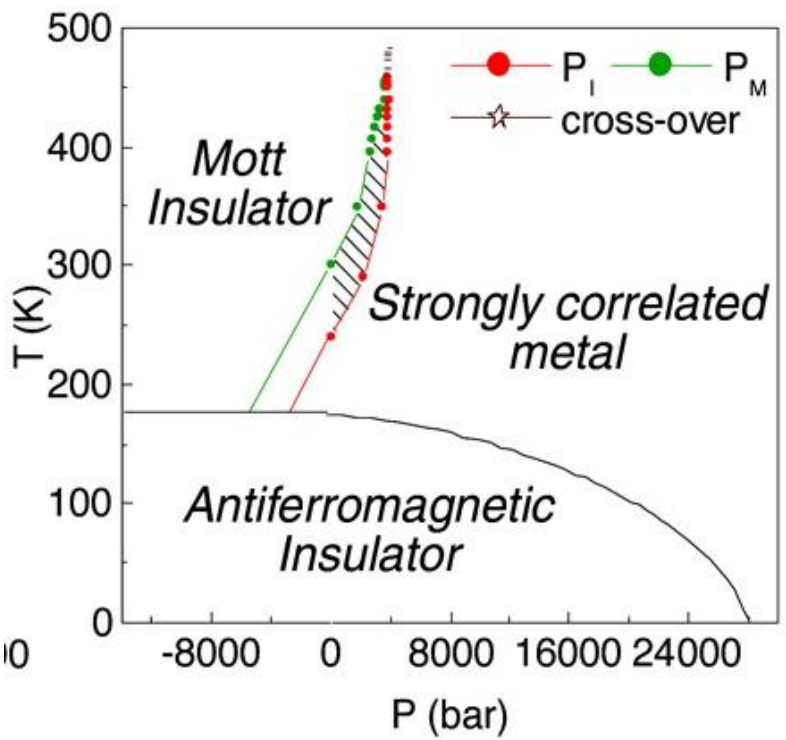

Electrical conductivity

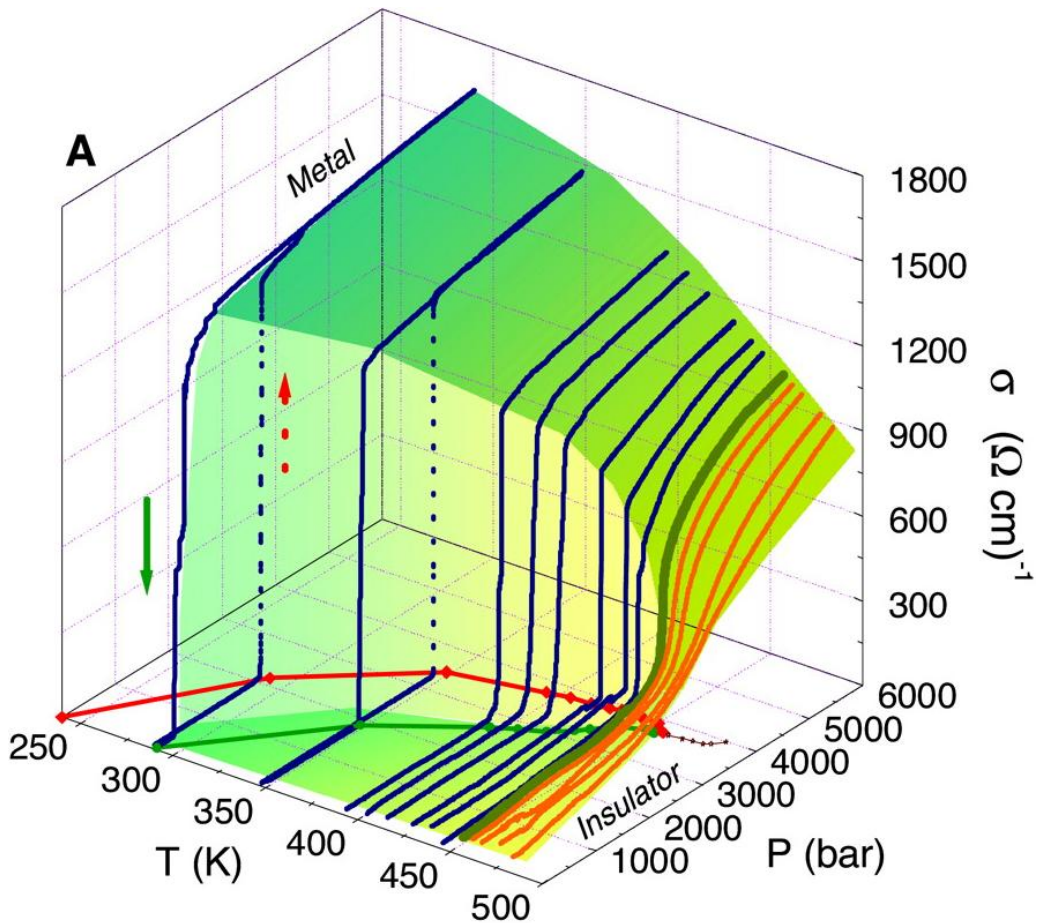

[Limelette et al., Science 302, 89 (2003)]

Ab initio calculations for correlated systems: LDA+DMFT

Recent "hot topic": kinks in photoemission spectra

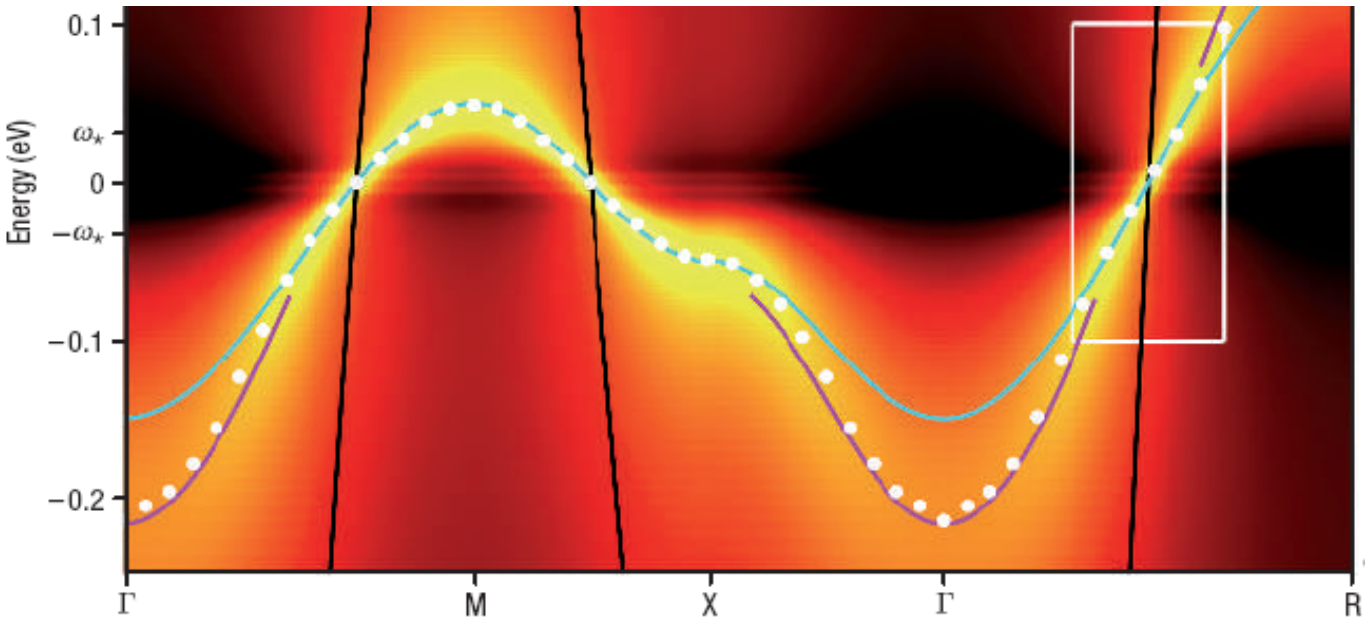

[Byzcuk et al., Nature Physics (2006)]

Itinerant ferromagnetism and half-metallicity

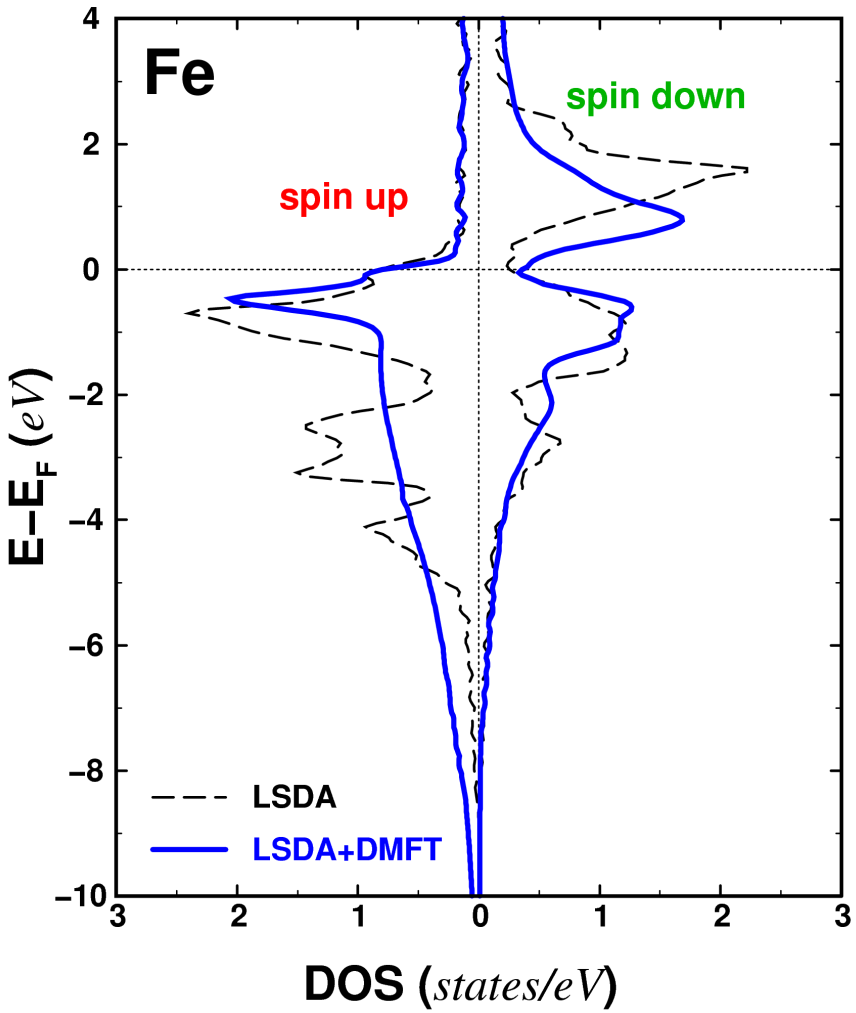

[Chioncel et. al, PRB (2003)]

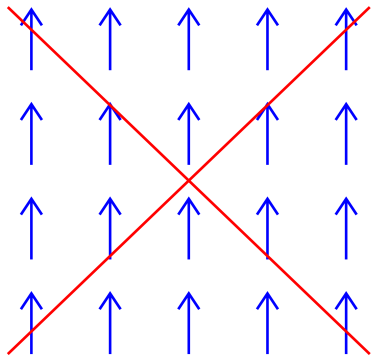

Spin models insufficient

Itinerant ferromagnetism and half-metallicity

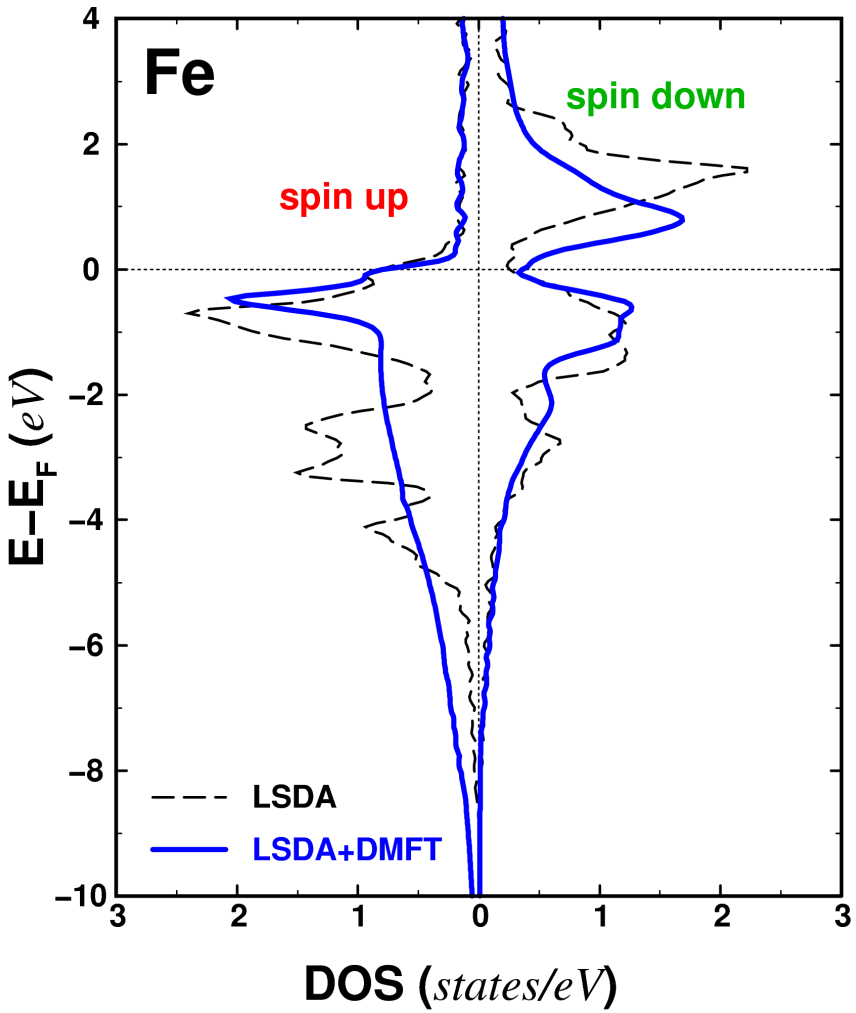

[Chioncel et. al, PRB (2003)]

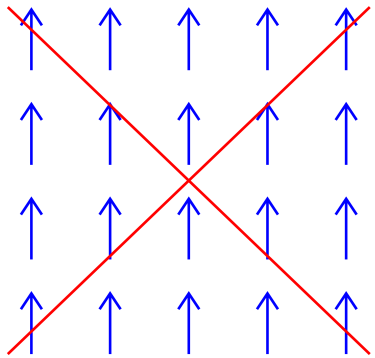

Spin models insufficient

Technological goal: TMR with half metals

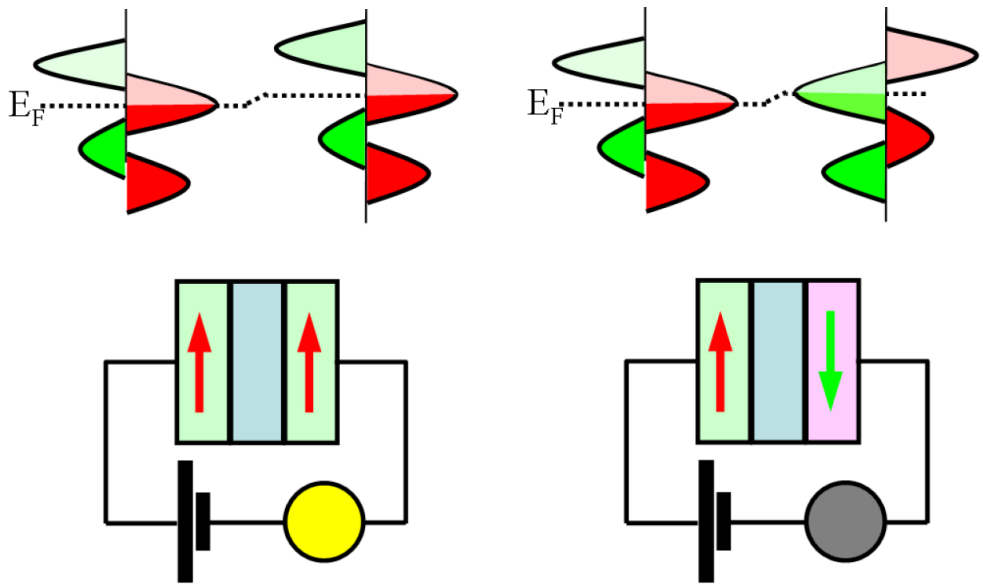

Complex phases of cuprate and organic superconductors

High-T_c physics contained in 2D Hubbard model?

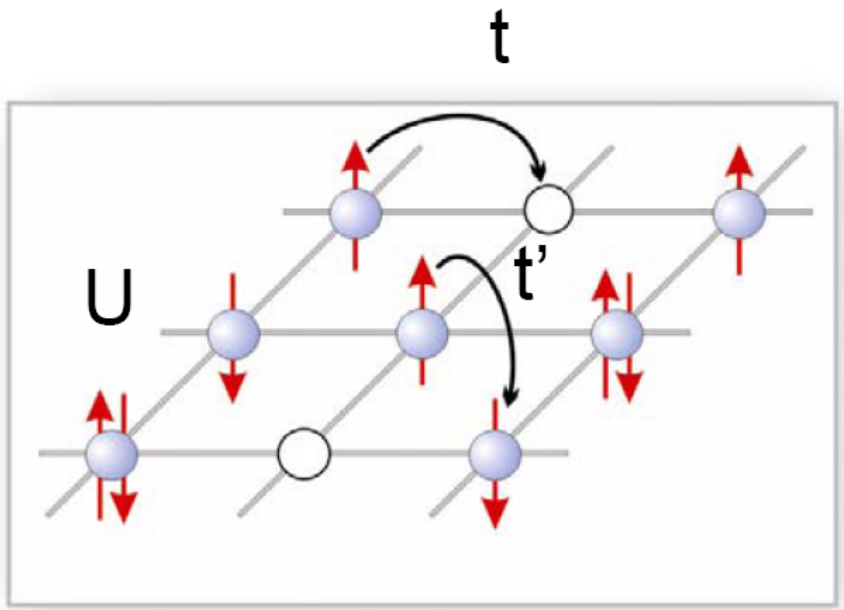

Are antiferromagnetic (AF) and Mott insulating phases essential for superconductivity?

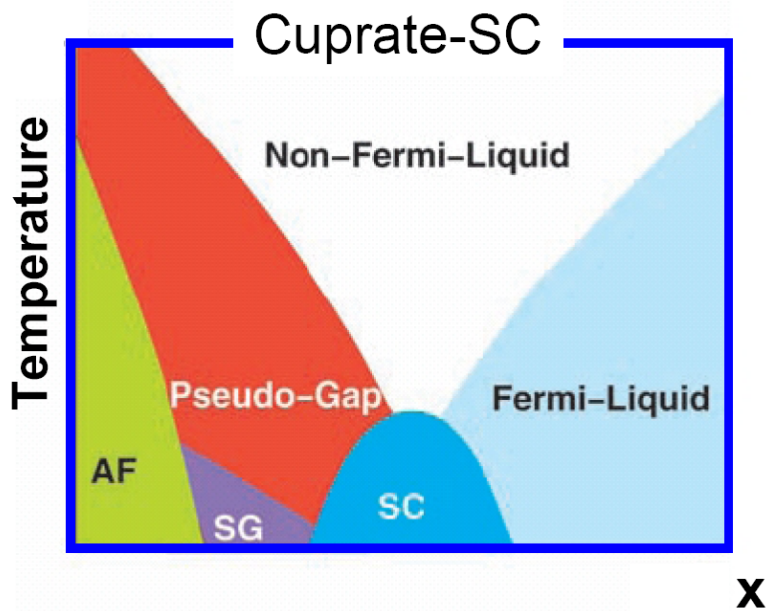

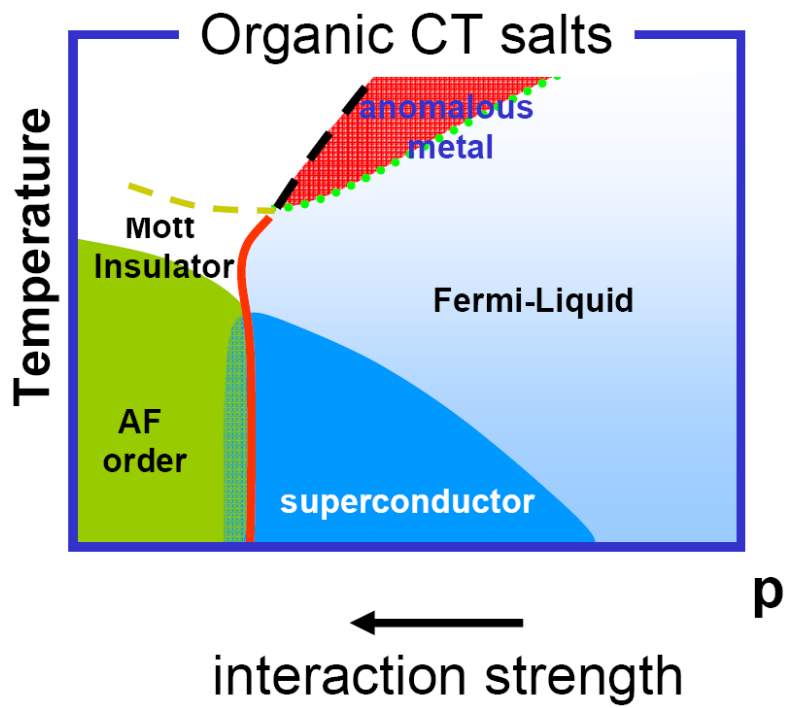

Approaches for correlated electron systems

Microscopic modeling I

General Hamiltonian for nuclei and electrons

$$H = \sum_{i=1}^{N_e} \frac{\boldsymbol{p}_i^{\,2}}{2m} + \sum_{k=1}^{L} \frac{\boldsymbol{P}_k^{\,2}}{2M_k} + \sum_{k<l} \frac{Z_k Z_l\, e^2}{|\boldsymbol{R}_k - \boldsymbol{R}_l|} - \sum_{i,k} \frac{Z_k\, e^2}{|\boldsymbol{r}_i - \boldsymbol{R}_k|} + \sum_{i<j} \frac{e^2}{|\boldsymbol{r}_i - \boldsymbol{r}_j|}$$

Approaches for correlated electron systems

Microscopic modeling I

General Hamiltonian for nuclei and electrons

$$H = \sum_{i=1}^{N_e} \frac{\boldsymbol{p}_i^2}{2m} + \sum_{k=1}^{L} \frac{\boldsymbol{P}_k^2}{2M_k} + \sum_{k<l} \frac{Z_k Z_l\, e^2}{|\boldsymbol{R}_k - \boldsymbol{R}_l|} - \sum_{i,k} \frac{Z_k\, e^2}{|\boldsymbol{r}_i - \boldsymbol{R}_k|} + \sum_{i<j} \frac{e^2}{|\boldsymbol{r}_i - \boldsymbol{r}_j|}$$

Born-Oppenheimer approximation (0^{th}order)

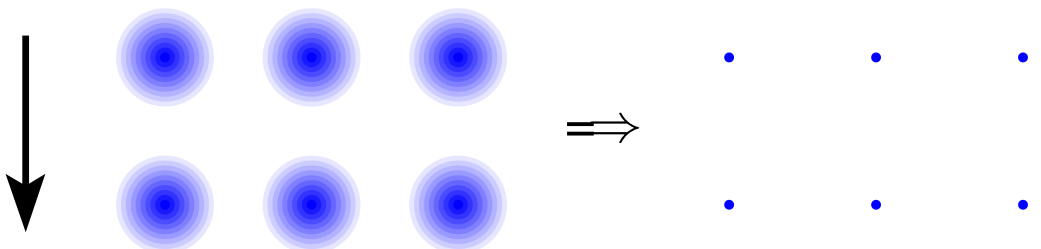

Approaches for correlated electron systems

Microscopic modeling I

General Hamiltonian for nuclei and electrons

$$H = \sum_{i=1}^{N_e} \frac{\boldsymbol{p}_i^2}{2m} + \sum_{k=1}^{L} \frac{\boldsymbol{P}_k^2}{2M_k} + \sum_{k<l} \frac{Z_k Z_l\, e^2}{|\boldsymbol{R}_k - \boldsymbol{R}_l|} - \sum_{i,k} \frac{Z_k\, e^2}{|\boldsymbol{r}_i - \boldsymbol{R}_k|} + \sum_{i<j} \frac{e^2}{|\boldsymbol{r}_i - \boldsymbol{r}_j|}$$

Born-Oppenheimer approximation (0^{th}order)

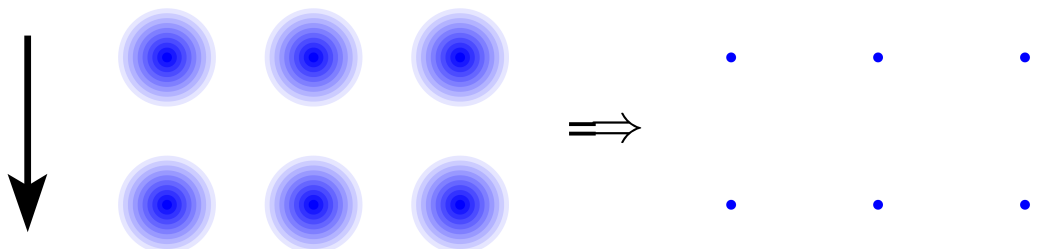

$$H = \sum_{i=1}^{N_e} \frac{\boldsymbol{p}_i^2}{2m} + \sum_{i} V(\boldsymbol{r}_i) + \sum_{i<j} \frac{e^2}{|\boldsymbol{r}_i - \boldsymbol{r}_j|}$$

Approaches for correlated electron systems

Microscopic modeling I

General Hamiltonian for nuclei and electrons

$$H = \sum_{i=1}^{N_e} \frac{\boldsymbol{p}_i^2}{2m} + \sum_{k=1}^{L} \frac{\boldsymbol{P}_k^2}{2M_k} + \sum_{k<l} \frac{Z_k Z_l\, e^2}{|\boldsymbol{R}_k - \boldsymbol{R}_l|} - \sum_{i,k} \frac{Z_k\, e^2}{|\boldsymbol{r}_i - \boldsymbol{R}_k|} + \sum_{i<j} \frac{e^2}{|\boldsymbol{r}_i - \boldsymbol{r}_j|}$$

Born-Oppenheimer approximation (0^{th}order)

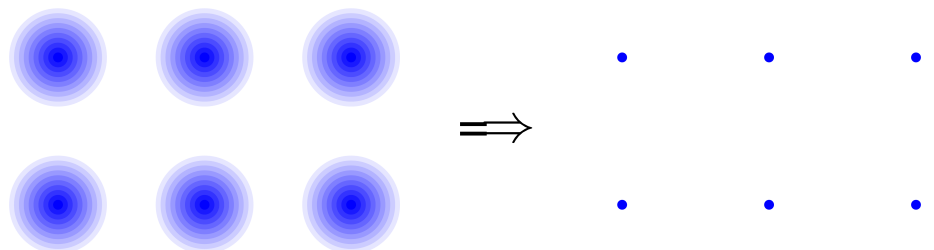

$$H = \sum_{i=1}^{N_e} \frac{\boldsymbol{p}_i^2}{2m} + \sum_{i} V(\boldsymbol{r}_i) + \sum_{i<j} \frac{e^2}{|\boldsymbol{r}_i - \boldsymbol{r}_j|}$$

Classes of theoretical approaches for electronic problem

- continuum methods: density functional theory (DFT), variational+diffusion QMC, . .
- methods for lattice electrons

Microscopic modeling II

$$H = \sum_{i=1}^{N_e} \frac{\boldsymbol{p}_i^2}{2m} + \sum_i V(\boldsymbol{r}_i) + \sum_{i<j} \frac{e^2}{|\boldsymbol{r}_i - \boldsymbol{r}_j|}$$

reduction to valence electrons

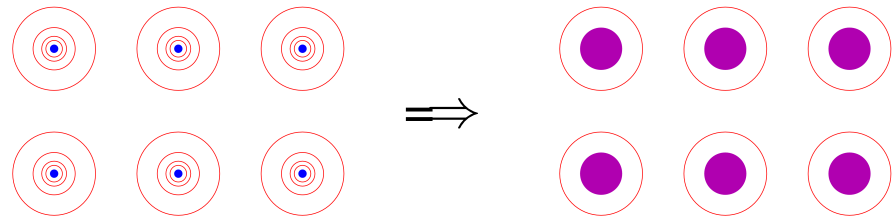

$$H = \sum_{i=1}^{N_v} \frac{\boldsymbol{p}_i^2}{2m} + \sum_{i=1}^{N_v} V^{\text{ion}}(\boldsymbol{r}_i) + \sum_{i=1}^{N_v-1} \sum_{j=i+1}^{N_v} V^{ee}(\boldsymbol{r}_i, \boldsymbol{r}_j)$$

Microscopic modeling II

$$H = \sum_{i=1}^{N_e} \frac{\boldsymbol{p}_i^2}{2m} + \sum_i V(\boldsymbol{r}_i) + \sum_{i<j} \frac{e^2}{|\boldsymbol{r}_i - \boldsymbol{r}_j|}$$

reduction to valence electrons

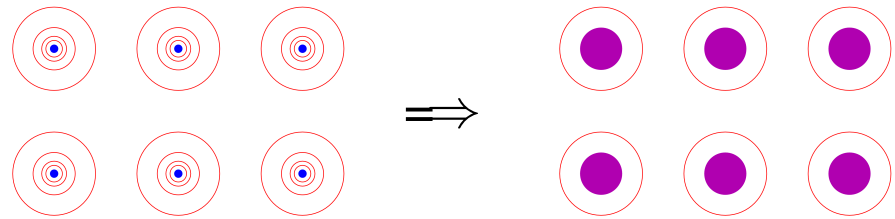

$$H = \sum_{i=1}^{N_v} \frac{\boldsymbol{p}_i^2}{2m} + \sum_{i=1}^{N_v} V^{\text{ion}}(\boldsymbol{r}_i) + \sum_{i=1}^{N_v-1} \sum_{j=i+1}^{N_v} V^{ee}(\boldsymbol{r}_i, \boldsymbol{r}_j)$$

occupation number formalism | Wannier orbitals

$$\hat{H} = \sum_{i\nu j\sigma} t_{ij}^{\nu} \, \hat{c}_{i\nu\sigma}^{\dagger} \, \hat{c}_{j\nu\sigma} + \frac{1}{2} \sum_{\nu\nu'\mu\mu'} \sum_{ijmn} \sum_{\sigma\sigma'} \mathcal{V}_{ijmn}^{\nu\nu'\mu\mu'} \, \hat{c}_{i\nu\sigma}^{\dagger} \, \hat{c}_{j\nu'\sigma'}^{\dagger} \, \hat{c}_{n\mu'\sigma'} \, \hat{c}_{m\mu\sigma}$$

Microscopic modeling II

$$H = \sum_{i=1}^{N_e} \frac{\boldsymbol{p}_i^2}{2m} + \sum_i V(\boldsymbol{r}_i) + \sum_{i<j} \frac{e^2}{|\boldsymbol{r}_i - \boldsymbol{r}_j|}$$

reduction to valence electrons ↓

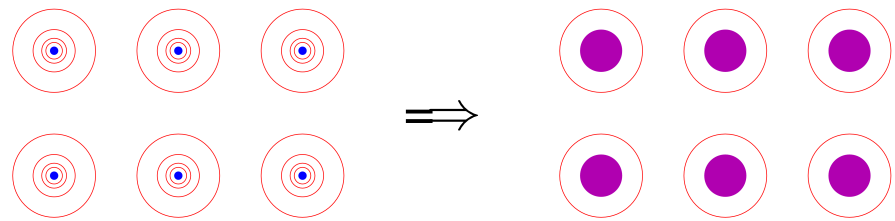

$$H = \sum_{i=1}^{N_v} \frac{\boldsymbol{p}_i^2}{2m} + \sum_{i=1}^{N_v} V^{\text{ion}}(\boldsymbol{r}_i) + \sum_{i=1}^{N_v-1} \sum_{j=i+1}^{N_v} V^{ee}(\boldsymbol{r}_i, \boldsymbol{r}_j)$$

occupation number formalism ↓ Wannier orbitals

$$\hat{H} = \sum_{i\nu j\sigma} t_{ij}^{\nu} \, \hat{c}_{i\nu\sigma}^{\dagger} \, \hat{c}_{j\nu\sigma} + \frac{1}{2} \sum_{\nu\nu'\mu\mu'} \sum_{ijmn} \sum_{\sigma\sigma'} \mathcal{V}_{ijmn}^{\nu\nu'\mu\mu'} \, \hat{c}_{i\nu\sigma}^{\dagger} \, \hat{c}_{j\nu'\sigma'}^{\dagger} \, \hat{c}_{n\mu'\sigma'} \, \hat{c}_{m\mu\sigma}$$

Hubbard model

$$\hat{H} = \sum_{(i,j),\sigma} t_{ij} \, (\hat{c}_{i\sigma}^{\dagger} \hat{c}_{j\sigma} + \text{h.c.}) + U \sum_i \hat{n}_{i\uparrow} \hat{n}_{i\downarrow}$$

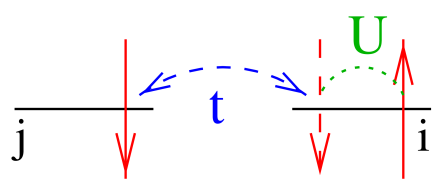

Approaches for Hubbard-type models

$$\hat{H} = \sum_{(i,j),\sigma} t_{ij} \left(\hat{c}^{\dagger}_{i\sigma} \hat{c}_{j\sigma} + \text{h.c.}\right) + U \sum_{i} \hat{n}_{i\uparrow} \hat{n}_{i\downarrow}$$

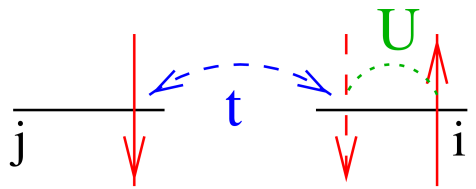

Perturbation theory

- $U \to 0$: Hartree-Fock
  2^{nd} order PT, . . .
- $t/U \to 0$ (for $n = 1$)
  $\rightsquigarrow$ Heisenberg model

finite clusters: ED, QMC

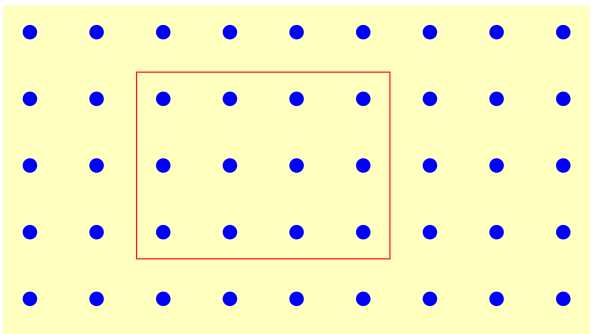

$d \to 1$: Bethe ansatz, DMRG

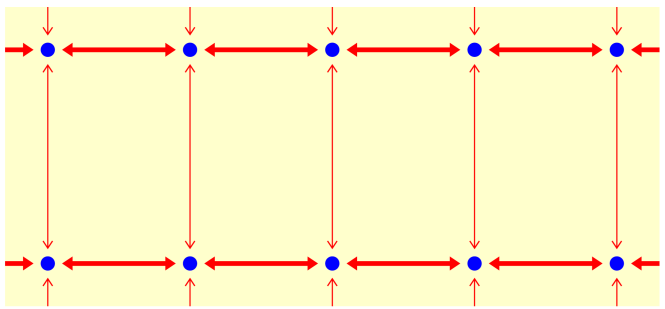

Approaches for Hubbard-type models

$$\hat{H} = \sum_{(i,j),\sigma} t_{ij} \left(\hat{c}^{\dagger}_{i\sigma} \hat{c}_{j\sigma} + \text{h.c.}\right) + U \sum_{i} \hat{n}_{i\uparrow} \hat{n}_{i\downarrow}$$

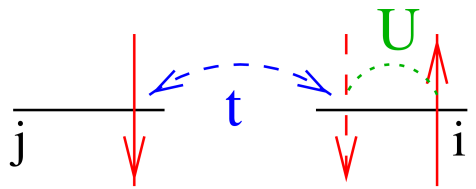

Perturbation theory

- $U \to 0$: Hartree-Fock
  2^{nd} order PT, . . .
- $t/U \to 0$ (for $n = 1$)
  $\rightsquigarrow$ Heisenberg model

finite clusters: ED, QMC

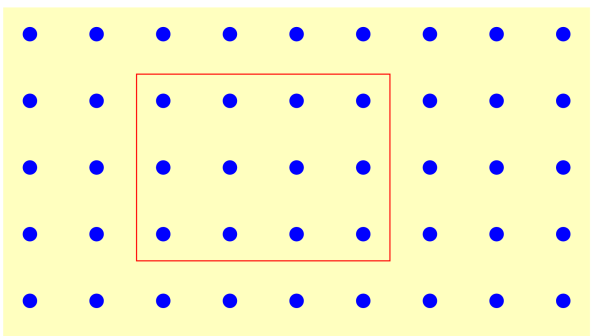

$d \to 1$: Bethe ansatz, DMRG

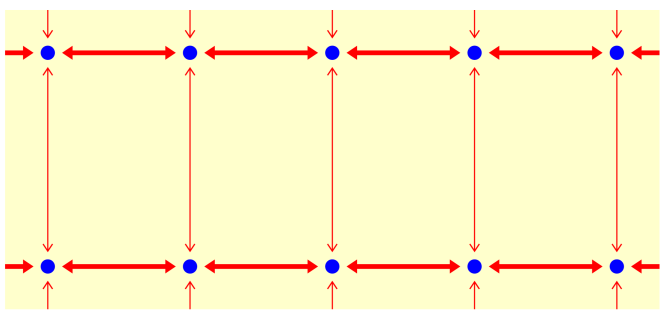

Dynamical mean-field theory (DMFT): local self-energy $\Sigma(\boldsymbol{k}, \omega) \equiv \Sigma(\omega)$

[Metzner, Vollhardt, PRL (1989), Georges, Kotliar, PRL (1992), Jarrell, PRL (1992)]

\+ non-perturbative $\rightsquigarrow$ valid at MIT

\+ dynamical on-site correlations preserved

\+ in thermodynamic limit

+/− exact for coordination $Z \to \infty$

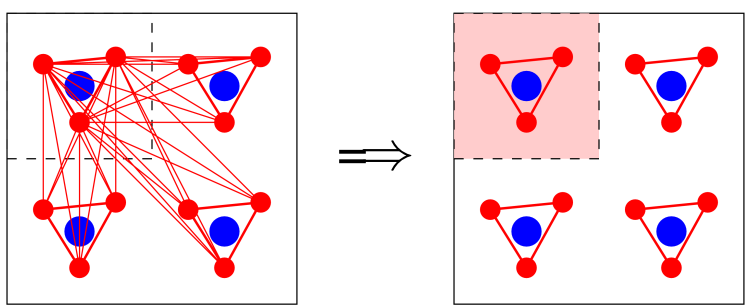

Excursus: Green function and self-energy

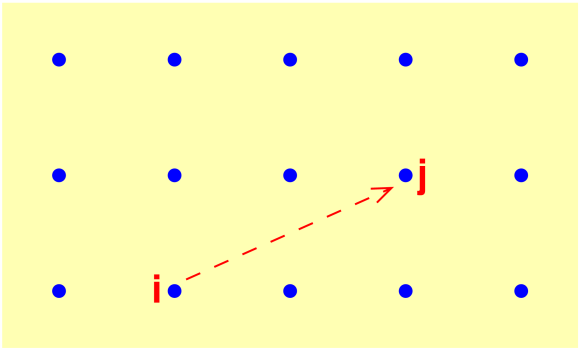

Single-particle Green function (lattice sites i, j):

$$G_{ij}(t_1, t_2) = -\langle c_j(t_2)\, c_i^\dagger(t_1)\rangle$$

Translation invariance in space and time: $G_{ij}(t_1, t_2) \equiv G_{j-i}(t_2 - t_1) \overset{\text{Fourier}}{\longrightarrow} G(\boldsymbol{k}, \omega)$

Excursus: Green function and self-energy

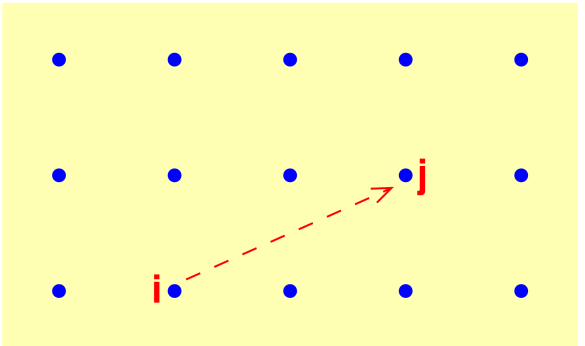

Single-particle Green function (lattice sites i, j):

$$G_{ij}(t_1, t_2) = -\langle c_j(t_2)\, c_i^\dagger(t_1)\rangle$$

Translation invariance in space and time: $G_{ij}(t_1, t_2) \equiv G_{j-i}(t_2 - t_1) \overset{\text{Fourier}}{\longrightarrow} G(\boldsymbol{k}, \omega)$

Noninteracting limit (dispersion $\varepsilon_{\boldsymbol{k}}$): $G^0(\boldsymbol{k}, \omega) = \dfrac{1}{\omega + \mu - \varepsilon_{\boldsymbol{k}}}$

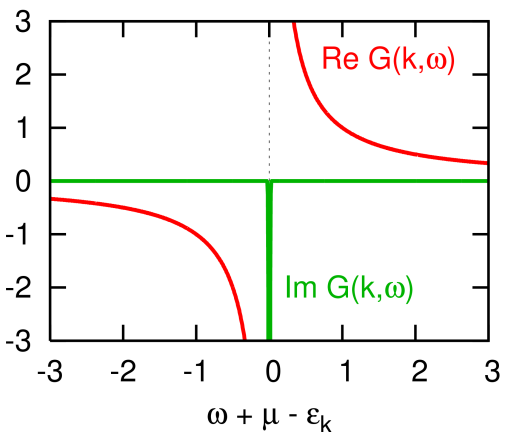

Excursus: Green function and self-energy

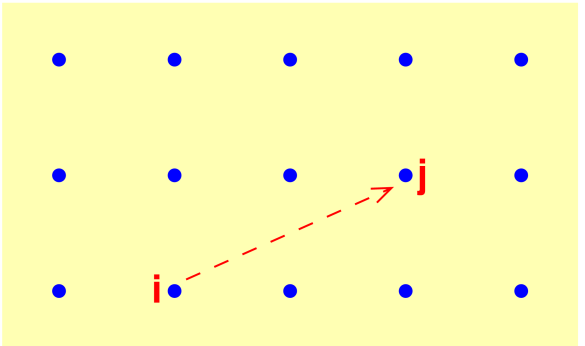

Single-particle Green function (lattice sites i, j):

$$G_{ij}(t_1, t_2) = -\langle c_j(t_2)\, c_i^\dagger(t_1)\rangle$$

Translation invariance in space and time: $G_{ij}(t_1, t_2) \equiv G_{j-i}(t_2 - t_1) \overset{\text{Fourier}}{\longrightarrow} G(\boldsymbol{k}, \omega)$

Noninteracting limit (dispersion $\varepsilon_{\boldsymbol{k}}$): $G^0(\boldsymbol{k}, \omega) = \dfrac{1}{\omega + \mu - \varepsilon_{\boldsymbol{k}}}$

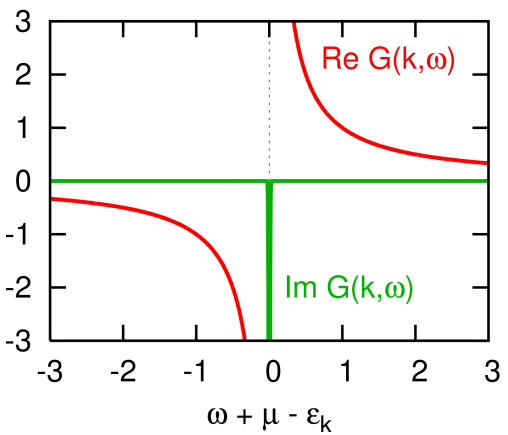

Self-energy Σ quantifies impact of interactions:

$$G(\boldsymbol{k}, \omega) = \frac{1}{\omega + \mu - \varepsilon_{\boldsymbol{k}} - \Sigma(\boldsymbol{k}, \omega)}$$

Excursus: Green function and self-energy

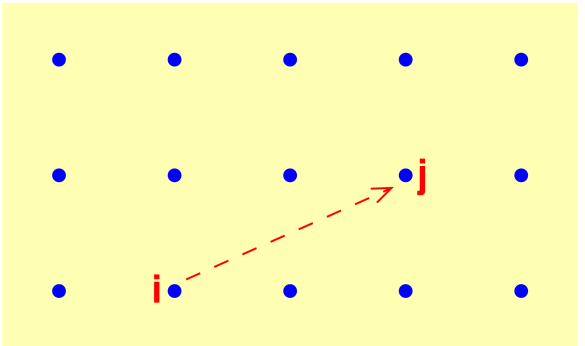

Single-particle Green function (lattice sites i, j):

$$G_{ij}(t_1, t_2) = -\langle c_j(t_2)\, c_i^\dagger(t_1)\rangle$$

Translation invariance in space and time: $G_{ij}(t_1, t_2) \equiv G_{j-i}(t_2 - t_1) \overset{\text{Fourier}}{\longrightarrow} G(\boldsymbol{k}, \omega)$

Noninteracting limit (dispersion $\varepsilon_{\boldsymbol{k}}$): $G^0(\boldsymbol{k}, \omega) = \dfrac{1}{\omega + \mu - \varepsilon_{\boldsymbol{k}}}$

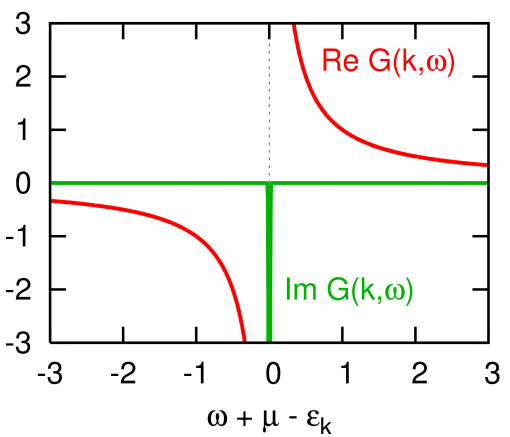

Self-energy Σ quantifies impact of interactions:

$$G(\boldsymbol{k}, \omega) = \frac{1}{\omega + \mu - \varepsilon_{\boldsymbol{k}} - \Sigma(\boldsymbol{k}, \omega)}$$

Locality of self-energy $\Sigma(\boldsymbol{k}, \omega) \equiv \Sigma(\omega)$ within DMFT simplifies local Green function:

$$G(\omega) \equiv G_{ii}(\omega) = \int d\varepsilon \frac{N^0(\varepsilon)}{\omega + \mu - \varepsilon - \Sigma(\omega)}; \qquad N^0(\varepsilon) = \frac{1}{N}\sum_{\boldsymbol{k}} \delta(\varepsilon - \varepsilon_{\boldsymbol{k}})$$

$\boldsymbol{k}$ integrated Dyson equation — noninteracting DOS

Mott transition within DMFT

Fully frustrated 1-band model,
energy scale: bandwidth $W = 4$

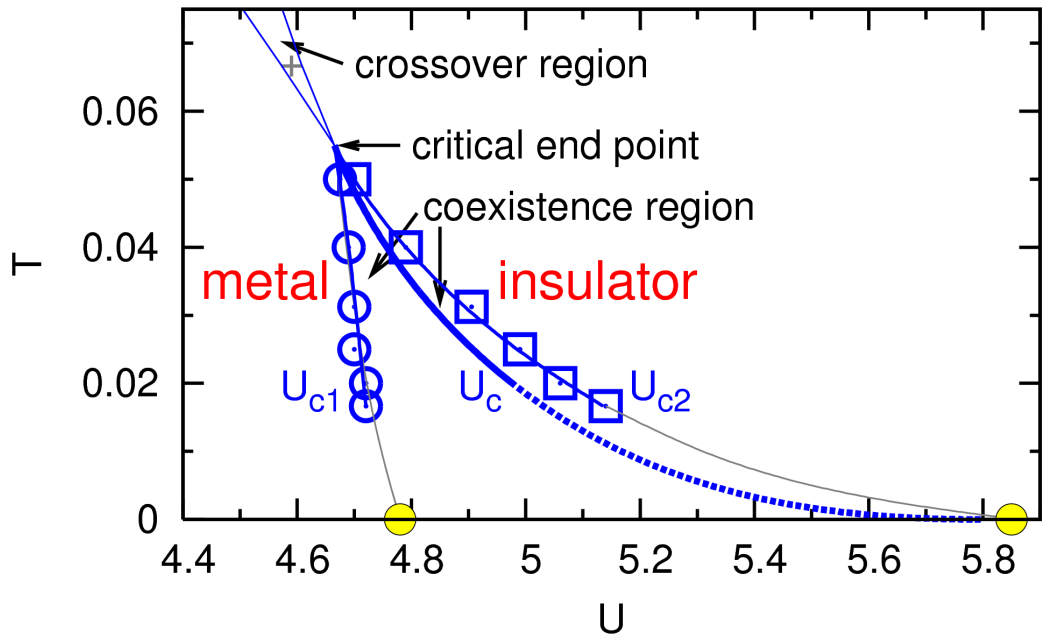

Mott transition within DMFT

Fully frustrated 1-band model,
energy scale: bandwidth $W = 4$

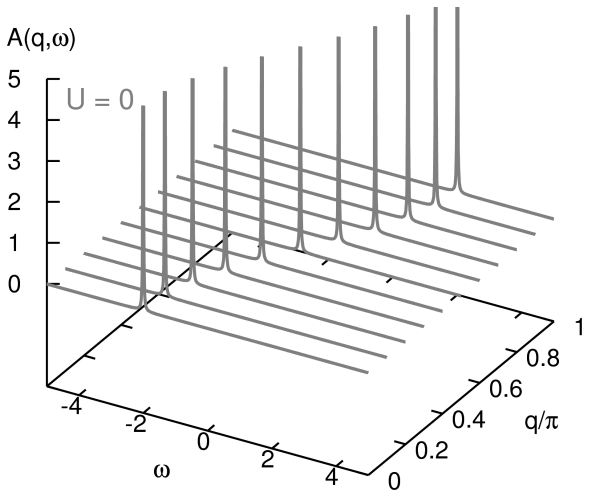

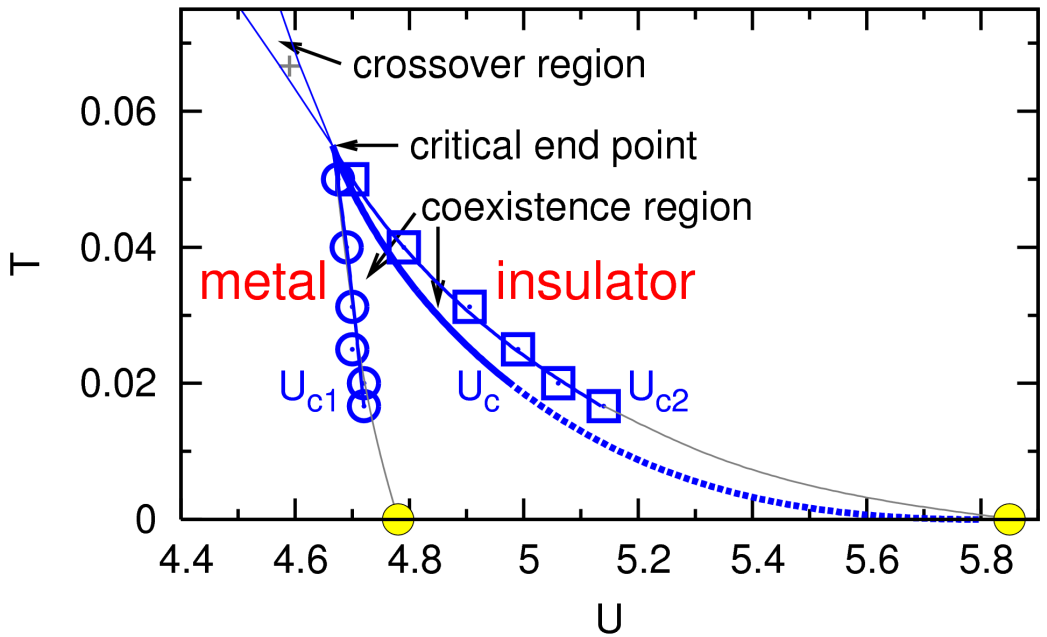

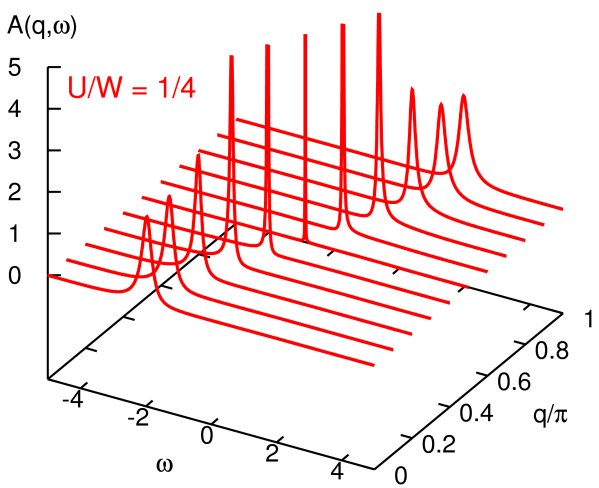

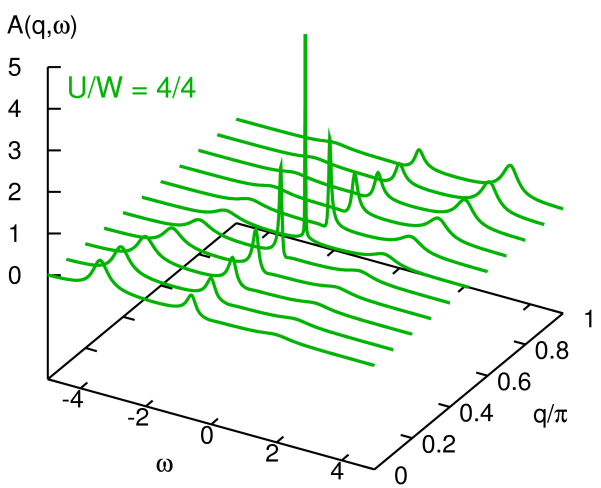

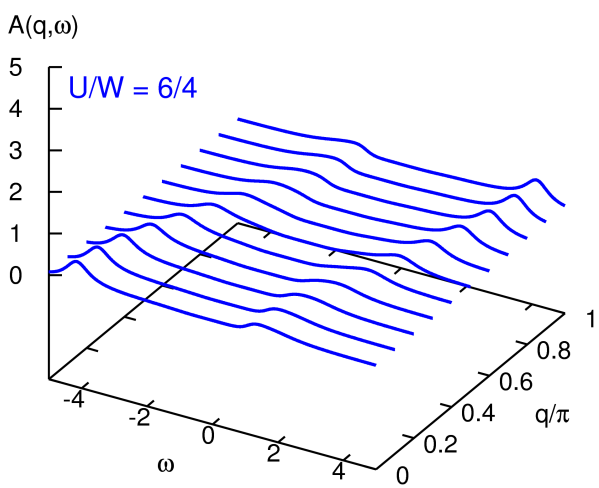

Iterative solution of DMFT equations

0. Initialize self-energy
1. Solve Dyson equation
2. Solve single impurity Anderson model (SIAM)

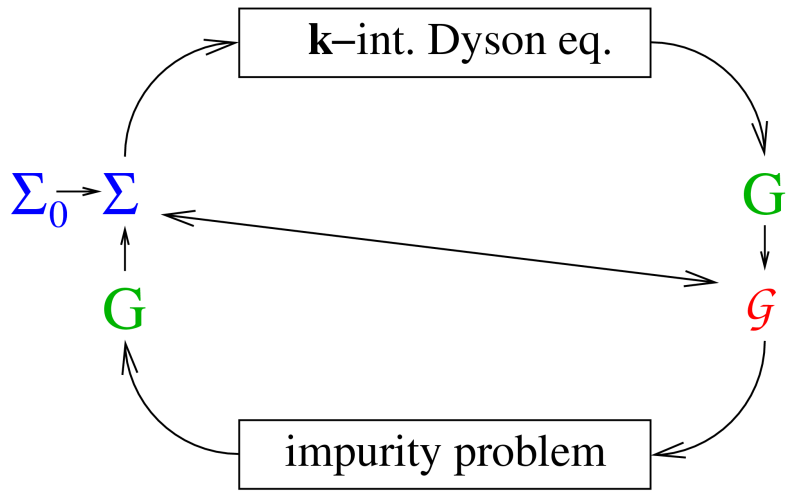

$\longleftarrow$ DOS / t_{ij} / $\varepsilon_{\nu \boldsymbol{k}}$

$\longleftarrow$ local interactions

Iterative solution of DMFT equations

0. Initialize self-energy
1. Solve Dyson equation
2. Solve single impurity Anderson model (SIAM)

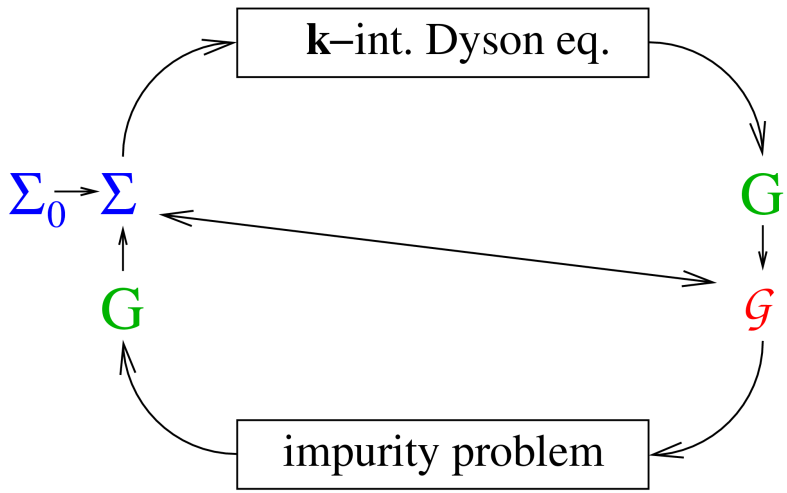

← DOS / t_{ij} / $\varepsilon_{\nu \boldsymbol{k}}$

← local interactions

Impurity solver:

- Iterative perturbation theory (IPT; not controlled)
- Quantum Monte-Carlo (QMC)

Iterative solution of DMFT equations

0. Initialize self-energy
1. Solve Dyson equation
2. Solve single impurity Anderson model (SIAM)

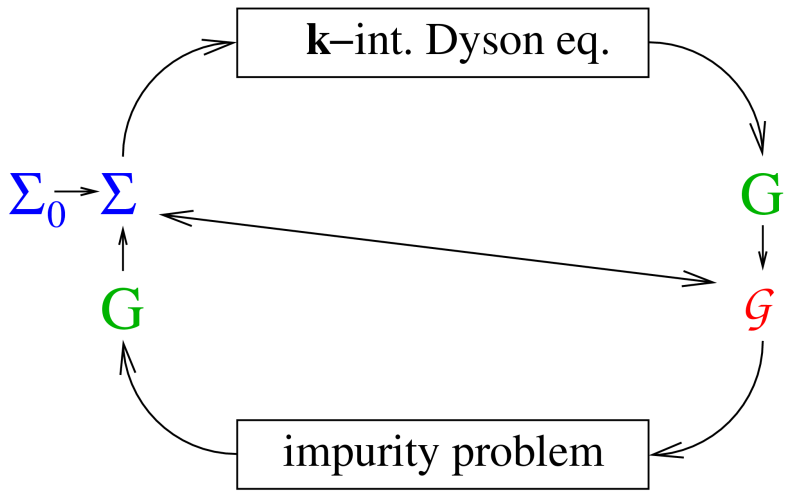

⟵ DOS / t_{ij} / $\varepsilon_{\nu \boldsymbol{k}}$

⟵ local interactions

Impurity solver:

- Iterative perturbation theory (IPT; not controlled)
- Quantum Monte-Carlo (QMC)
- Exact diagonalization (ED; large finite-size errors)
- Numerical renormalization group (NRG; 1-2 bands)
- Density matrix renormalization group (DMRG)
- Self-energy functional theory (SFT) + ED

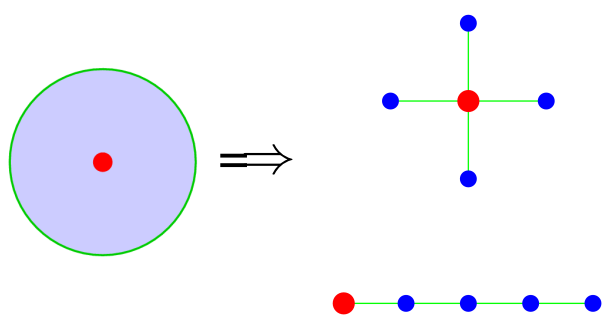

Auxiliary-field QMC algorithm [Hirsch, Fye (1986)]

Green function G in imaginary time (fermionic Grassmann variables ψ, ψ^*):

$$G_\sigma(\tau_2 - \tau_1) = \frac{1}{\mathcal{Z}} \int \mathcal{D}[\psi]\, \mathcal{D}[\psi^*]\ \psi_\sigma(\tau_1)\psi^*_\sigma(\tau_2)\ \exp\Big[\mathcal{A}_0 - U \sum_{\sigma\sigma'} \int_0^\beta d\tau\, \psi^*_\sigma \psi_\sigma \psi^*_{\sigma'} \psi_{\sigma'}\Big]$$

Auxiliary-field QMC algorithm [Hirsch, Fye (1986)]

Green function G in imaginary time (fermionic Grassmann variables ψ, ψ^*):

$$G_\sigma(\tau_2 - \tau_1) = \frac{1}{\mathcal{Z}} \int \mathcal{D}[\psi]\, \mathcal{D}[\psi^*]\ \psi_\sigma(\tau_1)\psi^*_\sigma(\tau_2)\ \exp\Big[\mathcal{A}_0 - U \sum_{\sigma\sigma'} \int_0^\beta d\tau\, \psi^*_\sigma \psi_\sigma \psi^*_{\sigma'} \psi_{\sigma'}\Big]$$

Discretization $\beta = \Lambda\, \Delta\tau$, Trotter decoupling $e^{-\beta(\hat{T}+\hat{V})} = \lim_{\Lambda\to\infty} \left[e^{-\Delta\tau \hat{T}} e^{-\Delta\tau \hat{V}}\right]^\Lambda$

Auxiliary-field QMC algorithm [Hirsch, Fye (1986)]

Green function G in imaginary time (fermionic Grassmann variables ψ, ψ^*):

$$G_\sigma(\tau_2-\tau_1) = \frac{1}{\mathcal{Z}} \int \mathcal{D}[\psi]\,\mathcal{D}[\psi^*]\ \psi_\sigma(\tau_1)\psi^*_\sigma(\tau_2)\ \exp\Big[\mathcal{A}_0 - U\sum_{\sigma\sigma'}\int_0^\beta d\tau\,\psi^*_\sigma\psi_\sigma\psi^*_{\sigma'}\psi_{\sigma'}\Big]$$

Discretization $\beta = \Lambda\,\Delta\tau$, Trotter decoupling $e^{-\beta(\hat{T}+\hat{V})} = \lim_{\Lambda\to\infty}\left[e^{-\Delta\tau\hat{T}}e^{-\Delta\tau\hat{V}}\right]^\Lambda$

Use $\hat{n}_\uparrow\hat{n}_\downarrow = \frac{1}{2}\left[\hat{n}_\uparrow + \hat{n}_\downarrow - \left(\hat{n}_\uparrow - \hat{n}_\downarrow\right)^2\right]$; discrete Hubbard-Stratonovich transformation

$$\exp\left[\Delta\tau U\left(\hat{n}_\uparrow - \hat{n}_\downarrow\right)^2/2\right] = \frac{1}{2}\sum_{s=\pm1}\exp\left[\lambda s\left(\hat{n}_\uparrow - \hat{n}_\downarrow\right)\right]; \qquad \cosh(\lambda) = \exp(\Delta\tau U/2)$$

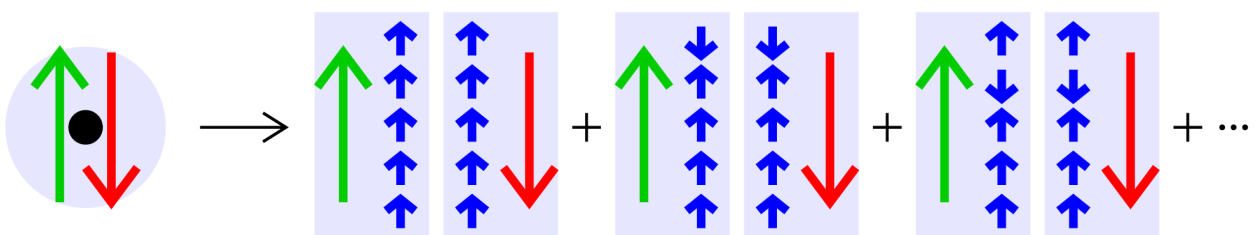

Wick theorem:

$$G = \frac{\sum M \det\{M\}}{\sum \det\{M\}}$$

Auxiliary-field QMC algorithm [Hirsch, Fye (1986)]

Green function G in imaginary time (fermionic Grassmann variables ψ, ψ^*):

$$G_\sigma(\tau_2-\tau_1) = \frac{1}{\mathcal{Z}} \int \mathcal{D}[\psi]\,\mathcal{D}[\psi^*]\ \psi_\sigma(\tau_1)\psi^*_\sigma(\tau_2)\ \exp\Big[\mathcal{A}_0 - U\sum_{\sigma\sigma'}\int_0^\beta d\tau\,\psi^*_\sigma\psi_\sigma\psi^*_{\sigma'}\psi_{\sigma'}\Big]$$

Discretization $\beta = \Lambda\,\Delta\tau$, Trotter decoupling $e^{-\beta(\hat{T}+\hat{V})} = \lim_{\Lambda\to\infty}\left[e^{-\Delta\tau\hat{T}}e^{-\Delta\tau\hat{V}}\right]^\Lambda$

Use $\hat{n}_\uparrow\hat{n}_\downarrow = \frac{1}{2}\left[\hat{n}_\uparrow + \hat{n}_\downarrow - \left(\hat{n}_\uparrow - \hat{n}_\downarrow\right)^2\right]$; discrete Hubbard-Stratonovich transformation

$$\exp\left[\Delta\tau U\left(\hat{n}_\uparrow - \hat{n}_\downarrow\right)^2/2\right] = \frac{1}{2}\sum_{s=\pm1}\exp\left[\lambda s\left(\hat{n}_\uparrow - \hat{n}_\downarrow\right)\right]; \qquad \cosh(\lambda) = \exp(\Delta\tau U/2)$$

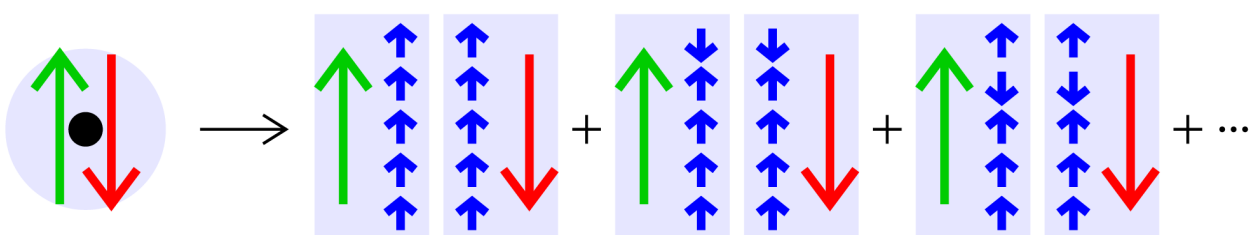

Wick theorem:

$$G = \frac{\sum M \det\{M\}}{\sum \det\{M\}}$$

Metropolis MC importance sampling over auxiliary Ising field $\{s\}$: 2^Λ configurations

\+ numerically exact, + no sign problem, − effort scales as T^{-3}

Contributions to DMFT-QMC error bars:

- statistical fluctuations + warm-up
- convergency (of self-consistency cycle)
- discretization (Trotter error and Fourier transform)

Contributions to DMFT-QMC error bars:

- statistical fluctuations + warm-up
- convergency (of self-consistency cycle)
- discretization (Trotter error and Fourier transform)

Example: half-filled Hubbard model, $U = 5$, $W = 4$, $T = 0.04$ (Mott insulator)

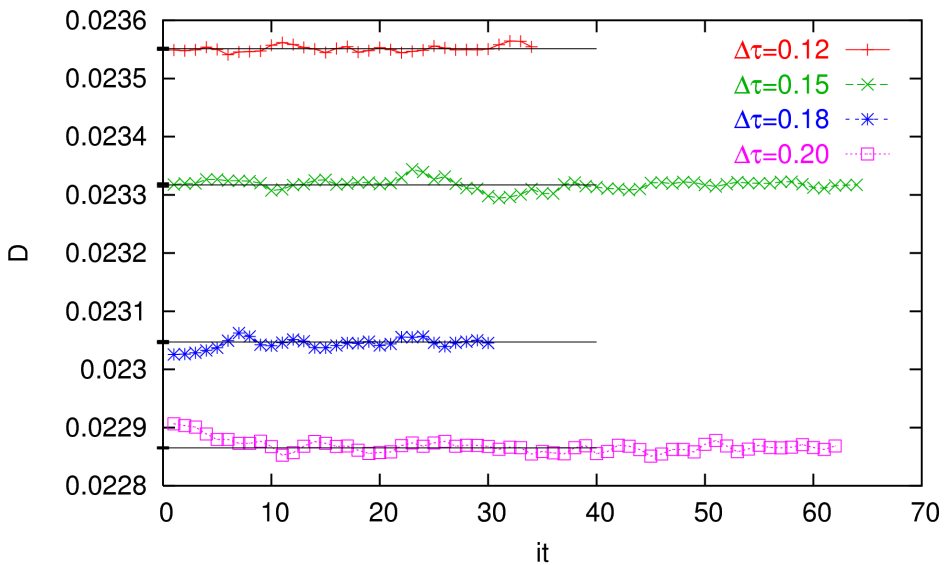

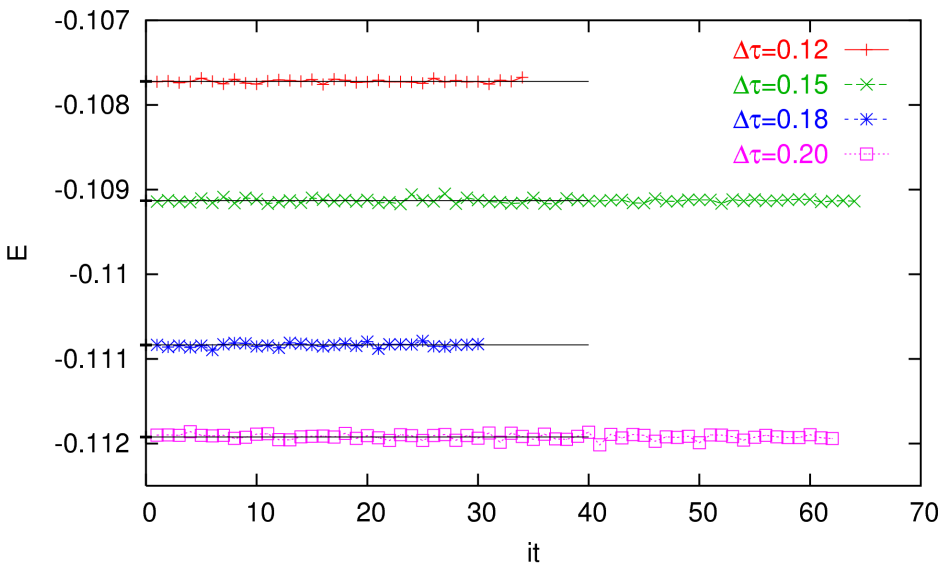

Contributions to DMFT-QMC error bars:

- statistical fluctuations + warm-up
- convergency (of self-consistency cycle)
- discretization (Trotter error and Fourier transform)

Example: half-filled Hubbard model, $U = 5$, $W = 4$, $T = 0.04$ (Mott insulator)

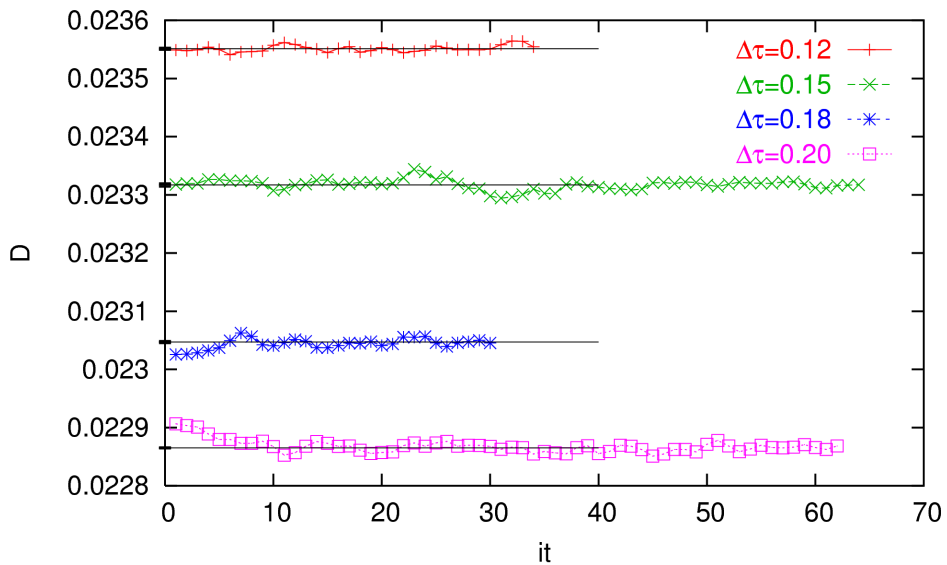

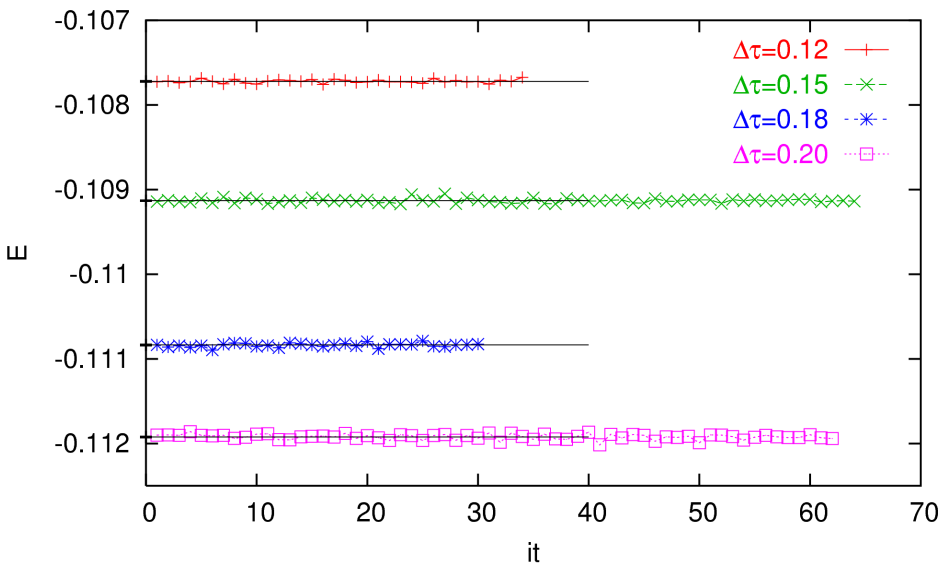

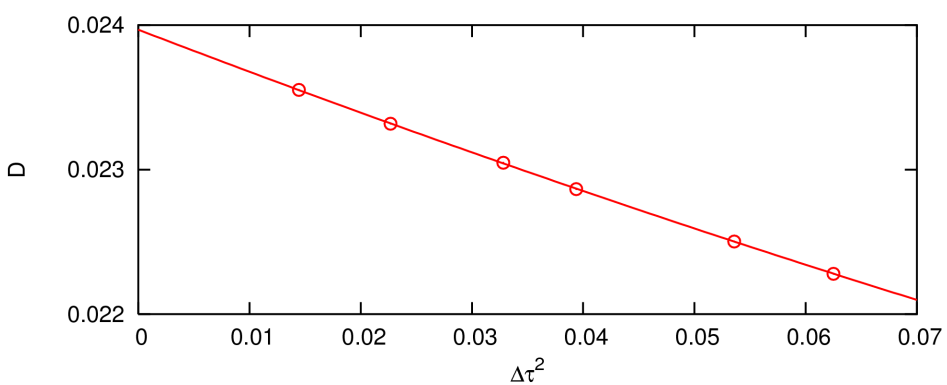

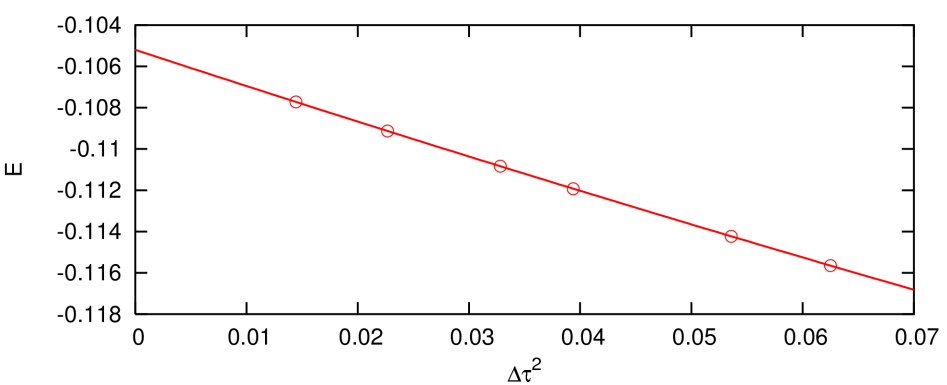

Special issue: Fourier transformations in DMFT-QMC cycle

Iterative solution of DMFT equations (for imaginary-time impurity solver)

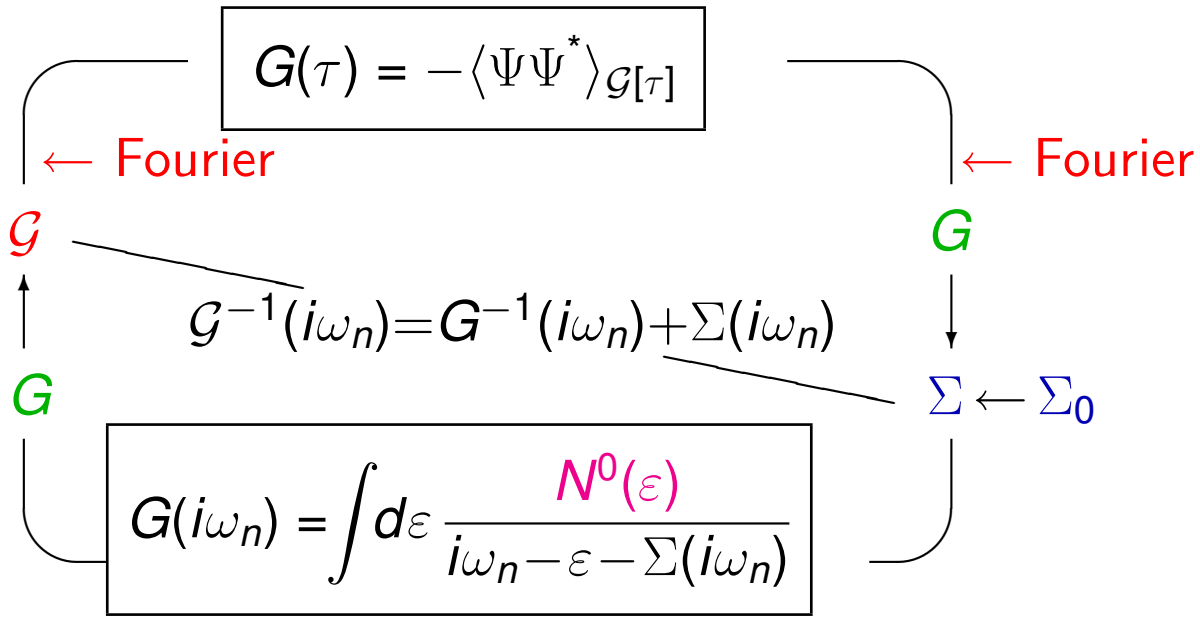

Special issue: Fourier transformations in DMFT-QMC cycle

Iterative solution of DMFT equations (for imaginary-time impurity solver)

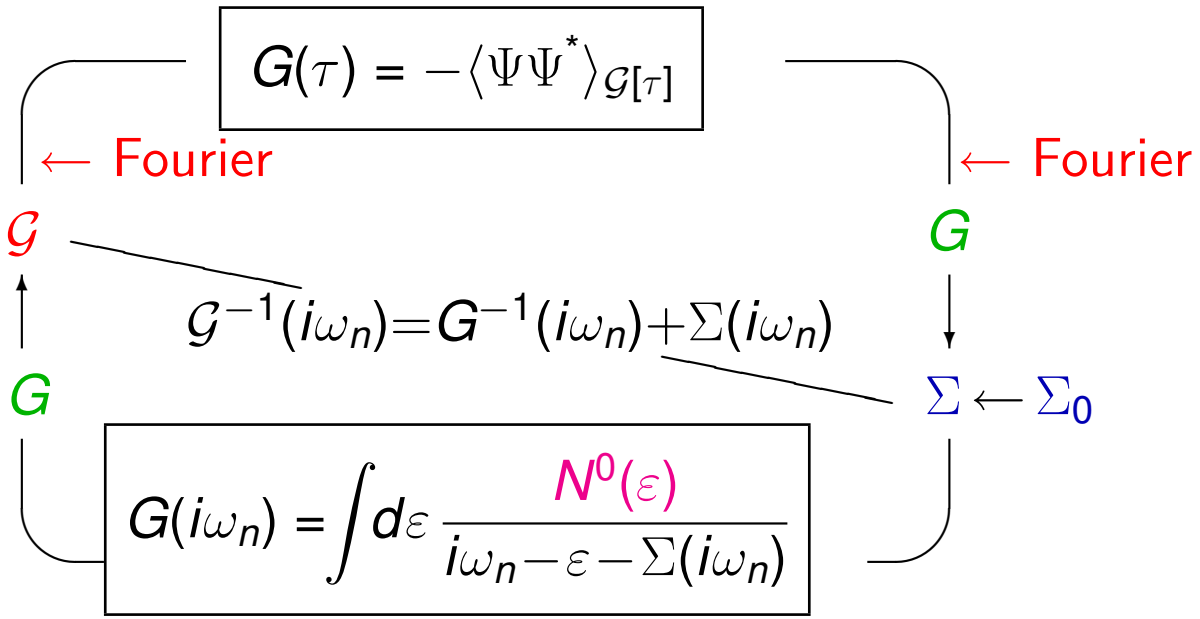

Naive discrete Fourier transformation $\rightsquigarrow$ oscillations (instead of $G(\omega) \overset{\omega\to\infty}{\longrightarrow} 1/\omega$)

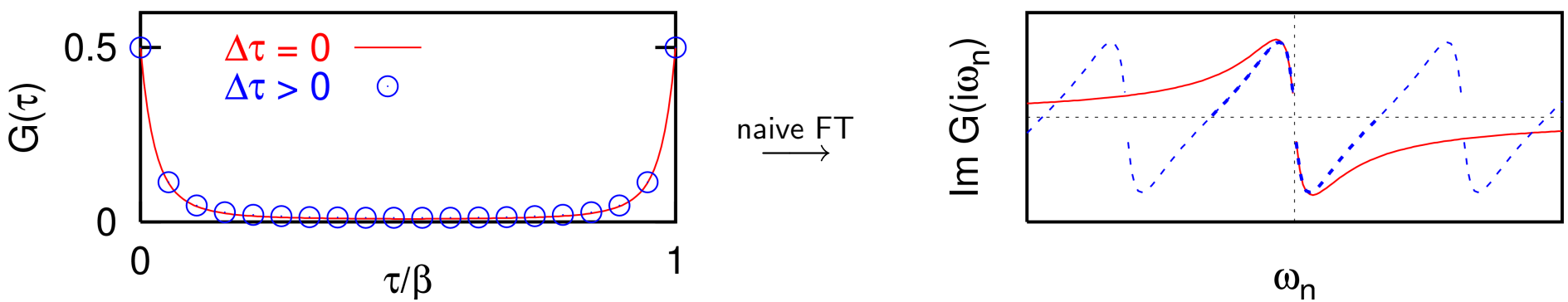

Special issue: Fourier transformations in DMFT-QMC cycle

Iterative solution of DMFT equations (for imaginary-time impurity solver)

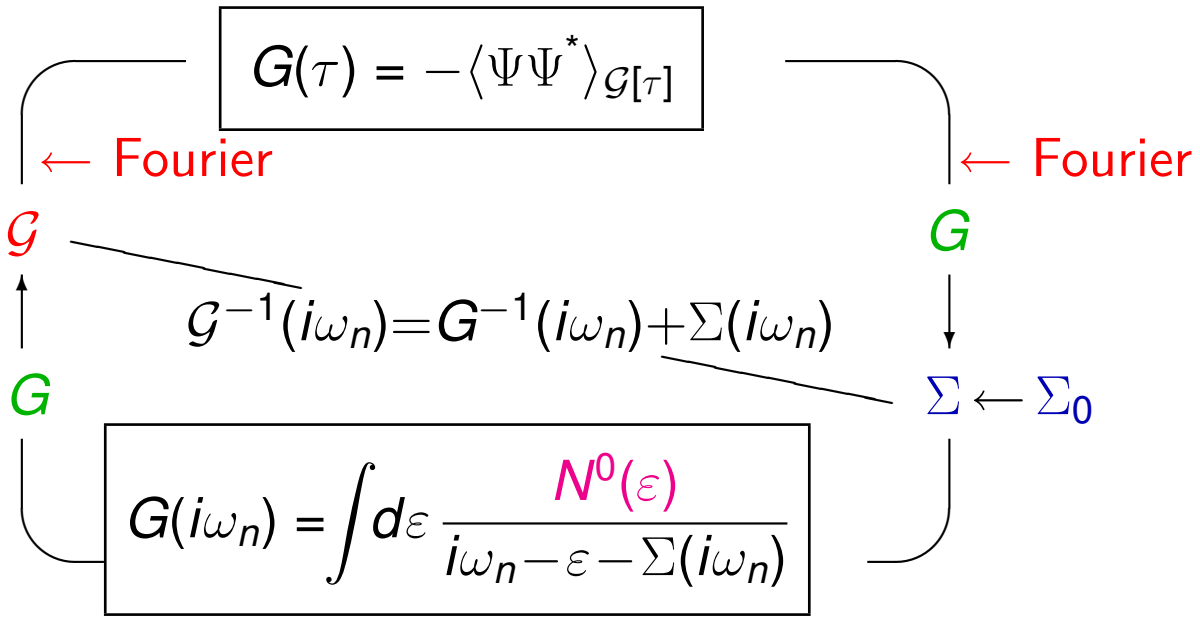

Naive discrete Fourier transformation $\rightsquigarrow$ oscillations (instead of $G(\omega) \overset{\omega\to\infty}{\longrightarrow} 1/\omega$)

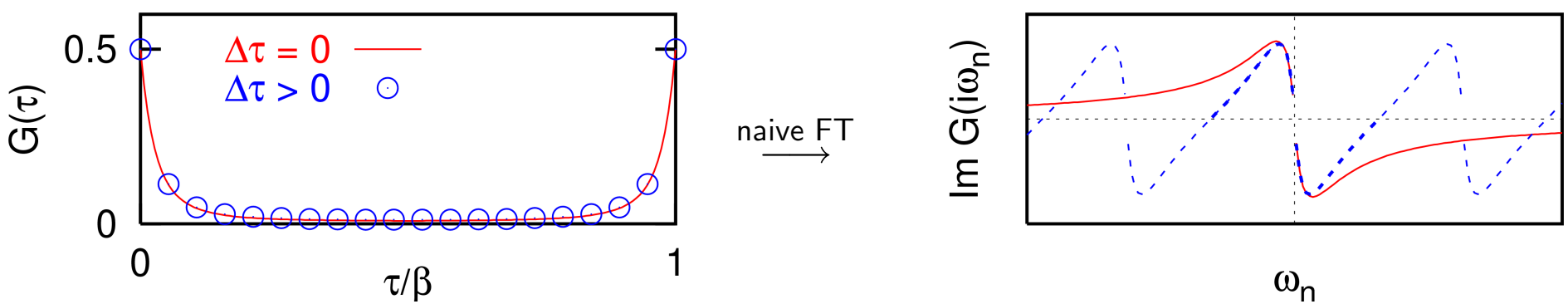

1st solution: correct unphysical behavior for $|\omega| \lesssim \omega_{\text{Nyquist}}$ by transformation [Ulmke]

2^{nd} solution: interpolate $G_{\text{QMC}}(\tau)$ by cubic splines [Jarrell, Krauth, Gull, . . .]

But: $\dfrac{d^2G(\tau)}{d\tau^2}$ maximal for $\tau \to 0, \beta$ $\quad \rightsquigarrow$ natural boundary conditions inappropriate

2^{nd} solution: interpolate $G_{\text{QMC}}(\tau)$ by cubic splines [Jarrell, Krauth, Gull, . . .]

But: $\dfrac{d^2G(\tau)}{d\tau^2}$ maximal for $\tau \to 0, \beta$ $\rightsquigarrow$ natural boundary conditions inappropriate

- adjust boundary cond. [Oudovenko]
- spline-fit only difference w.r.t. reference problem:
  - IPT [Jarrell]

2nd solution: interpolate $G_{\mathrm{QMC}}(\tau)$ by cubic splines [Jarrell, Krauth, Gull, . . .]

But: $\dfrac{d^2G(\tau)}{d\tau^2}$ maximal for $\tau \to 0, \beta$ $\rightsquigarrow$ natural boundary conditions inappropriate

- adjust boundary cond. [Oudovenko]
- spline-fit only difference w.r.t. reference problem:
  - IPT [Jarrell]
  - high-frequency expansion for $\Sigma(\omega)$ + param. [Knecht, NB]

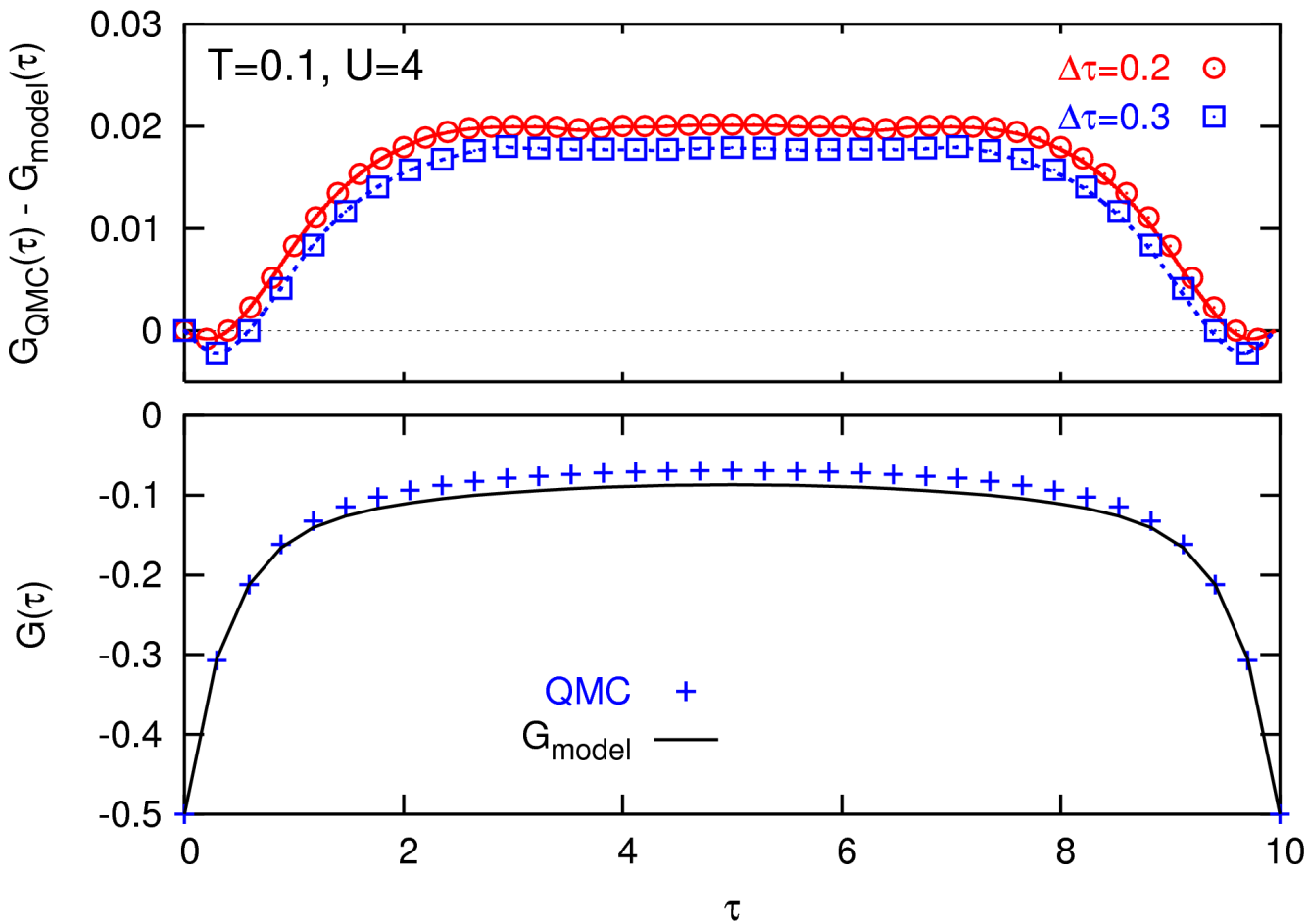

$$\Sigma_\sigma(\omega) = U\left(\langle\hat{n}_{-\sigma}\rangle - \tfrac{1}{2}\right)\omega^0 + U^2\langle\hat{n}_{-\sigma}\rangle\left(1 - \langle\hat{n}_{-\sigma}\rangle\right)\omega^{-1} + \mathcal{O}(\omega^{-2})$$

Sensitive test: self-energy $\Sigma(i\omega_n)$ for insulating phase ($T = 0.1$, $U = 5.0$)

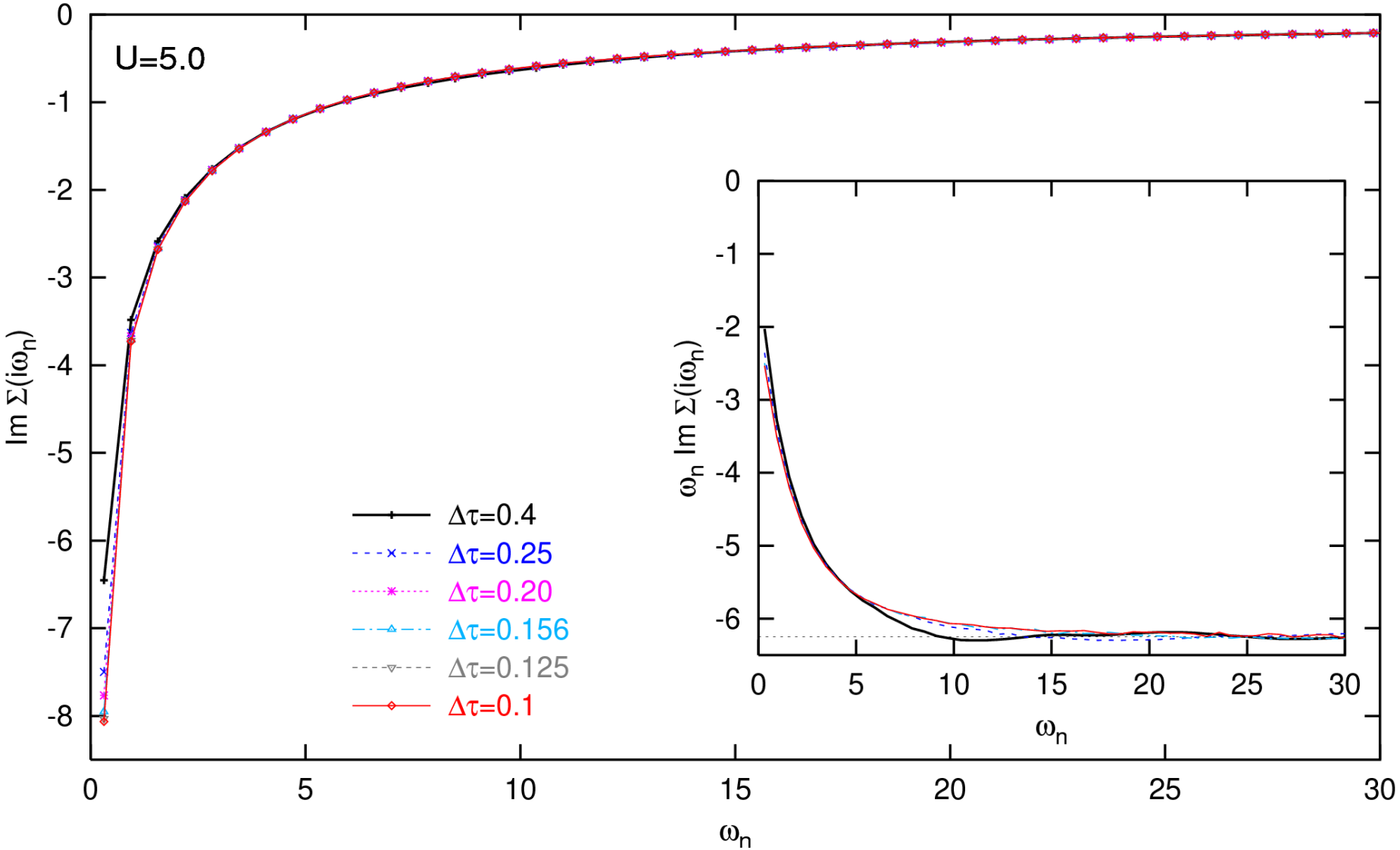

Rapid convergence at all frequencies for "QMC + $1/\omega$" DMFT solver

Selected applications

High-precision calculations for 1-band model, extrapolation $T \to 0$:

benchmark results (E, D, Z) unmatched by ED, DMRG, PQMC, NRG

revealed errors in weak-coupling expansions

Orbital-selective Mott transitions in 2-band model

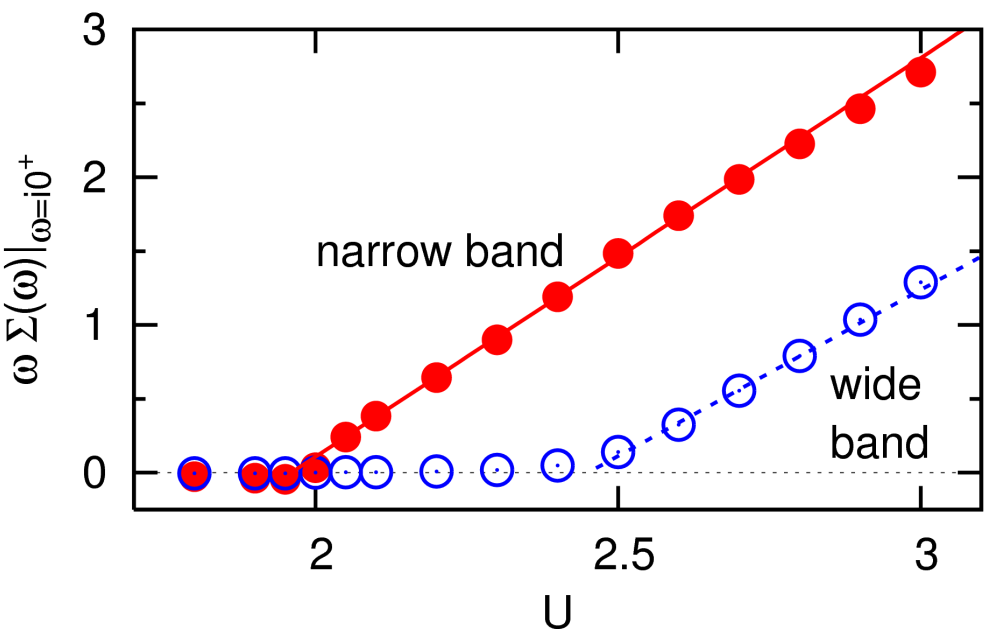

[C. Knecht, NB, and P.G.J. van Dongen, PRB 72, 081103(R) (2005)]

Efficiency of QMC DMFT solvers

New development: continuous-time QMC algorithms

1. weak-coupling expansion

[Rubtsov, Savkin, Lichtenstein, PRB (2005)]

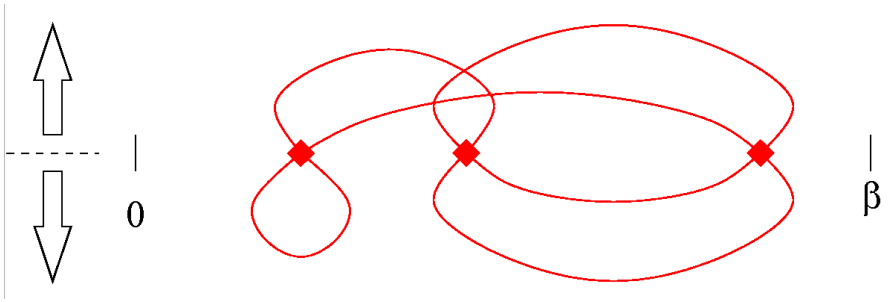

2. hybridization expansion

[Werner et al., PRL (2006)]

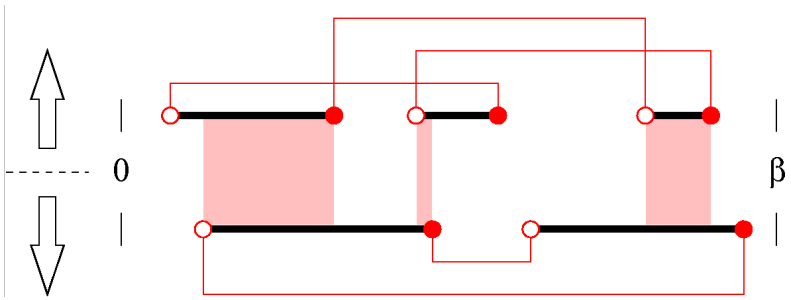

Efficiency of QMC DMFT solvers

New development: continuous-time QMC algorithms

1. weak-coupling expansion

[Rubtsov, Savkin, Lichtenstein, PRB (2005)]

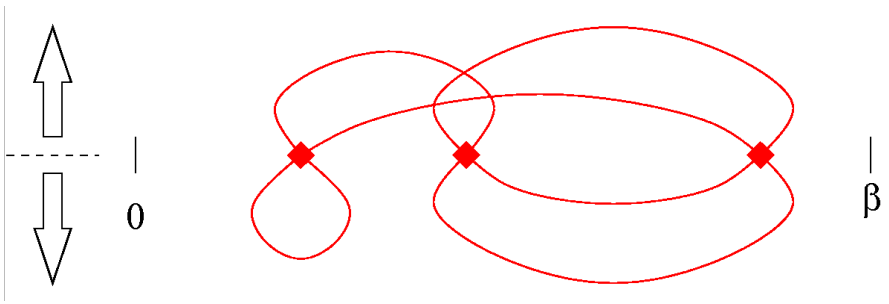

2. hybridization expansion

[Werner et al., PRL (2006)]

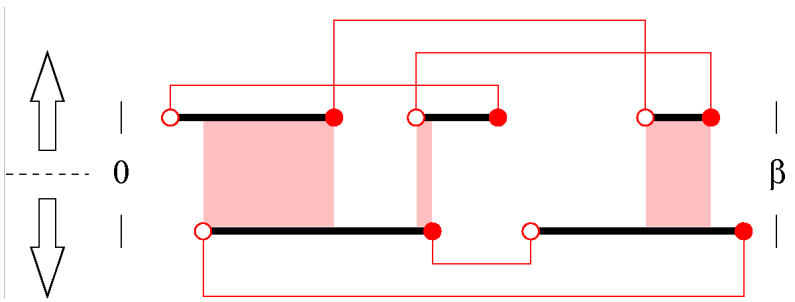

CT-QMC methods: smaller matrices

All QMC methods: effort $\propto \Lambda^3$

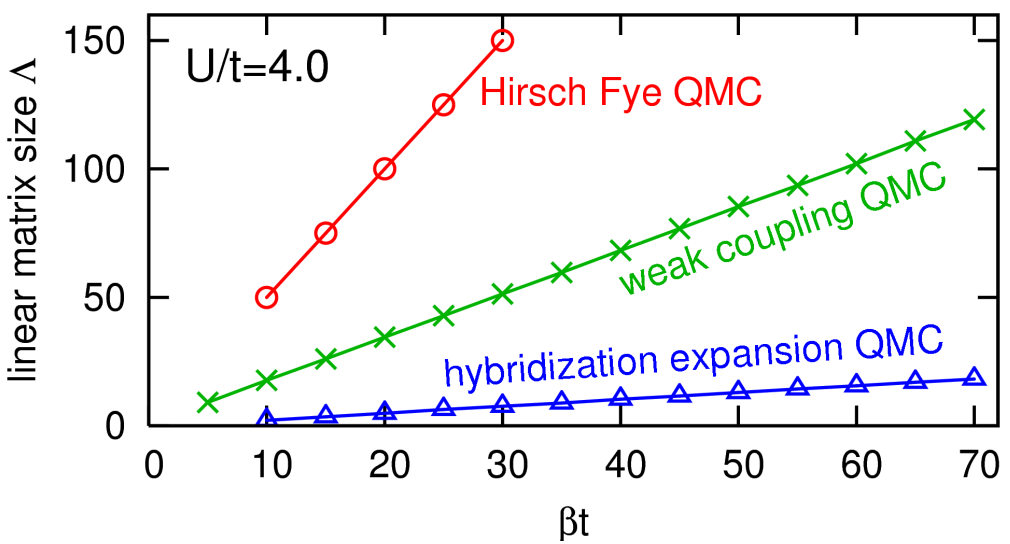

Efficiency of QMC DMFT solvers

New development: continuous-time QMC algorithms

1. weak-coupling expansion

[Rubtsov, Savkin, Lichtenstein, PRB (2005)]

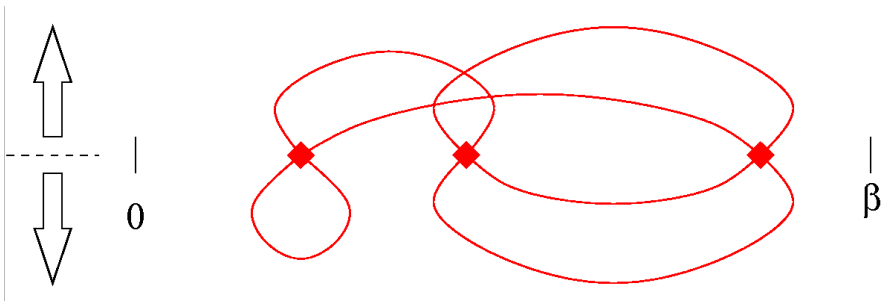

2. hybridization expansion

[Werner et al., PRL (2006)]

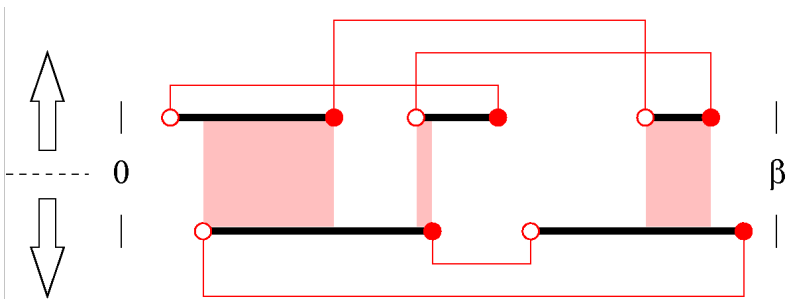

CT-QMC methods: smaller matrices

All QMC methods: effort $\propto \Lambda^3$

Claim [Troyer (2006)]:
"CT-QMC more efficient than HF-QMC by orders of magnitude"

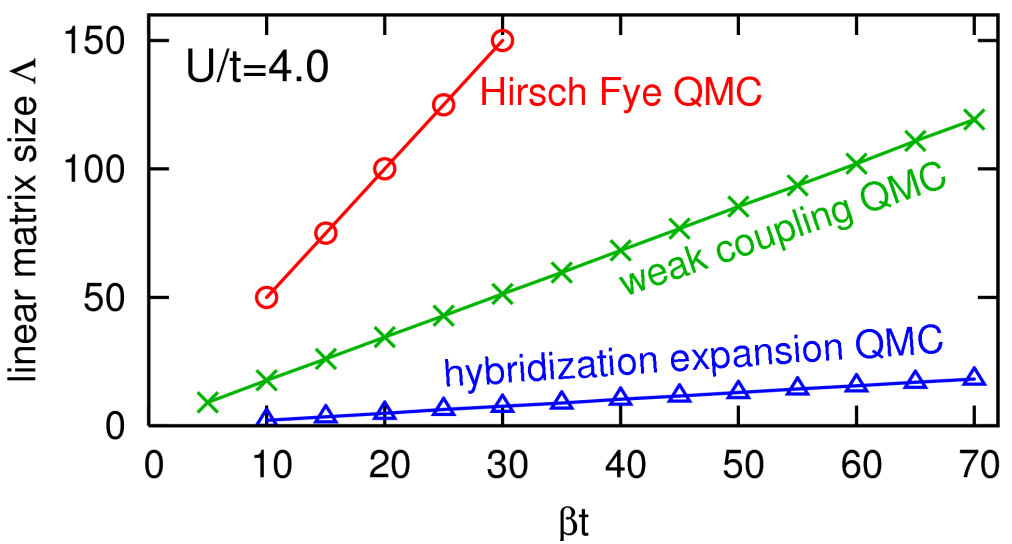

Comparisons at constant CPU time: kinetic energy (at $U = W = 4$)

140 CPU hours on AMD Opteron 244 (serial) / mix of Opterons (parallel)

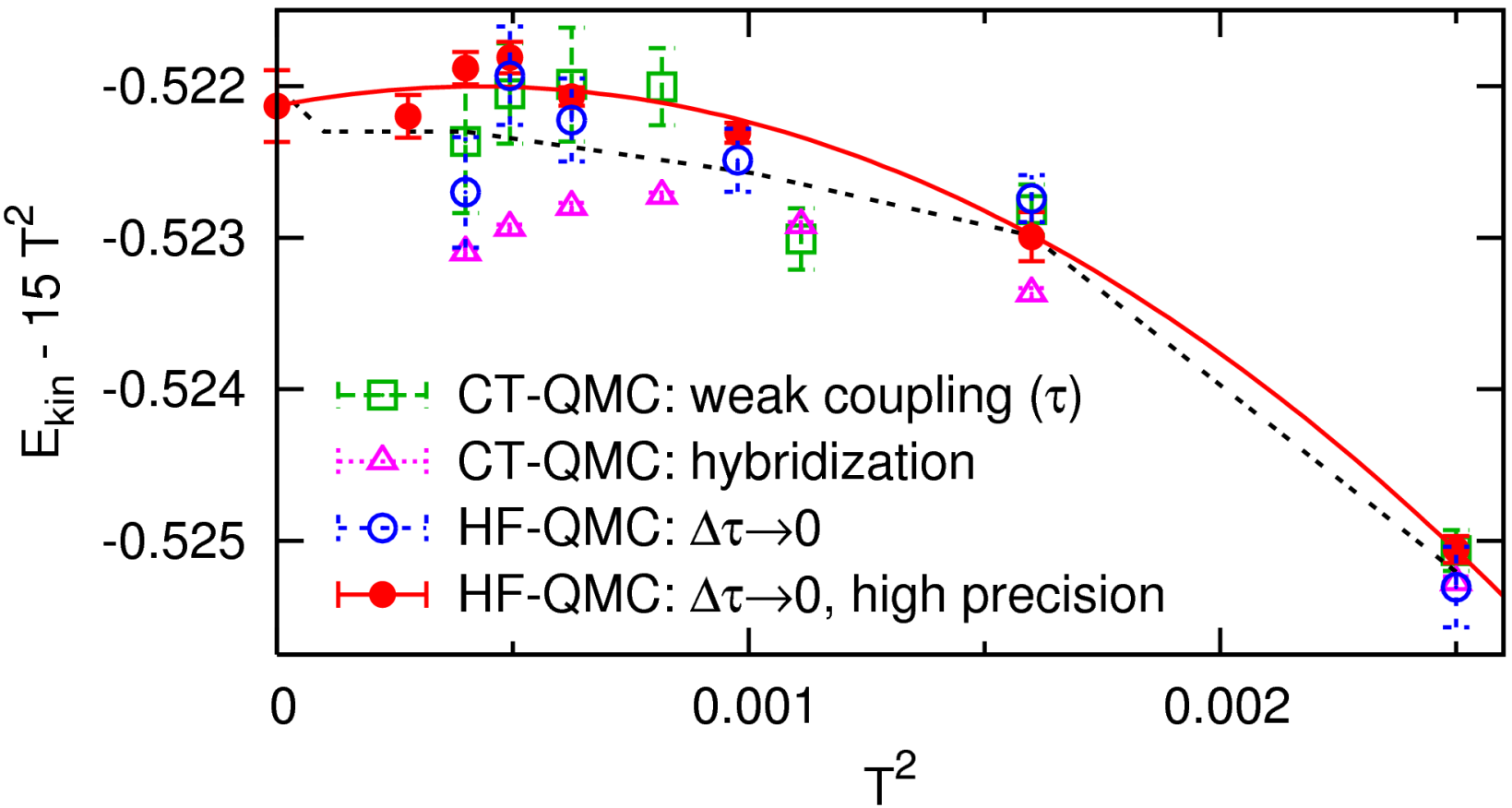

Similar precision for HF-QMC and weak-coupling CT-QMC

Systematic errors in hybridization CT-QMC data! [NB, PRB **76**, 205120 (2007)]

Comparison for total energy (at $U = W = 4$)

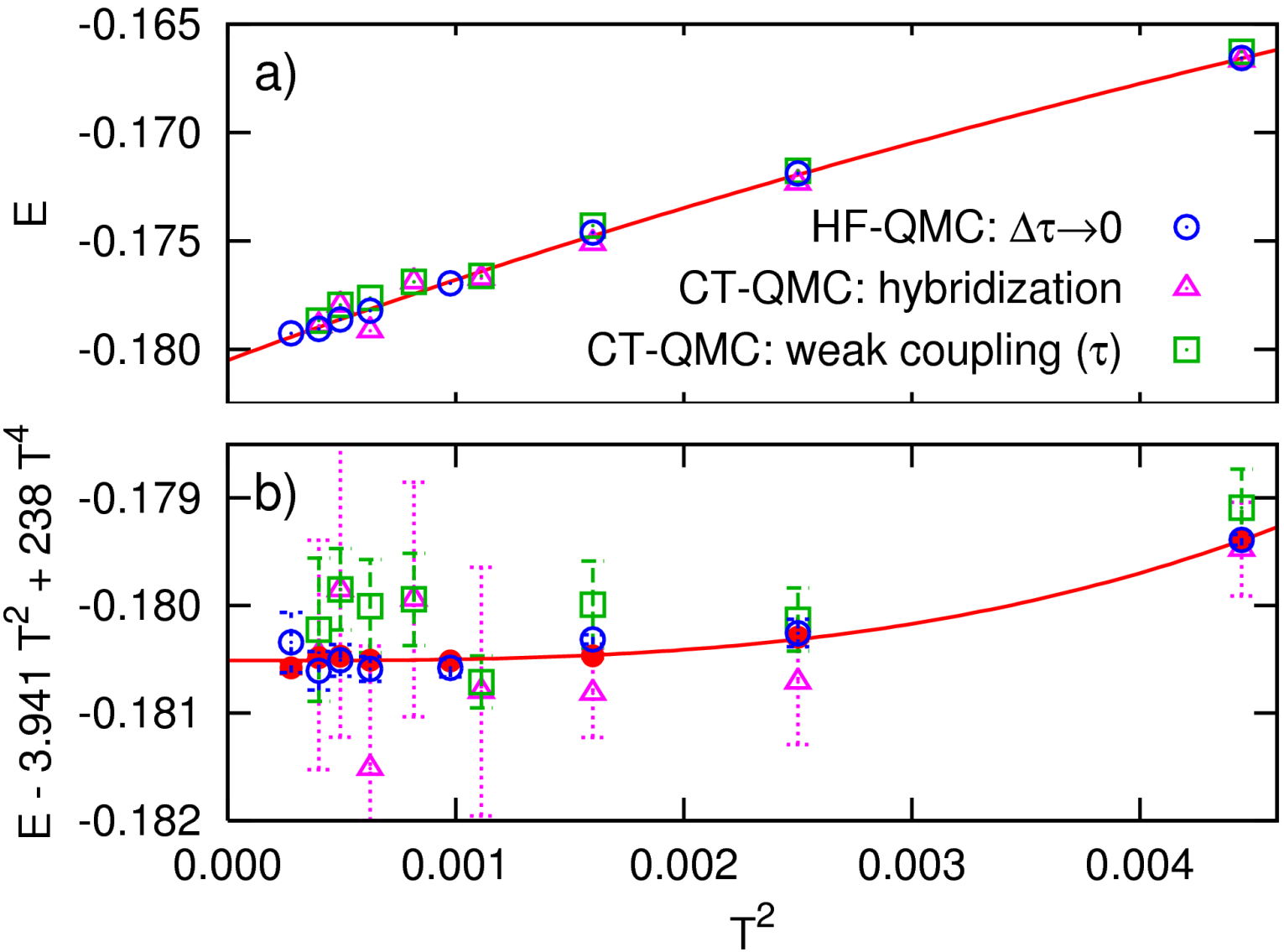

HF-QMC more efficient (higher precision at same cost) [NB, PRB **76**, 205120 (2007)]

Unbiased Green functions and spectra from HF-QMC

State of the art: analytic continuation (using MEM) of imaginary-time Green function at fixed finite (often large) $\Delta\tau \rightsquigarrow$ bias

Unbiased Green functions and spectra from HF-QMC

State of the art: analytic continuation (using MEM) of imaginary-time Green function at fixed finite (often large) $\Delta\tau$ $\rightsquigarrow$ bias

Reason: no obvious extrapolation scheme for $G(\tau)$

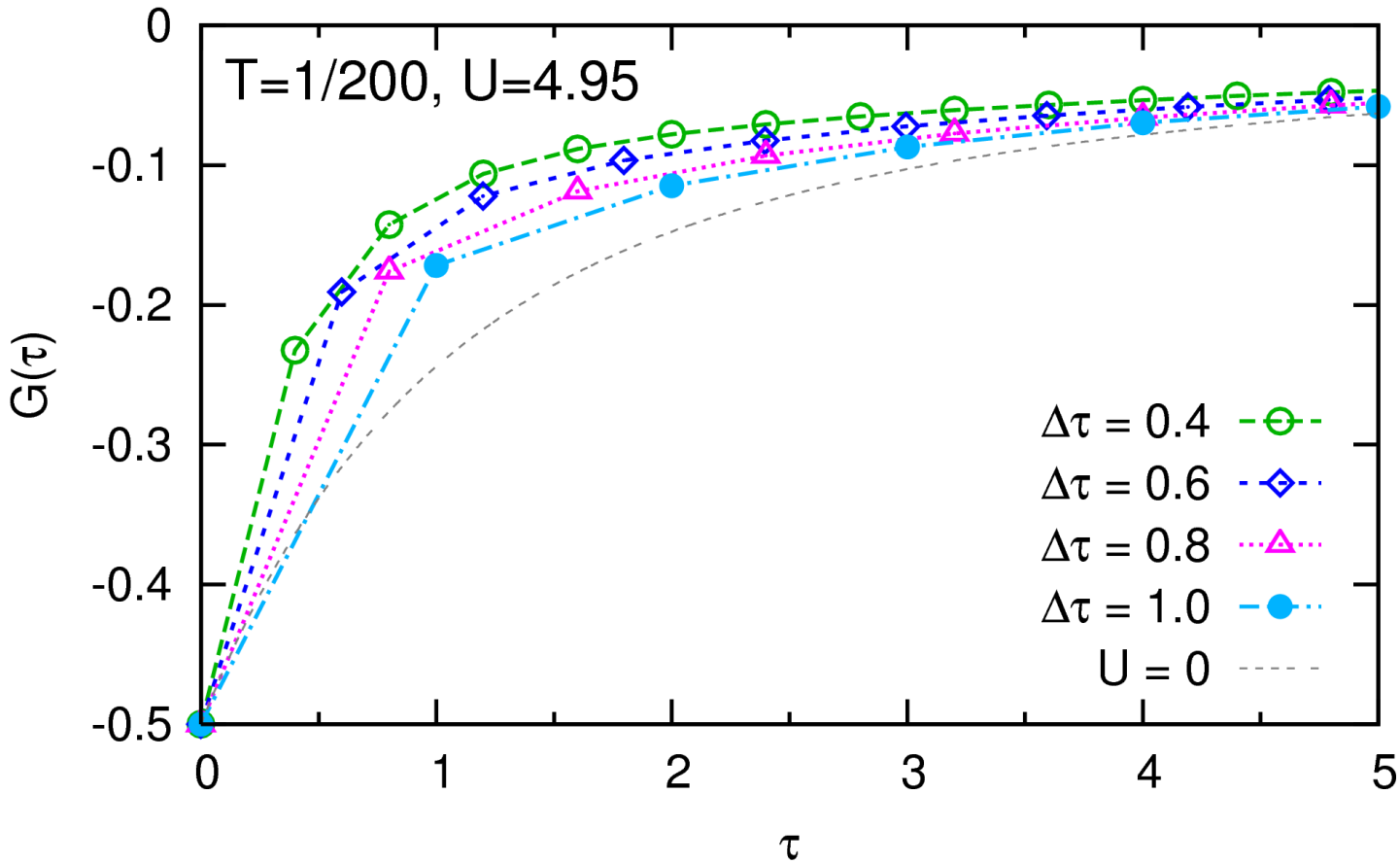

Low temperature ("beyond HF-QMC"): large $\Delta\tau$ $\rightsquigarrow$ large biases [NB, arXiv:0712.1290]

Unbiased Green functions and spectra from HF-QMC

State of the art: analytic continuation (using MEM) of imaginary-time Green function at fixed finite (often large) $\Delta\tau \rightsquigarrow$ bias

Reason: no obvious extrapolation scheme for $G(\tau)$

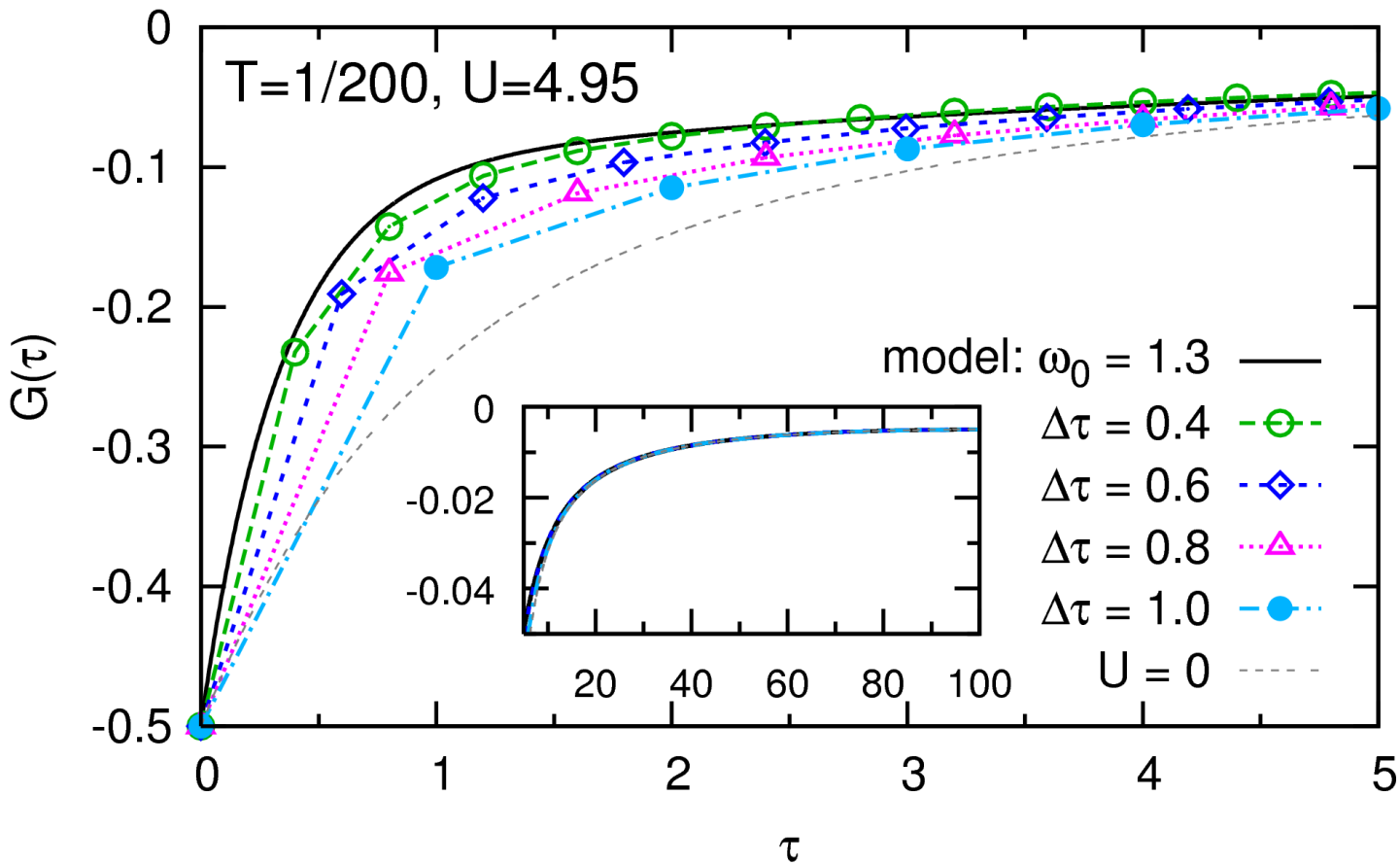

Low temperature ("beyond HF-QMC"): large $\Delta\tau \rightsquigarrow$ large biases [NB, arXiv:0712.1290]

New Green function extrapolation scheme

1. average $G(\tau)$ over parallel runs for same impurity model

2. average $\log[-G(\tau)]$ over iterations ($\sim$ geometric average for $G(\tau)$)

3. interpolate via difference Green function $G_{\mathrm{QMC}}(\tau) - G_{\mathrm{model}}(\tau) \rightsquigarrow$ common grid

New Green function extrapolation scheme

1. average $G(\tau)$ over parallel runs for same impurity model
2. average $\log[-G(\tau)]$ over iterations ($\sim$ geometric average for $G(\tau)$)
3. interpolate via difference Green function $G_{\mathrm{QMC}}(\tau) - G_{\mathrm{model}}(\tau) \rightsquigarrow$ common grid
4. extrapolate $\log[-G(\tau)]$ using cubic least-squares fits, overweighting low $\Delta\tau$

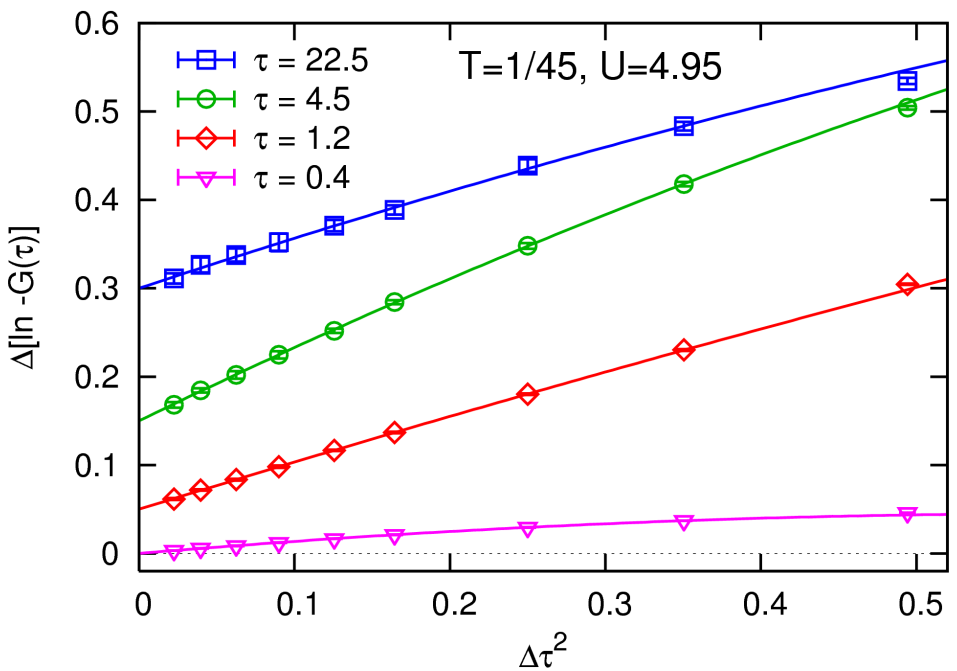

Result: unbiased, numerically exact Green function

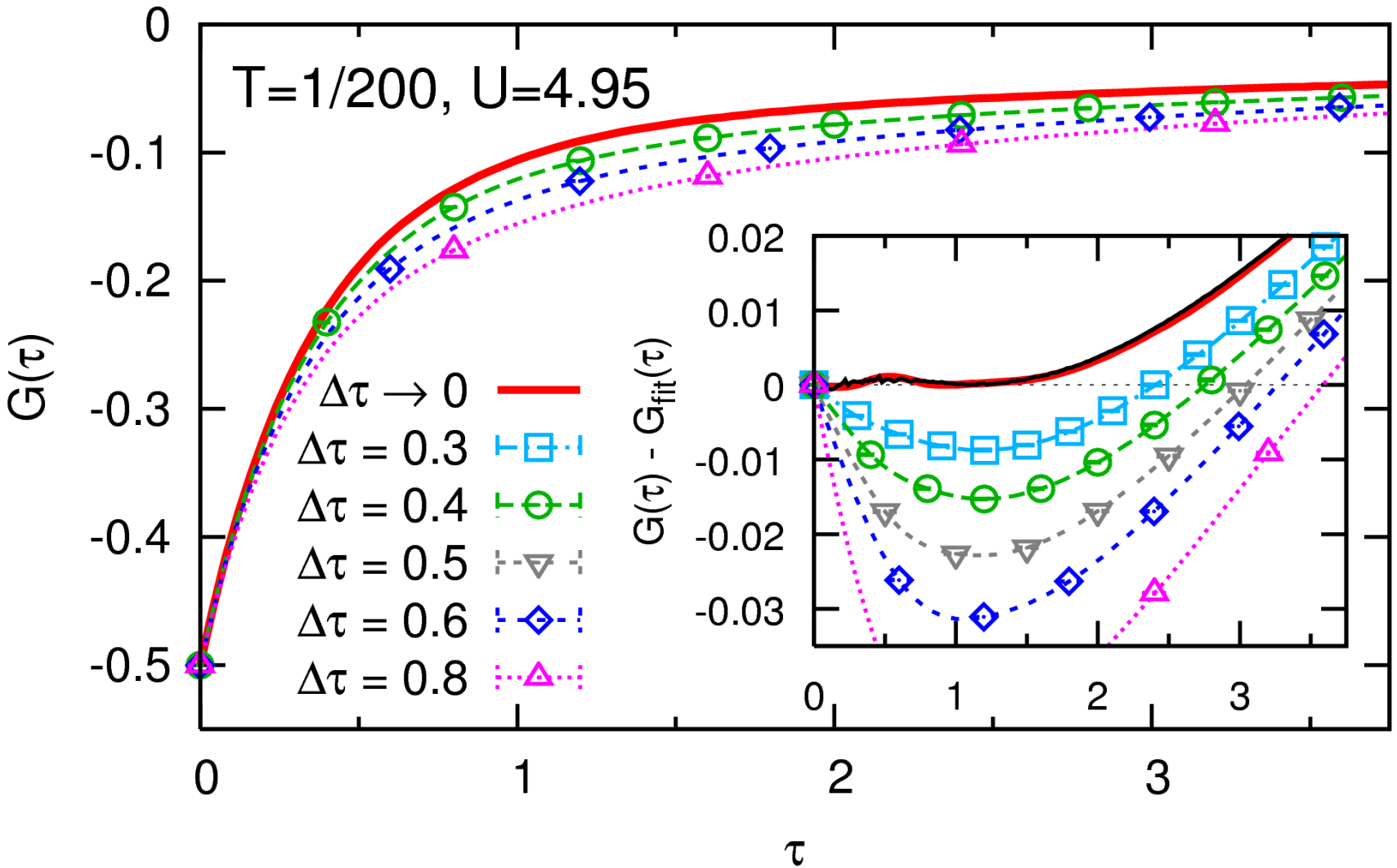

[NB, arXiv:0712.1290]

Excellent agreement with hybridization expansion CT-QMC [Werner et al., PRL (2006)]

2nd and 1st order derivatives of Green function

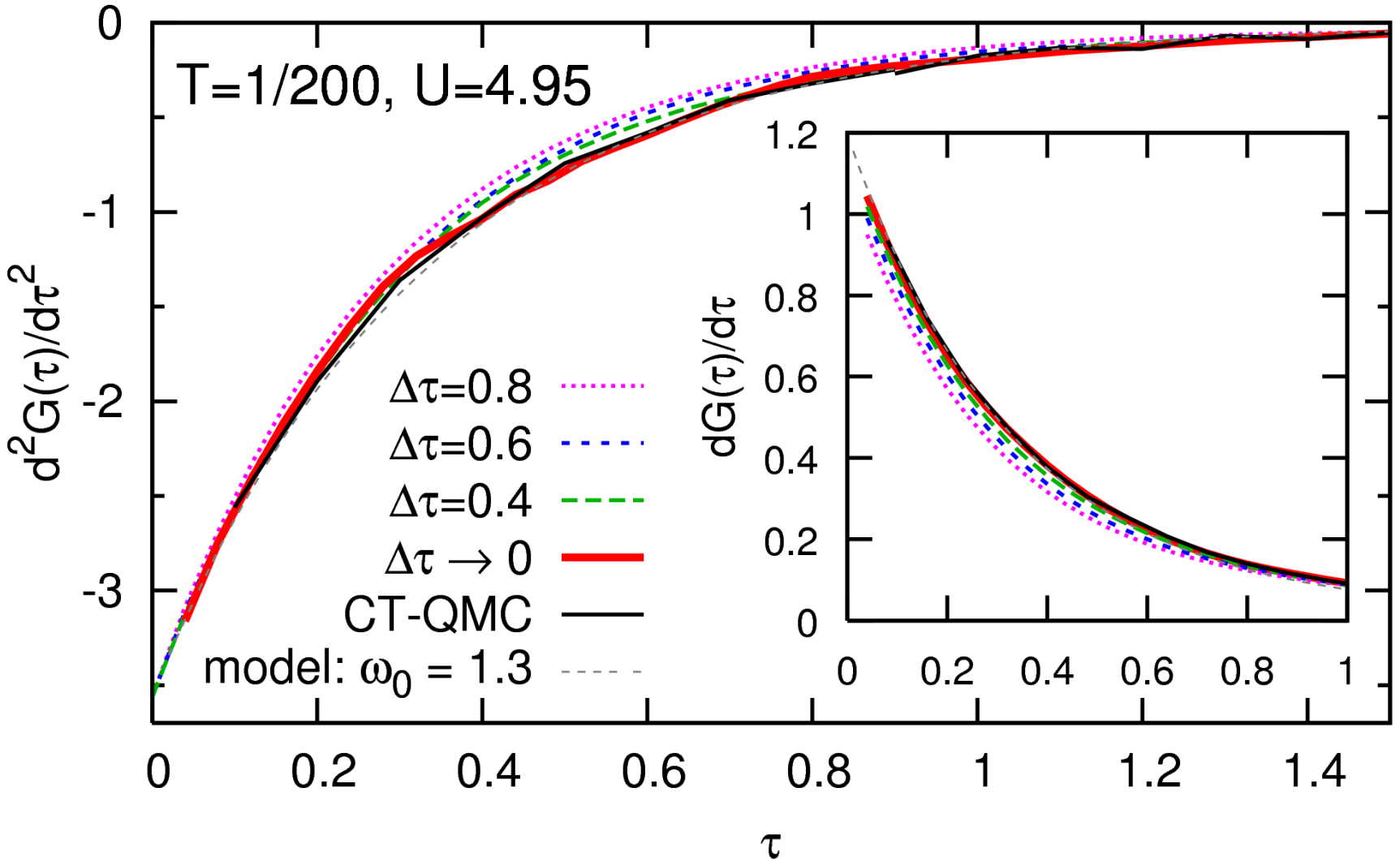

Exact asymptotics $\left.\frac{d^2G(\tau)}{d\tau^2}\right|_{\tau=0+} = \frac{1}{2} + \frac{U^2}{8}$; $\left.\frac{dG(\tau)}{d\tau}\right|_{\tau=0+}$ nonuniversal

Why average and extrapolation on logarithmic scale?

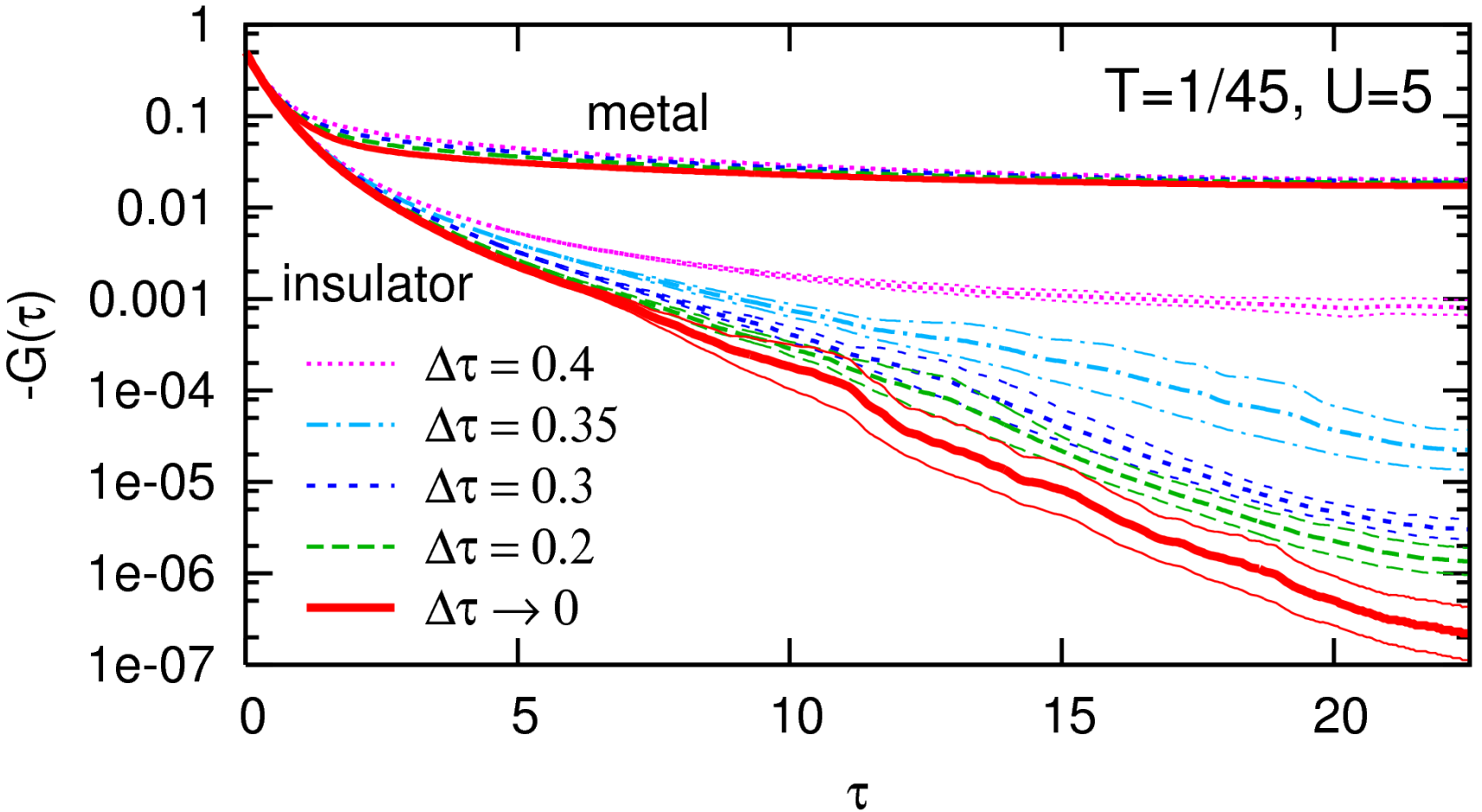

Difference metal–insulator and $\Delta\tau$ dependence involves orders of magnitude!

Even maximum statistical/iteration errors nearly order of magnitude

Low-τ resolution limited by $\Delta\tau$? No!

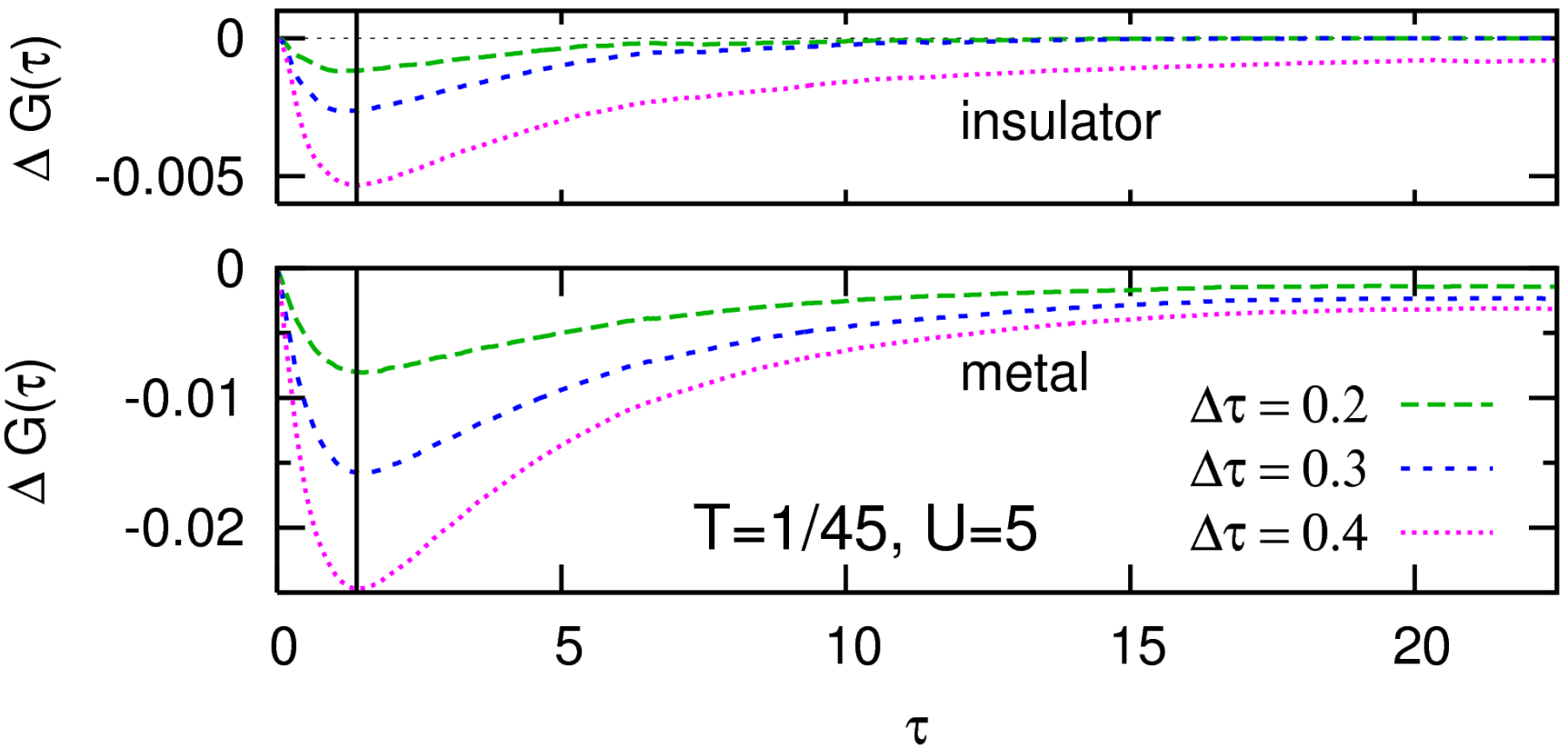

Uniform $\Delta\tau$ dependence, position of max error independent of $\Delta\tau$ and phase!

Analytic continuation using Padé approximant for self-energy

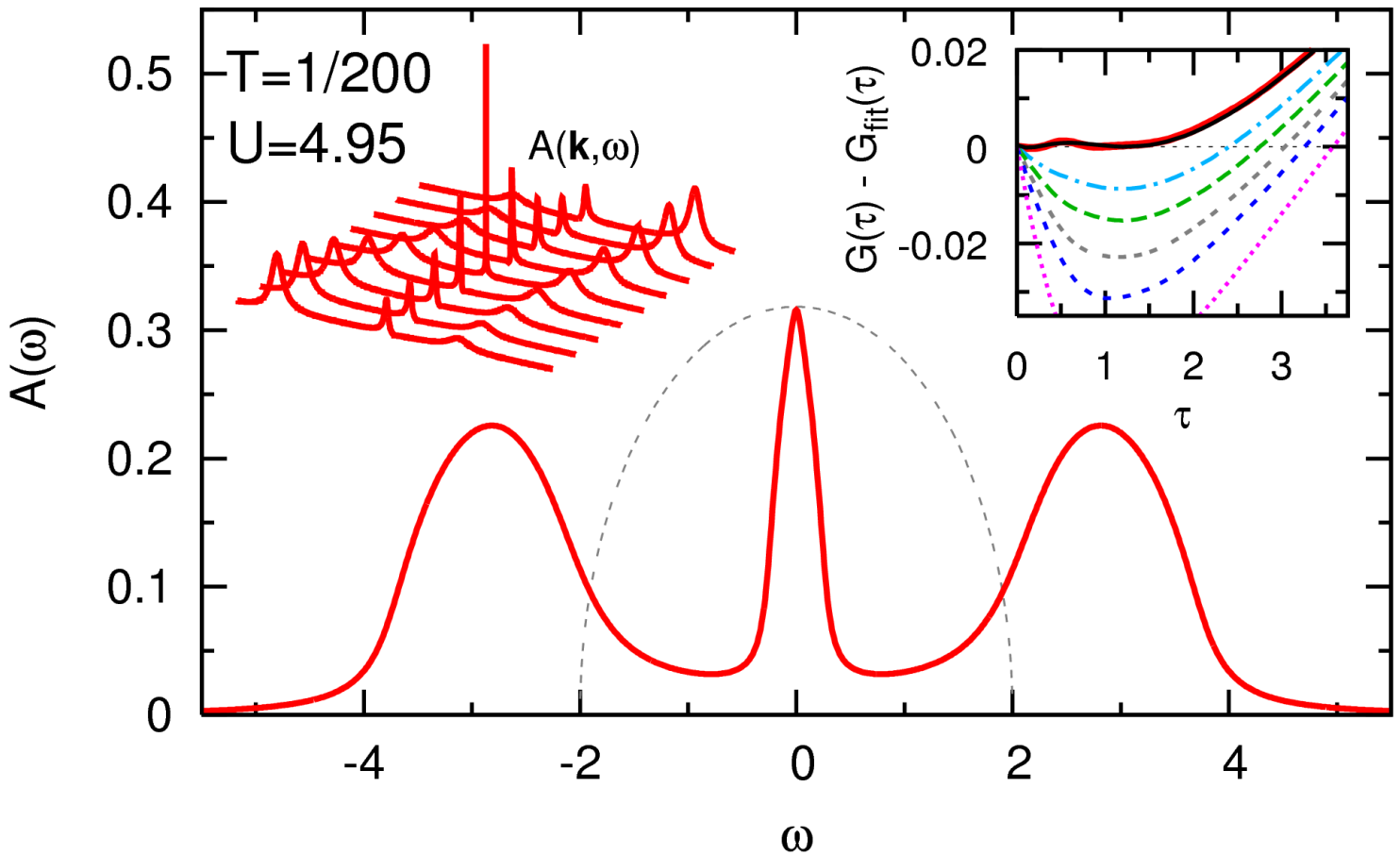

First spectra without discretization error from HF-QMC, at ultra-low T

Method directly applicable, e.g., to LDA+DMFT calculations [NB, arXiv:0712.1290]

Multigrid Hirsch-Fye quantum Monte Carlo algorithm

State of the art: (a) conventional HF-QMC

(b) *a posteriori* extrapolation of selected observables

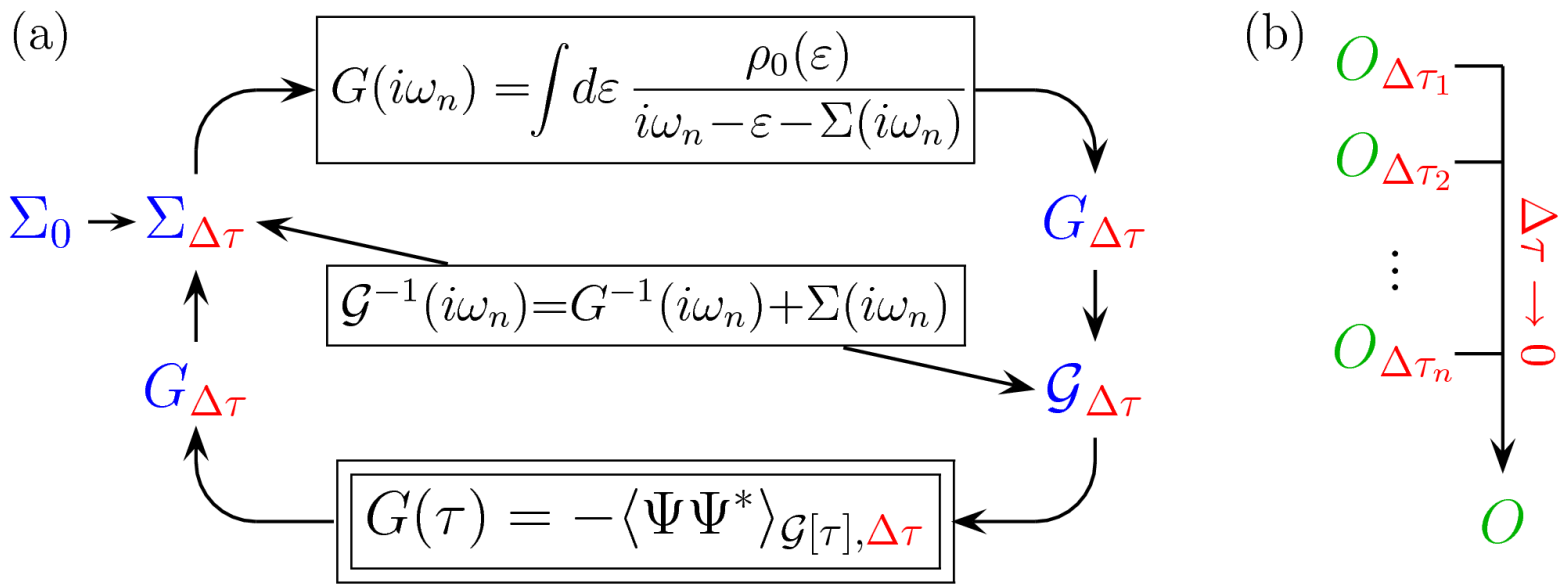

Multigrid Hirsch-Fye quantum Monte Carlo algorithm

State of the art: (a) conventional HF-QMC

(b) *a posteriori* extrapolation of selected observables

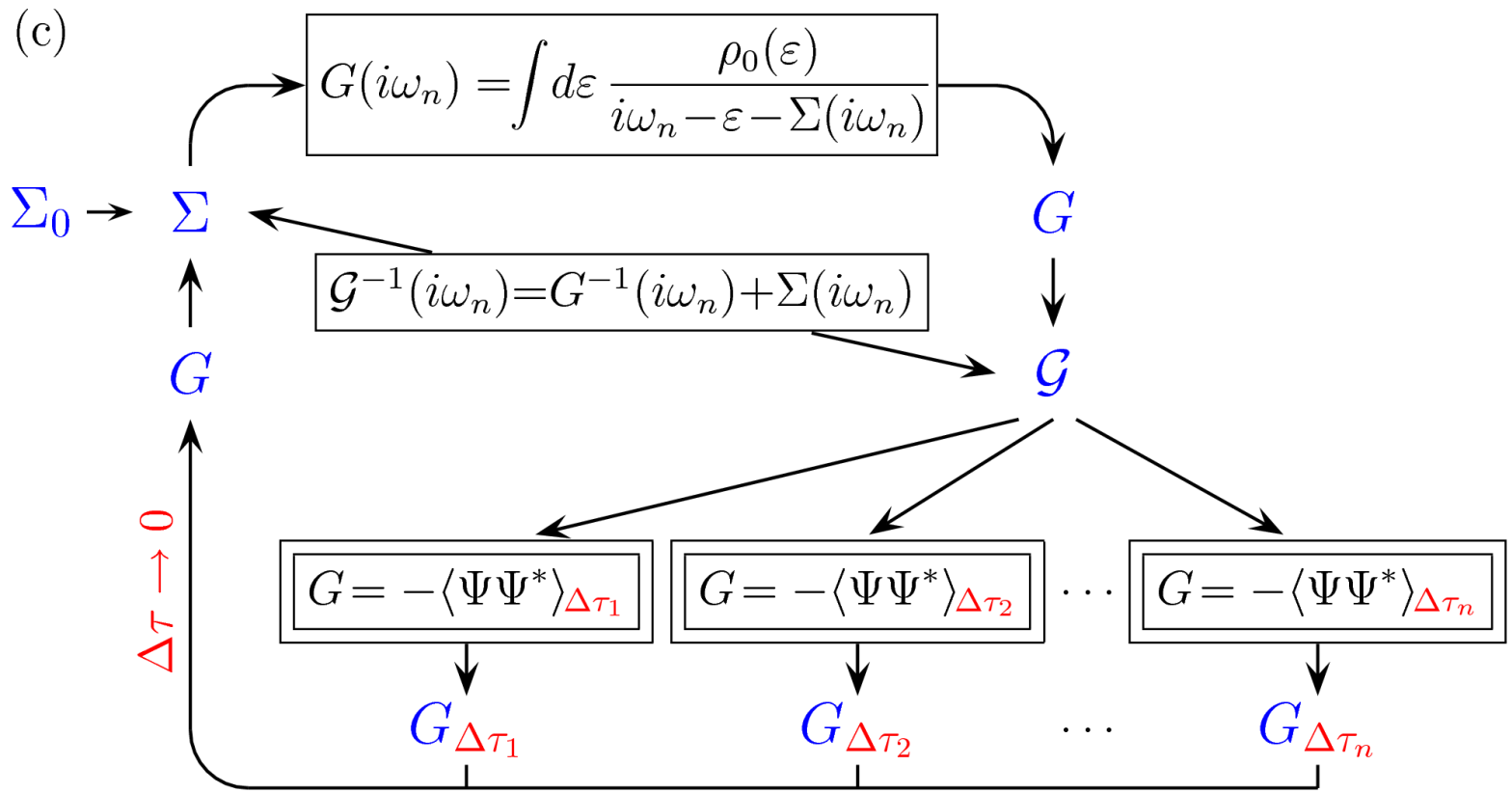

(c) Multigrid HF-QMC: internal elimination of Trotter error

$\rightsquigarrow$ quasi continuous time algorithm [NB, arXiv:0801.1222]

Schematic comparison via generalized Ginzburg-Landau functionals

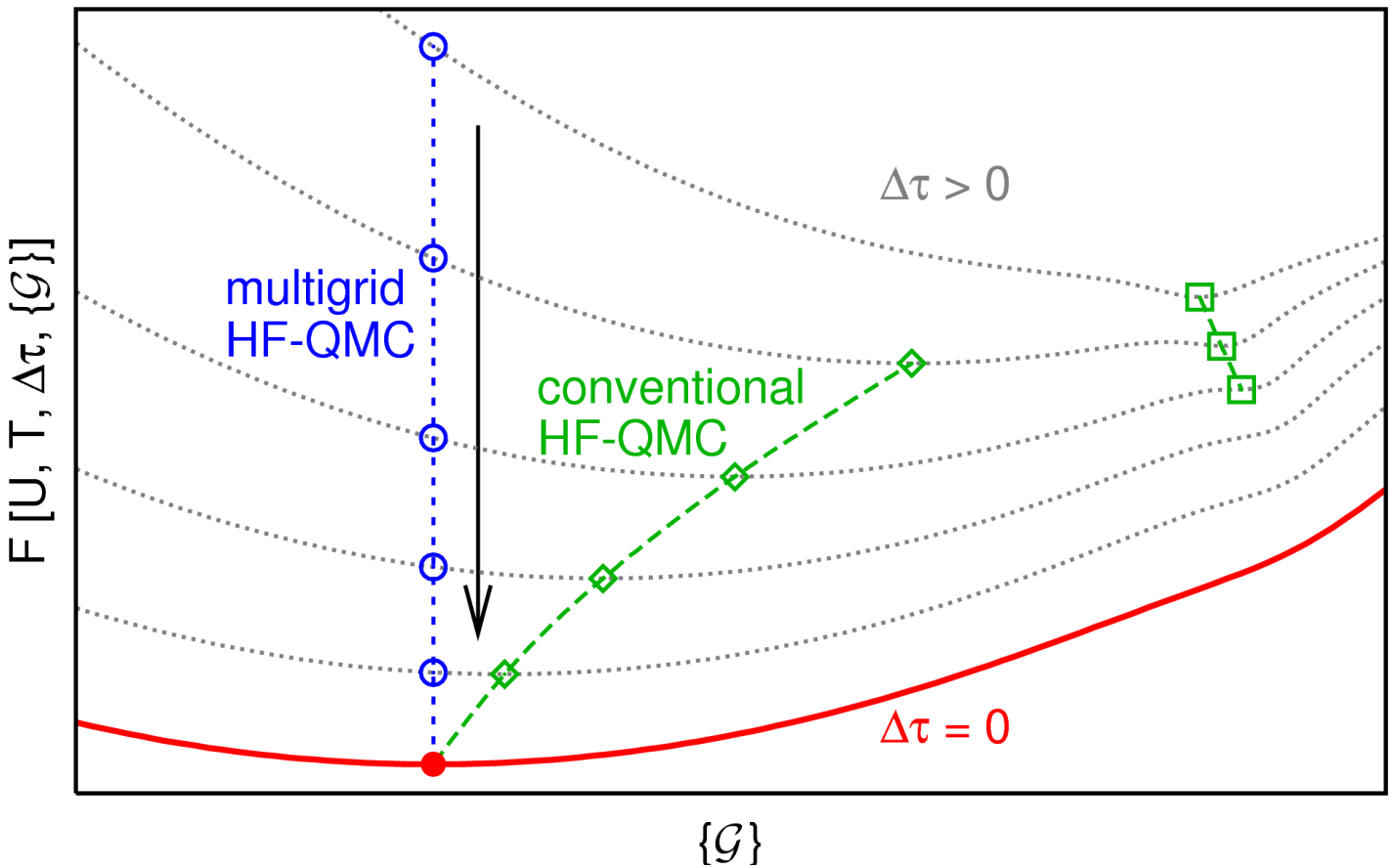

conventional Hirsch-Fye QMC: DMFT fixed point shifts with $\Delta\tau$

multigrid Hirsch-Fye QMC: DMFT iteration towards exact fixed point

Comparison: double occupancy $D = \langle n_{i\uparrow} n_{i\downarrow} \rangle$ near Mott transition

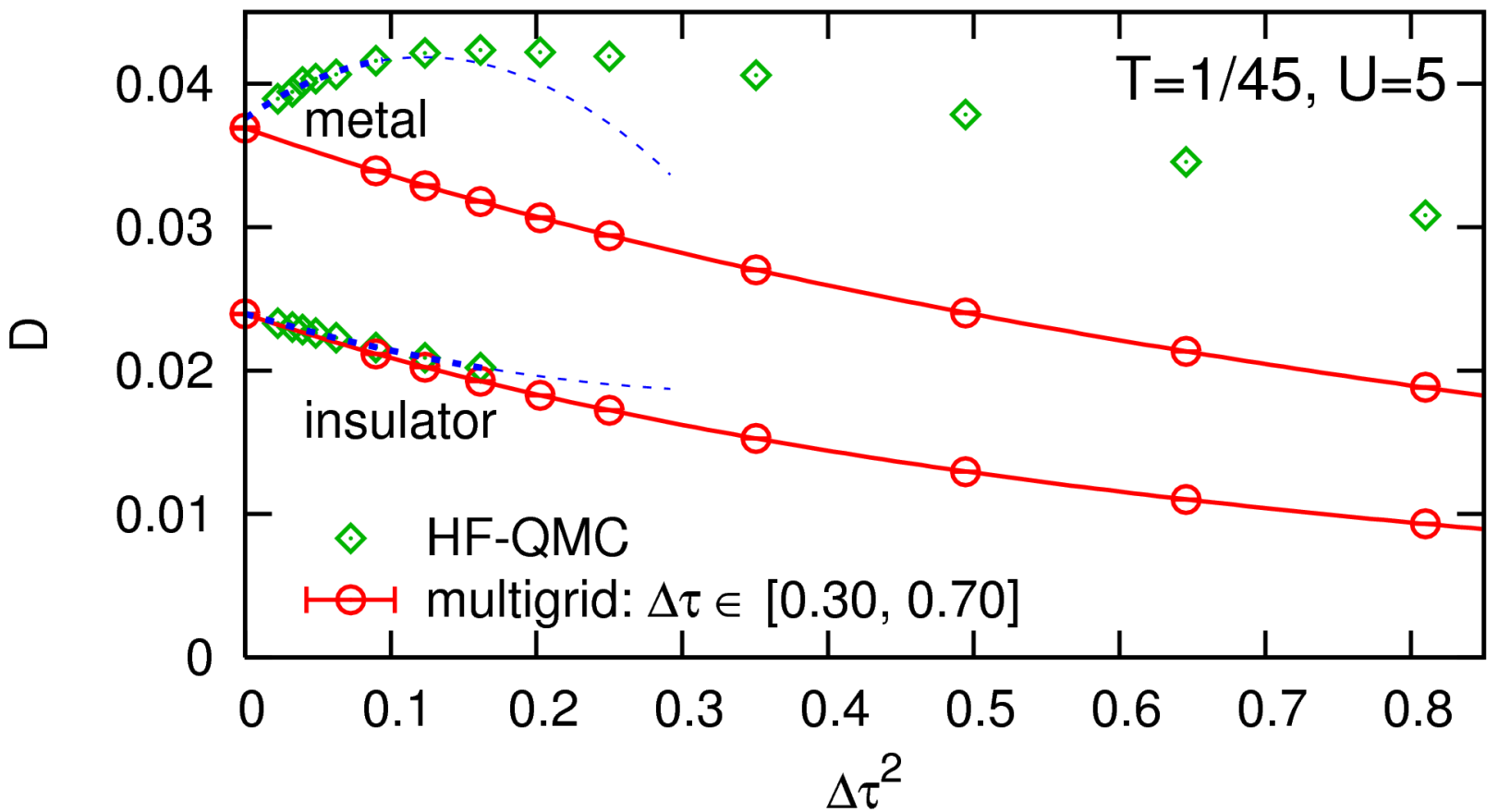

Conventional HF-QMC: no insulating solution for $\Delta\tau \gtrsim 0.4$

very irregular $\Delta\tau$ dependence beyond $\Delta\tau \approx 0.3$

Multigrid HF-QMC: vastly larger useful range of $\Delta\tau$

Systematic study: impact of grid range (on double occupancy)

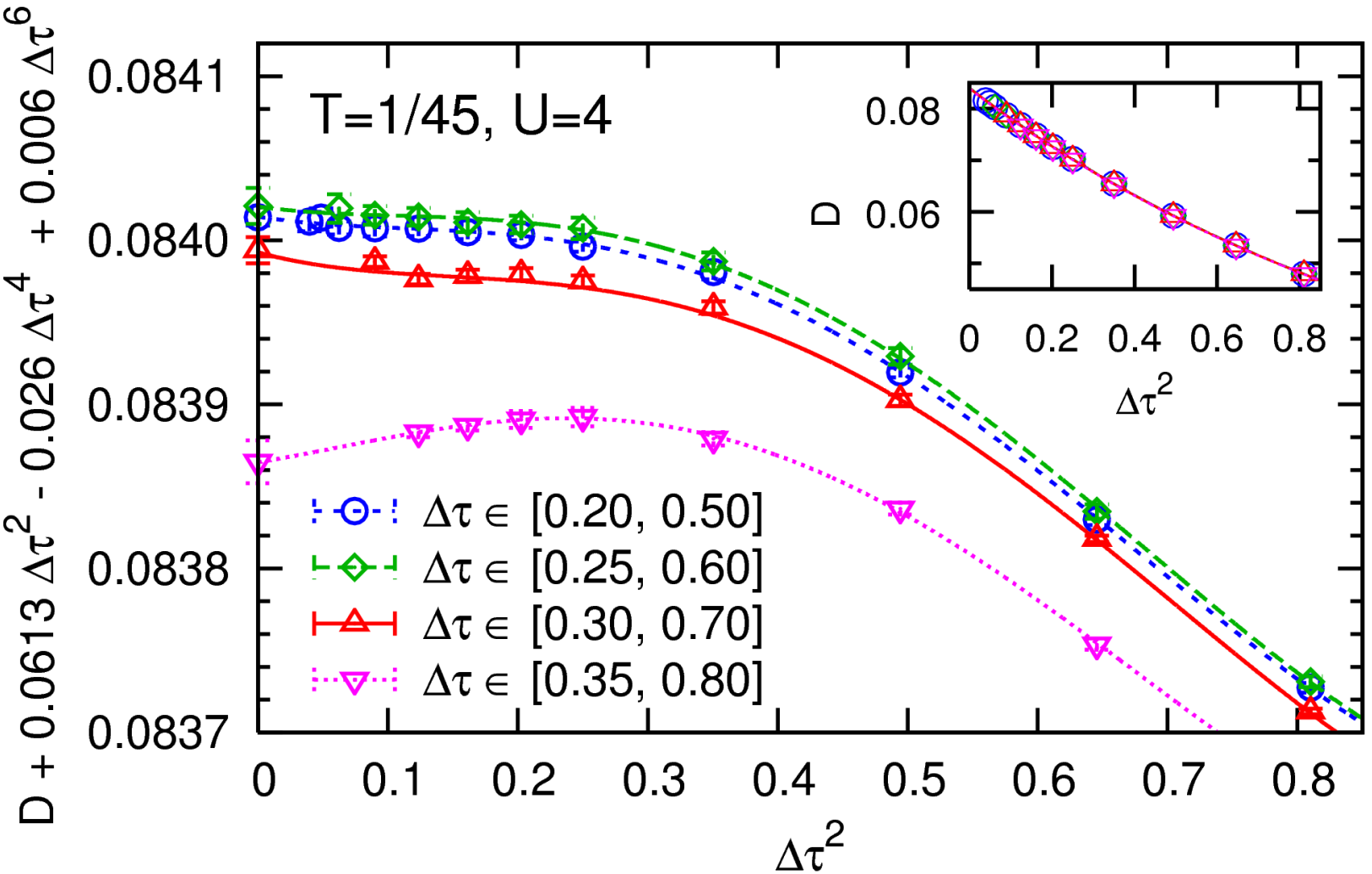

Multigrid HF-QMC usually "numerically exact" for $\tau_{\text{min}} \lesssim 0.3$

Efficiency: potential energy $E_{\mathrm{pot}} = UD$

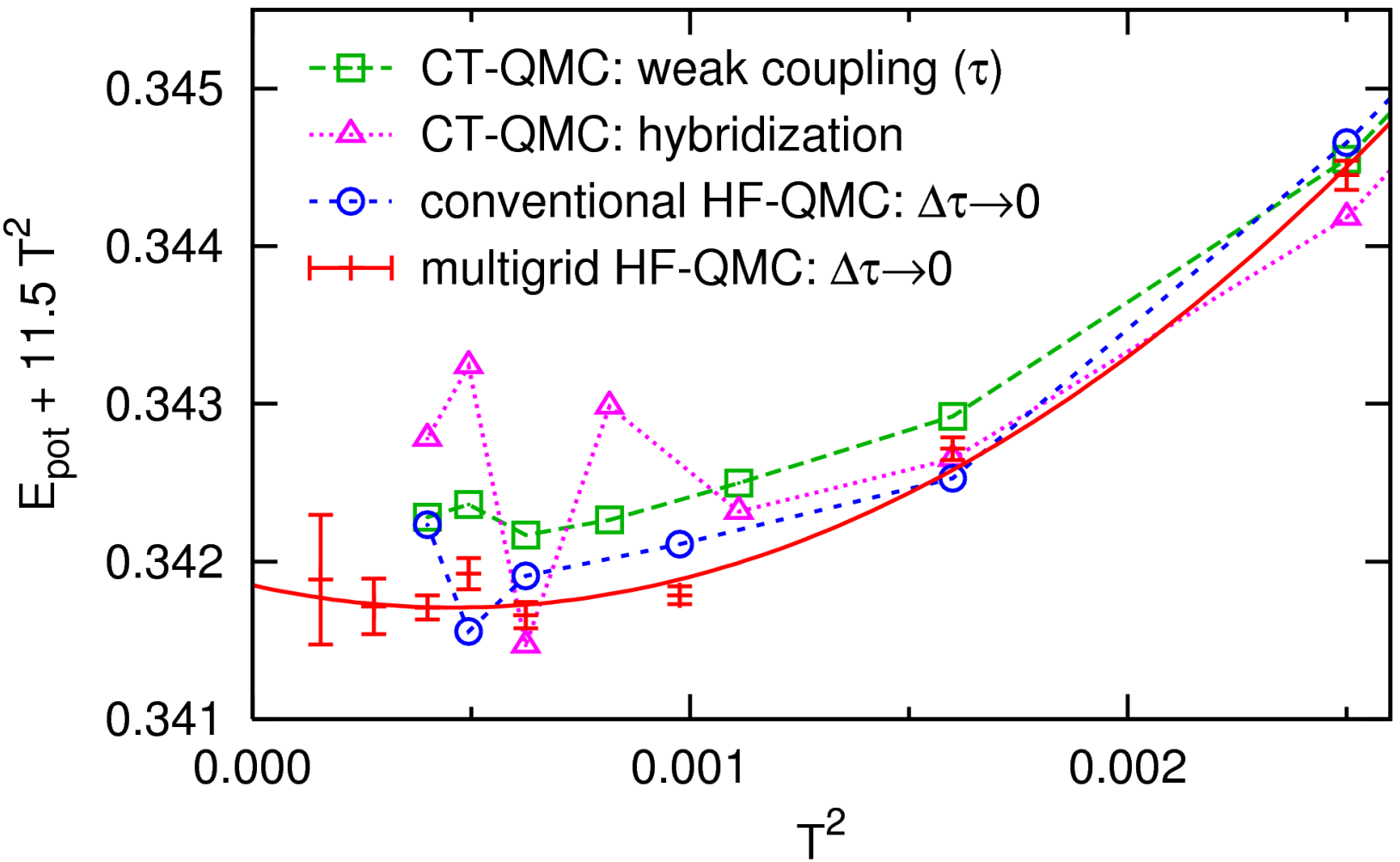

No more "difficult observables" for multigrid HF-QMC

Higher precision than CT-QMC methods at same effort

Spectral weight transfer at the Mott transition

Question: how does the Mott metal-insulator transition take place, precisely?

Spectral weight transfer at the Mott transition

Question: how does the Mott metal-insulator transition take place, precisely?

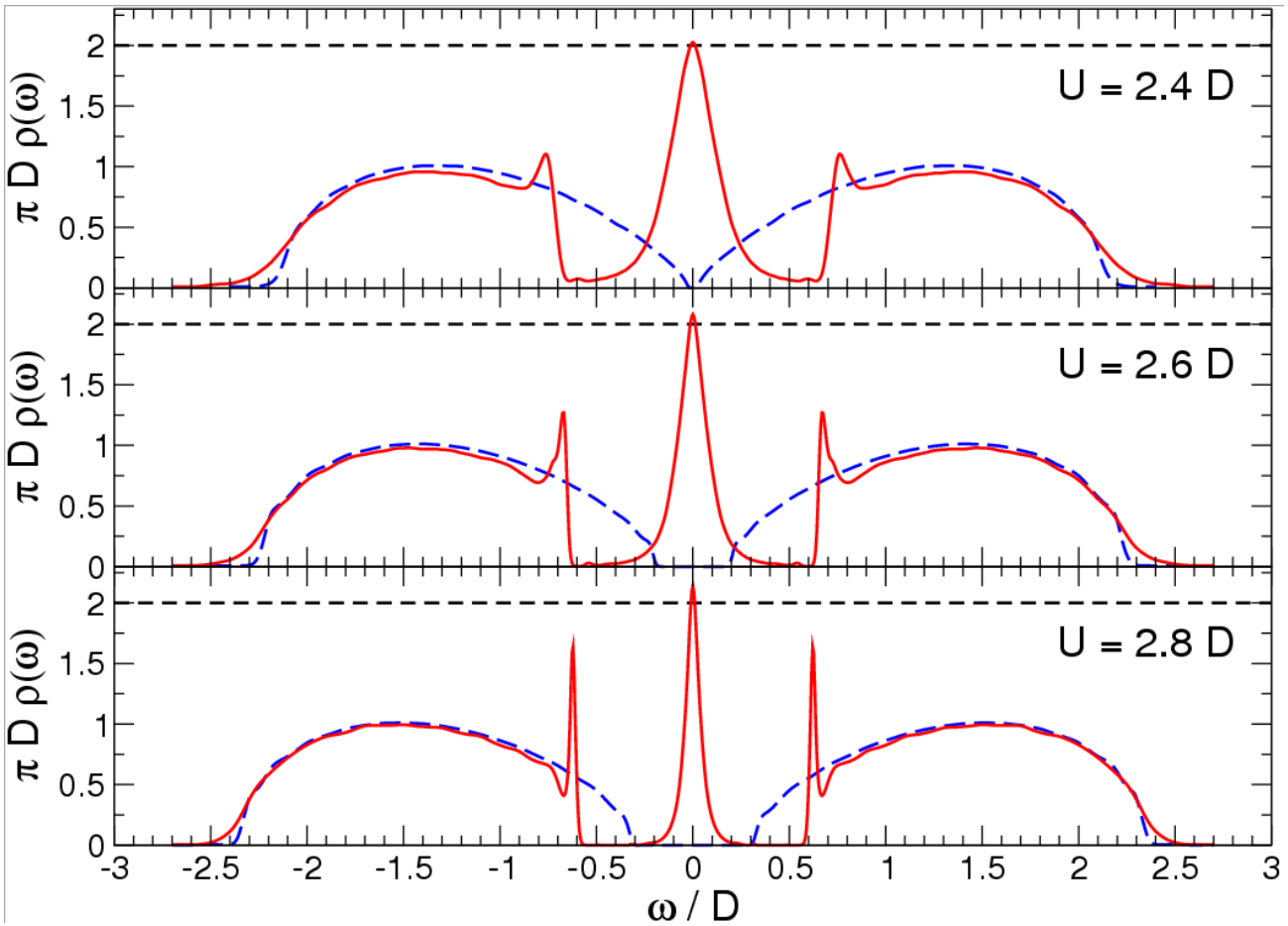

Dynamical DMRG $\rightsquigarrow$ Hubbard band subpeaks in metallic phase (at $T = 0$)

[Karski, Raas, Uhrig, PRB (2005)]

Spectral weight transfer at the Mott transition

Question: how does the Mott metal-insulator transition take place, precisely?

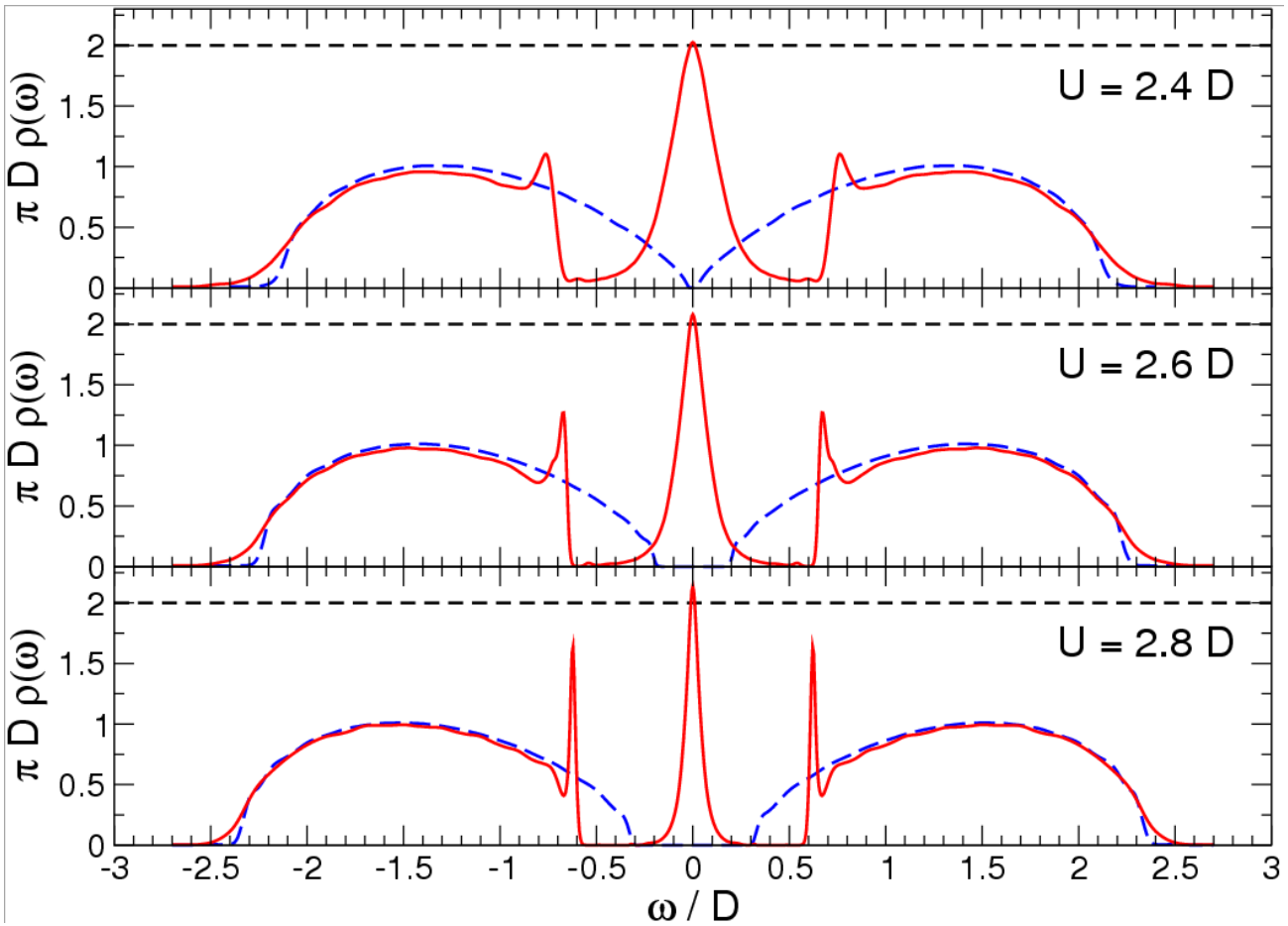

Dynamical DMRG $\rightsquigarrow$ Hubbard band subpeaks in metallic phase (at $T = 0$)

[Karski, Raas, Uhrig, PRB (2005)]

Verify using multigrid HF-QMC. . .

Analysis via difference of spectral functions (symmetric in ω) at $U = 5.2$

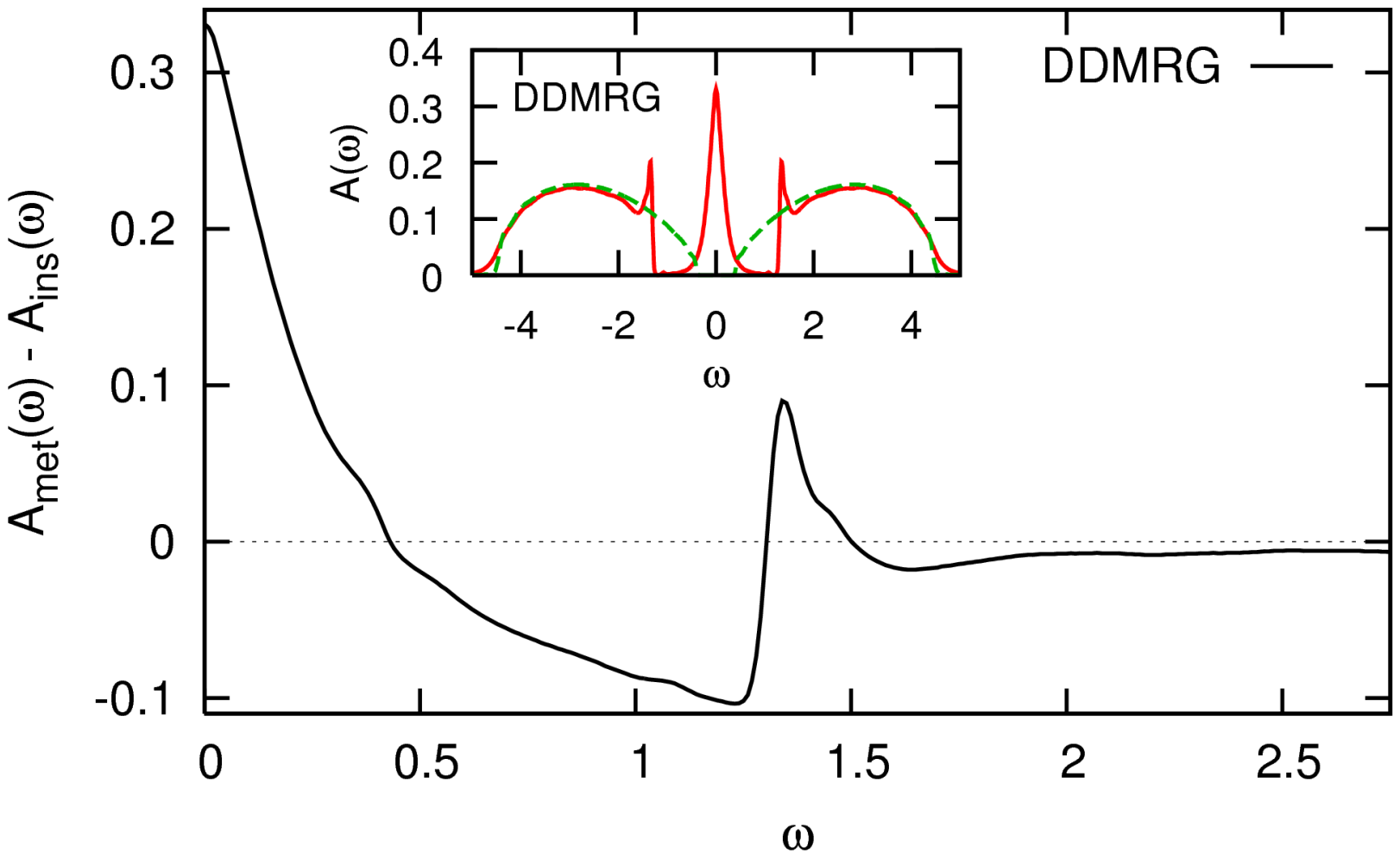

Problems for QMC: (i) analytic continuation of QMC data ill-conditioned

(ii) no $T \longrightarrow 0$ extrapolation of spectra

Difference Green functions in imaginary time

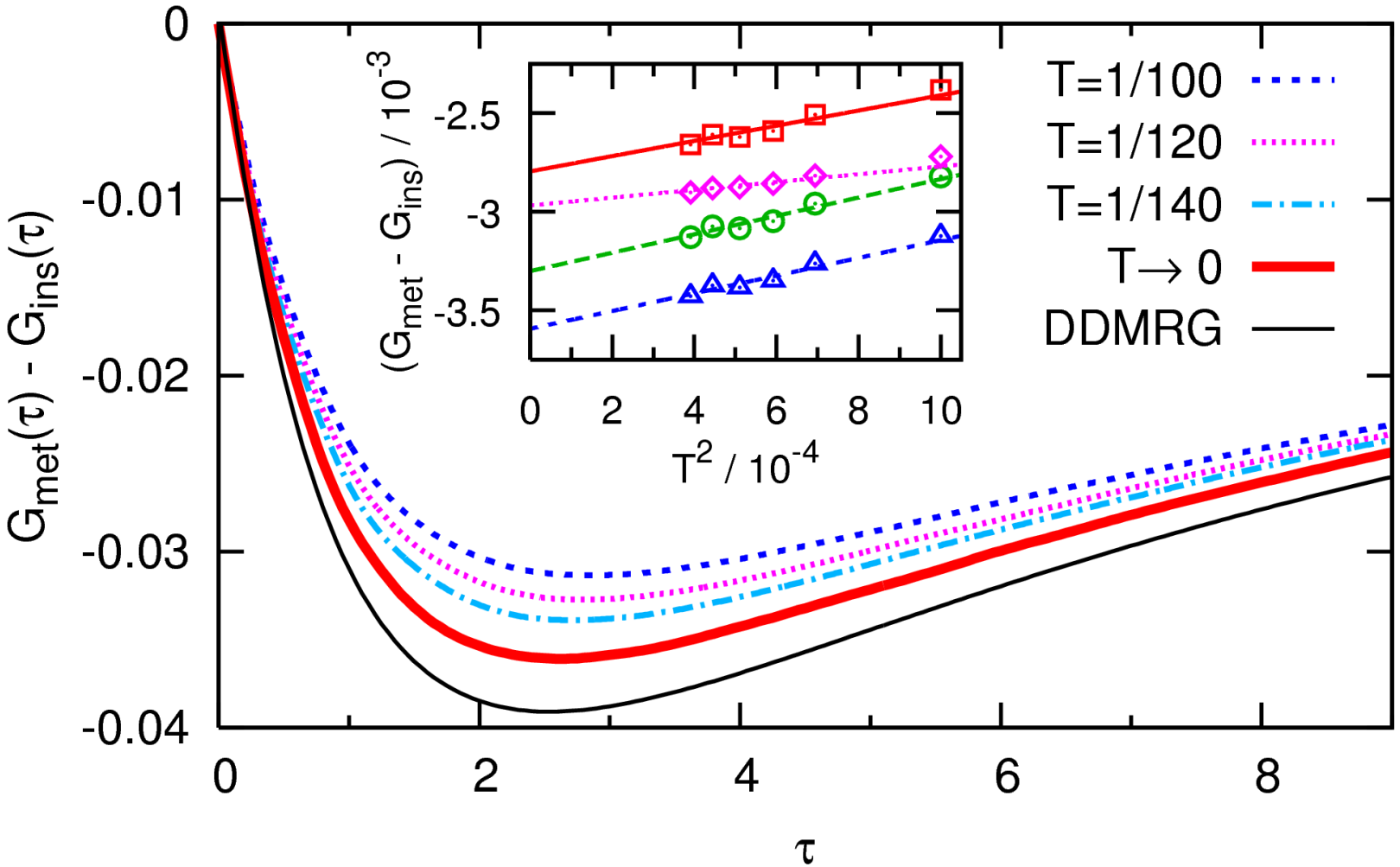

Multigrid HF-QMC data precise within linewidths [NB, arXiv:0801.1222]

DDMRG overestimates spectral weight transfer at $U = 5.2$ by about 10%!

Difference spectra

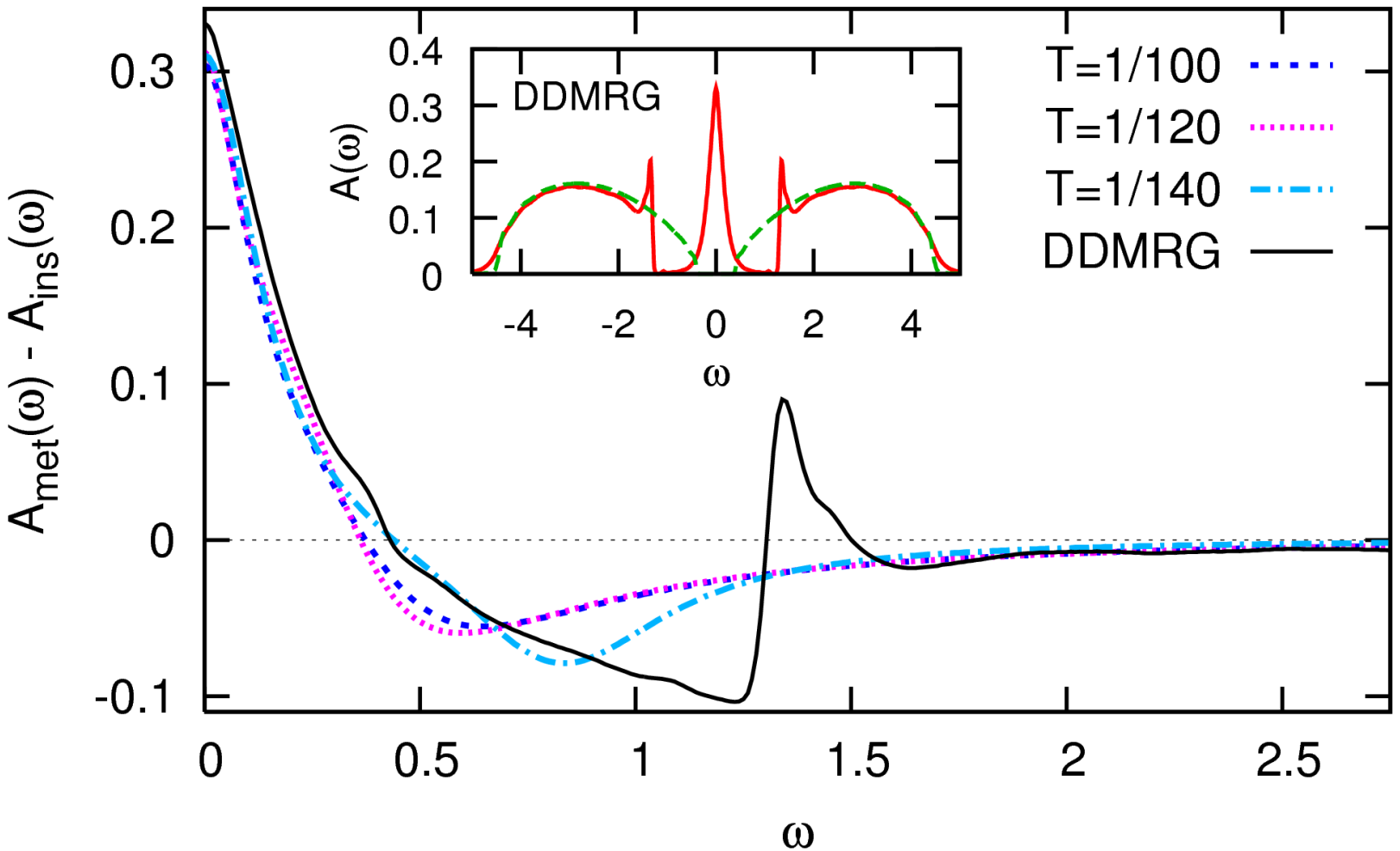

Similarities, but no indication for feature at $\omega = 1.3$ in QMC data

QMC spectral data via Padé interpolation, may be overly smooth [NB, arXiv:0801.1222]

Thermal breakdown of a Fermi liquid

Fermi liquid theory:	linear specific heat	$c_V = \gamma T$	
	linear entropy	$S = \gamma T$	
	quadratic resistivity	$\rho \propto T^2$	for "low enough" T

When/how do these laws break down?

Thermal breakdown of a Fermi liquid

Fermi liquid theory: linear specific heat $c_V = \gamma T$

linear entropy $S = \gamma T$

quadratic resistivity $\rho \propto T^2$ for "low enough" T

When/how do these laws break down?

Exact diagonalization study (8 sites)

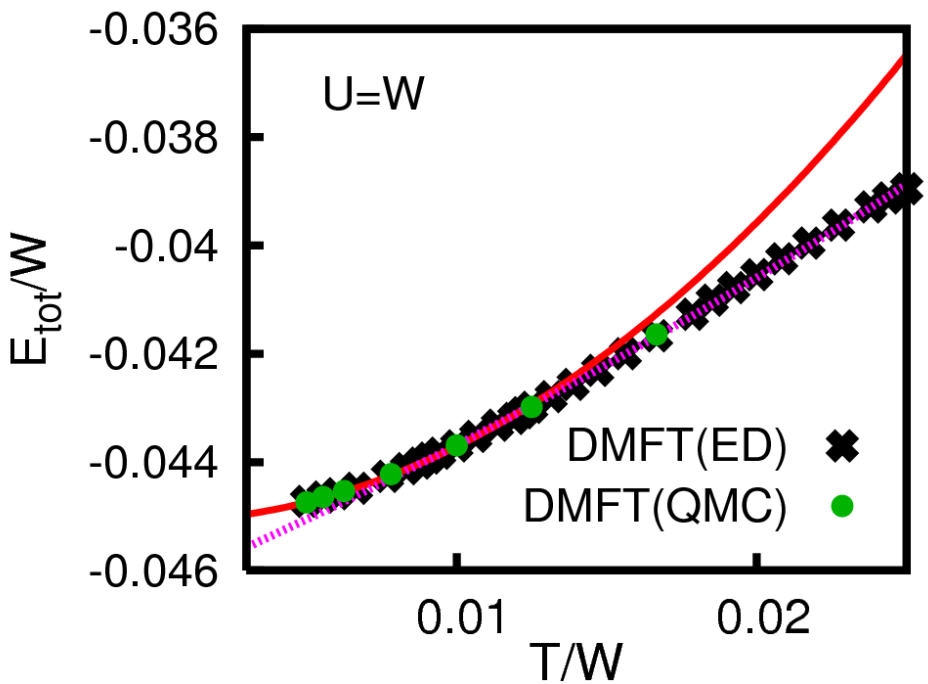

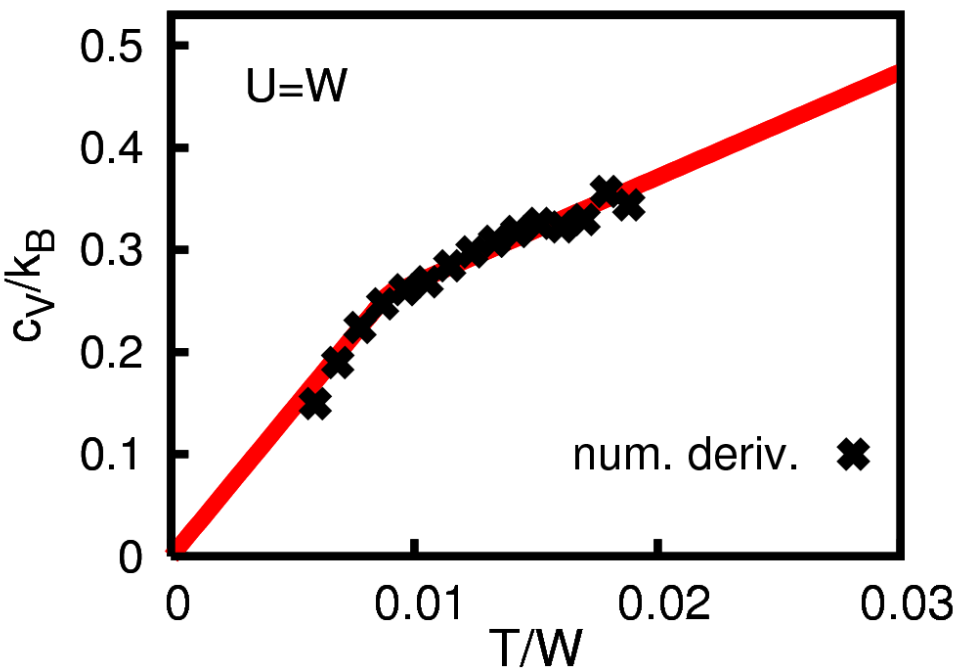

Distinct kink in c_V! [A. Toschi, M. Capone, C. Castellani, K. Held, arXiv:0712.3723]

Theoretical explanation: kink in self-energy $\rightsquigarrow$ kink in c_V

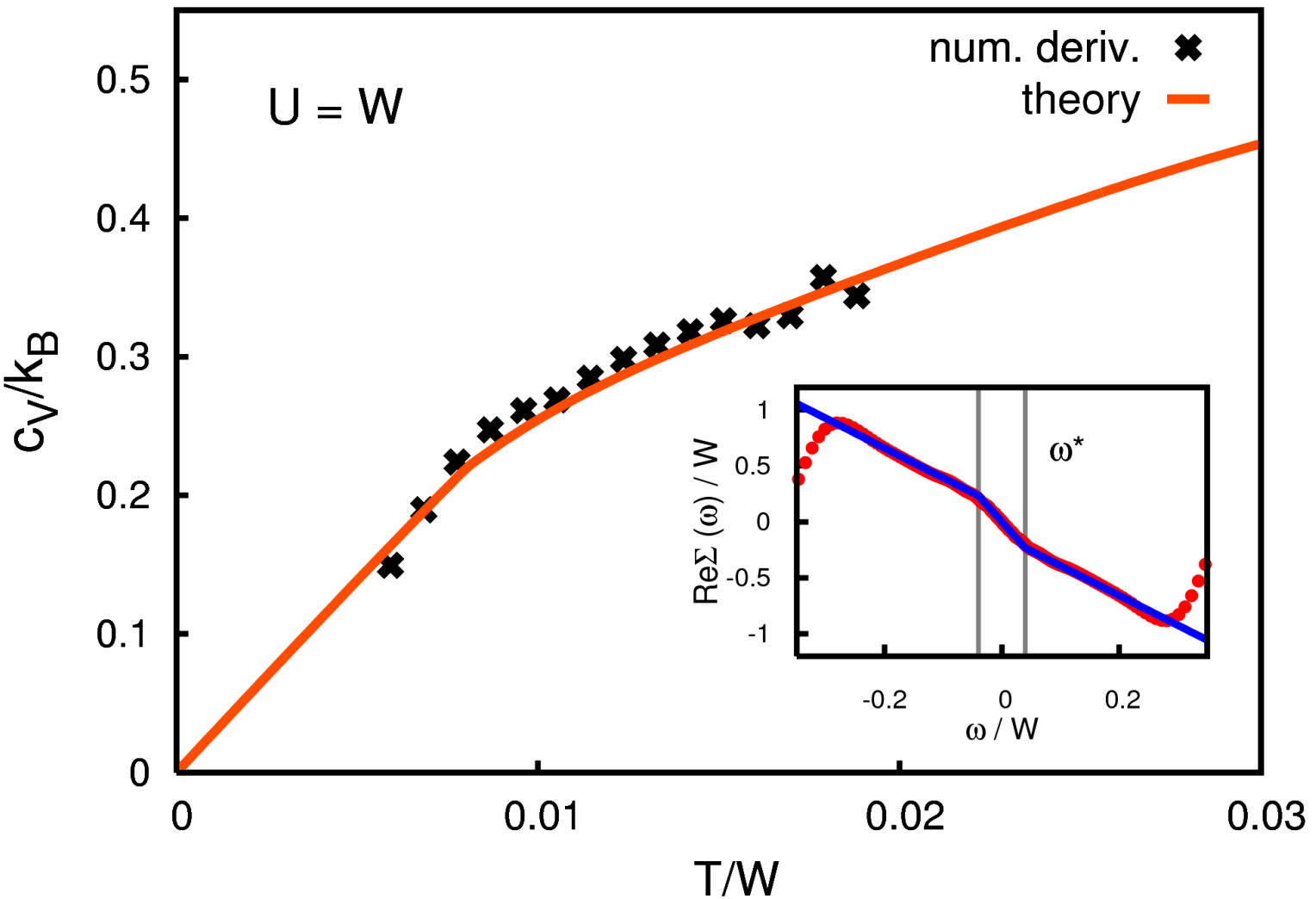

[A. Toschi, M. Capone, C. Castellani, K. Held, arXiv:0712.3723]

Kink feature visible in specific heat of heavy fermion LiV_2O_4?

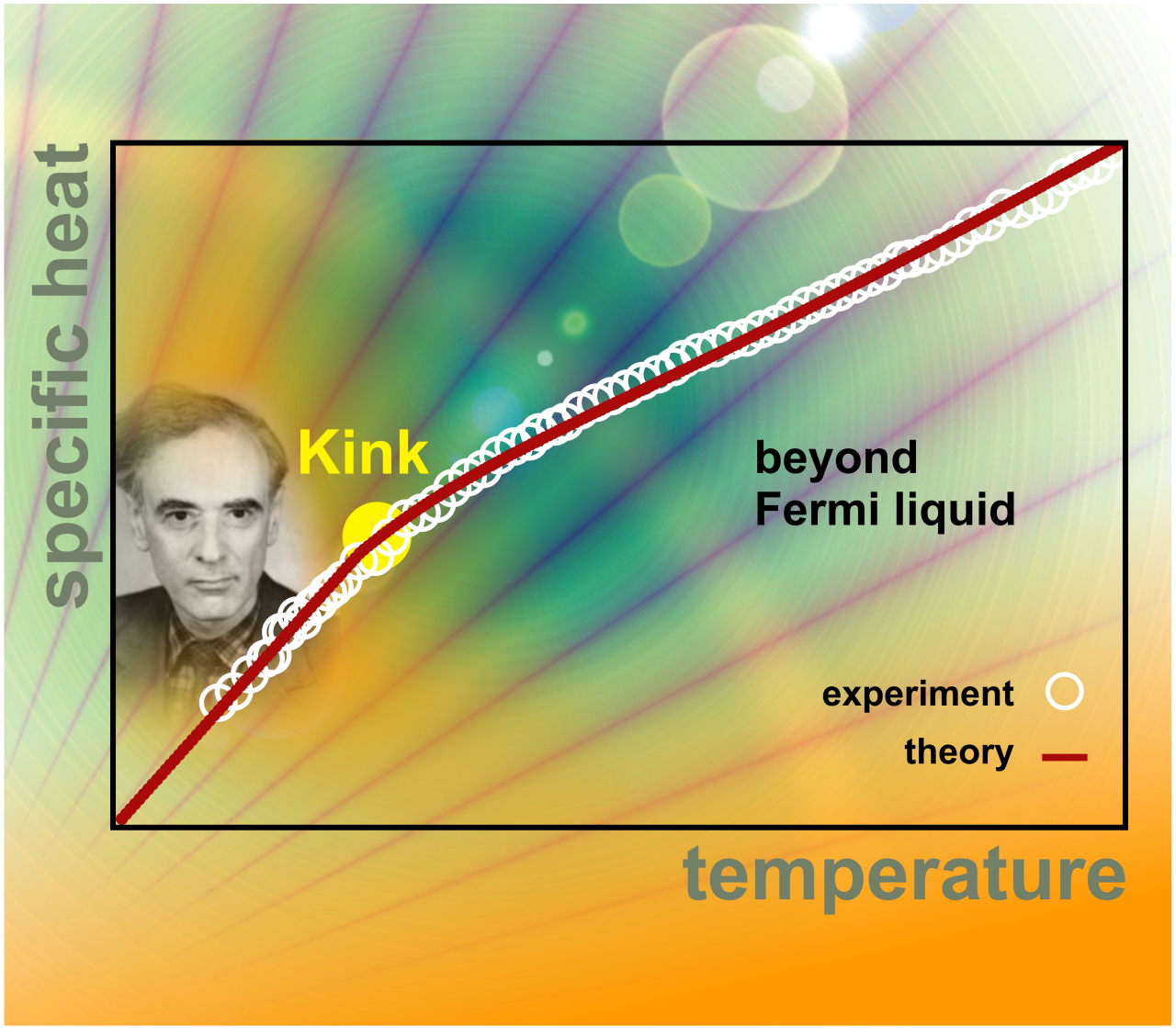

[A. Toschi, M. Capone, C. Castellani, K. Held, arXiv:0712.3723]

Check using QMC. . .

Conventional HF-QMC at constant discretization $\Delta\tau$,

numerical derivatives from parabolic interpolation of tripels

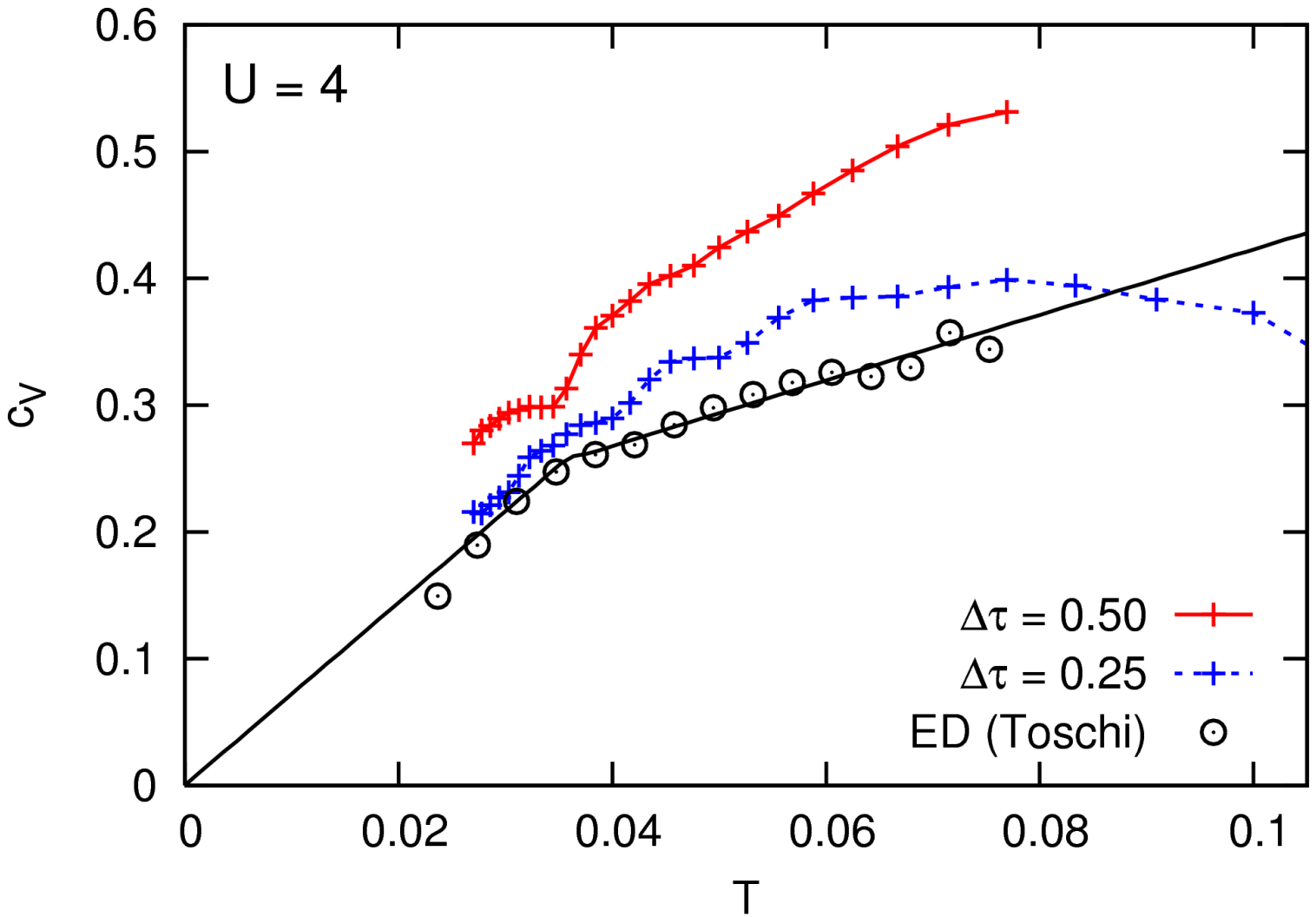

Roughly consistent with ED, but: no significant kinks, maximum at $T \approx 0.08$?

Best (only?) way to exclude kink: rescale data to straight line!

Best (only?) way to exclude kink: rescale data to straight line!

(i) consider c_V/T

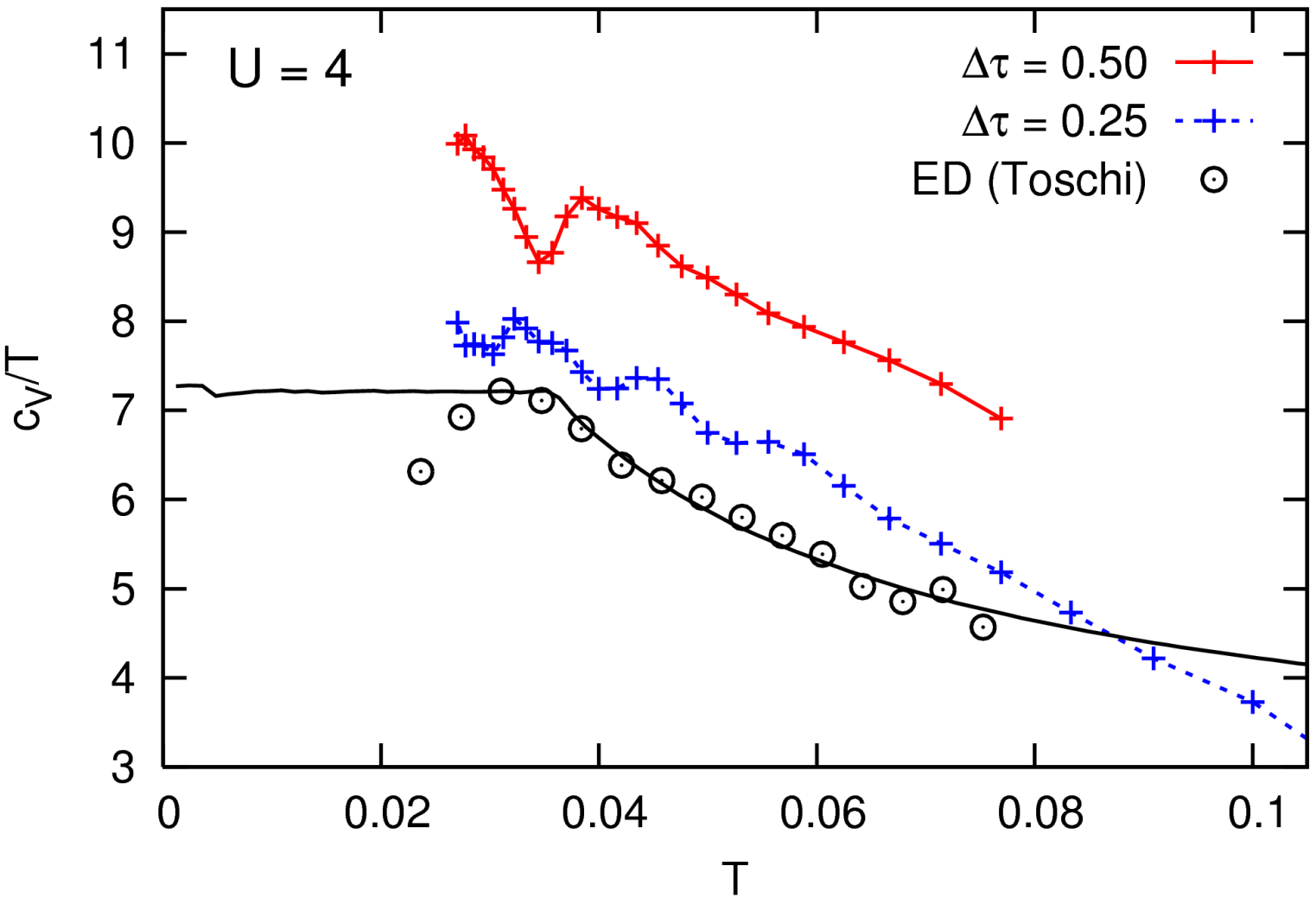

Best (only?) way to exclude kink: rescale data to straight line!

(i) consider c_V/T (ii) $T \longrightarrow T^2$

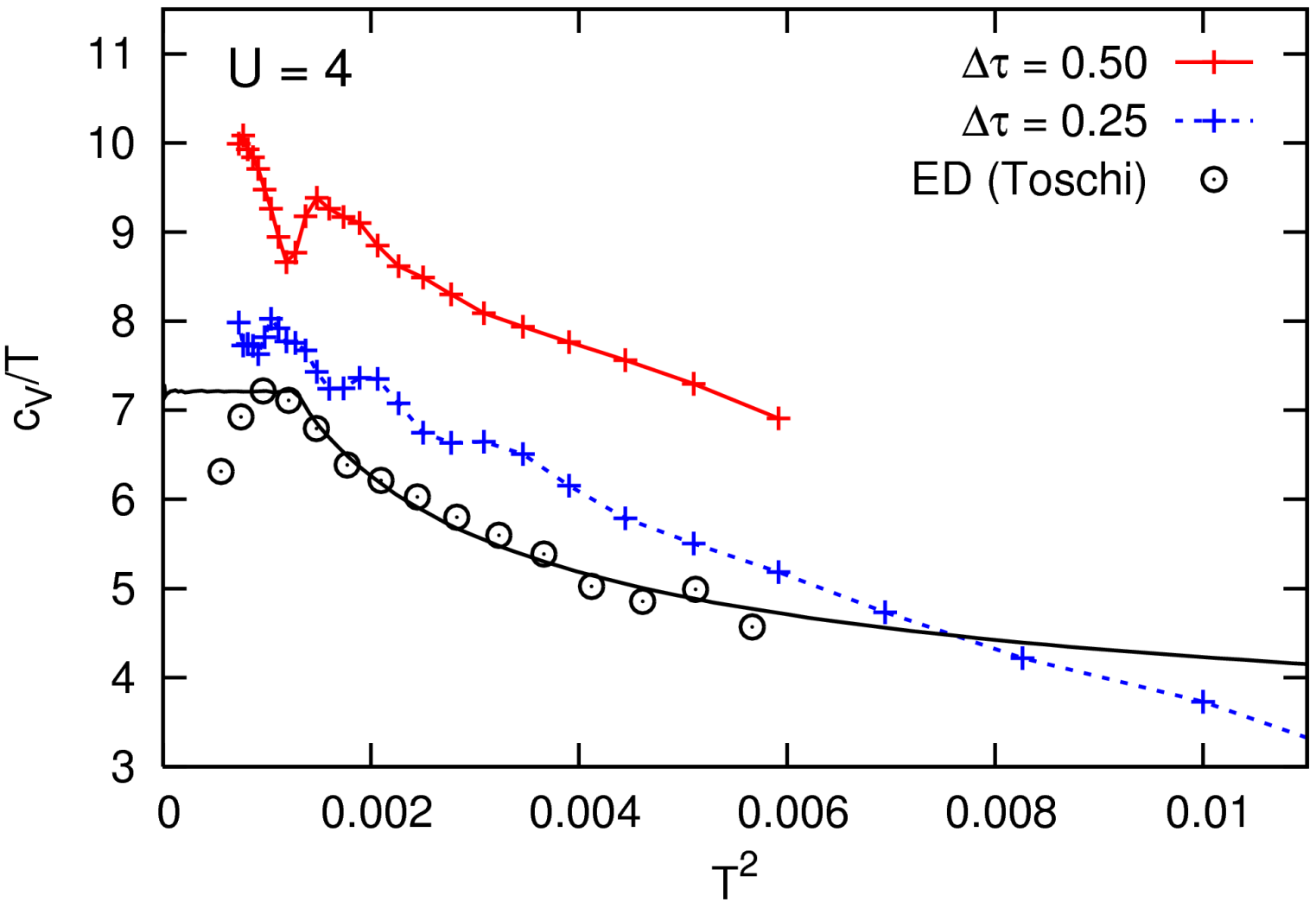

Best (only?) way to exclude kink: rescale data to straight line!

(i) consider c_V/T (ii) $T \longrightarrow T^2$ (iii) logarithmic scale

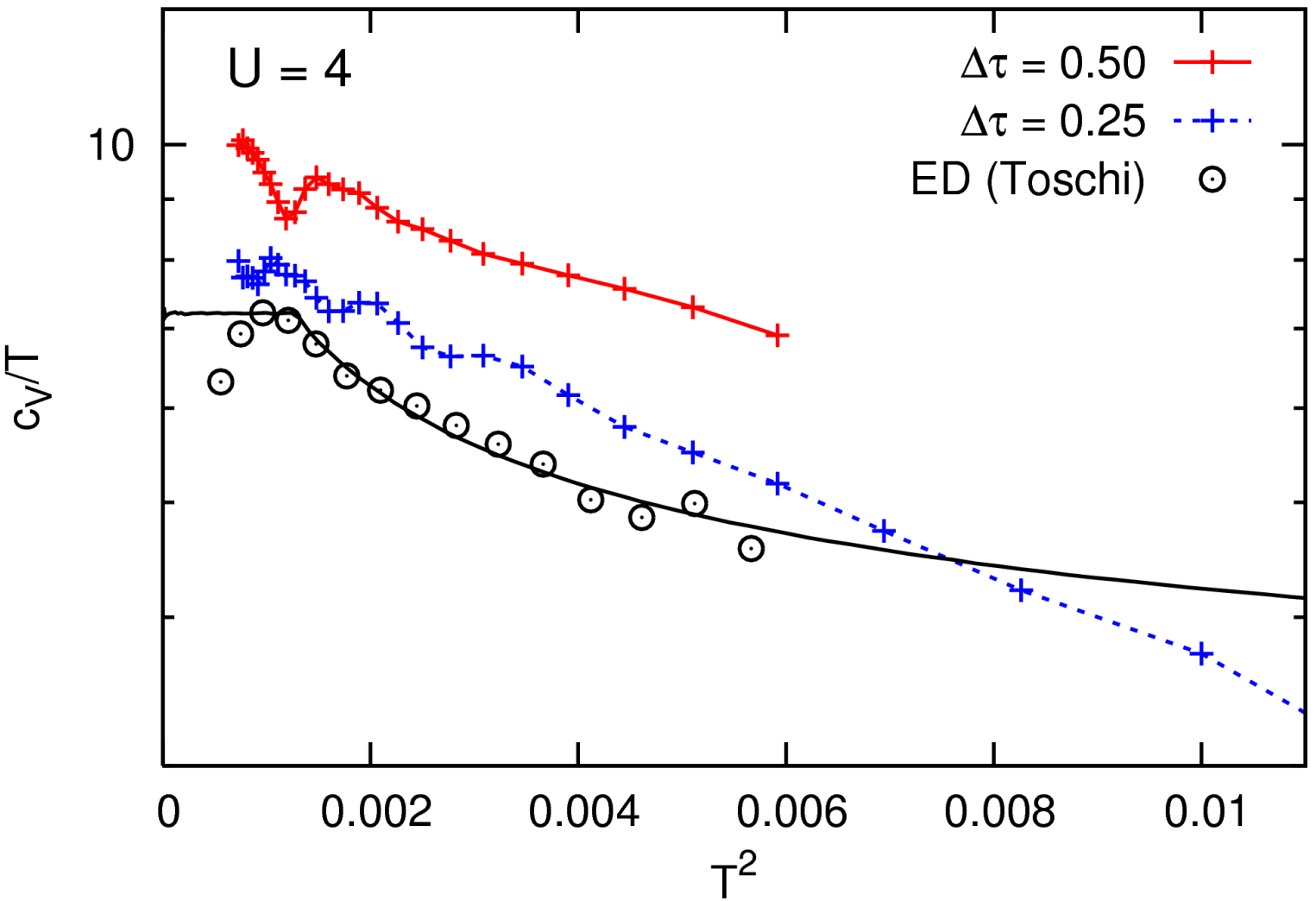

New hypothesis (for quasiparticle contribution): $c_V(T) \approx \gamma T\, e^{-aT^2}$

Now: more QMC sweeps + iterations, extended T range, smaller $\Delta\tau$ derivatives with error bars (via parabolic least-squares fits to 5-tupels)

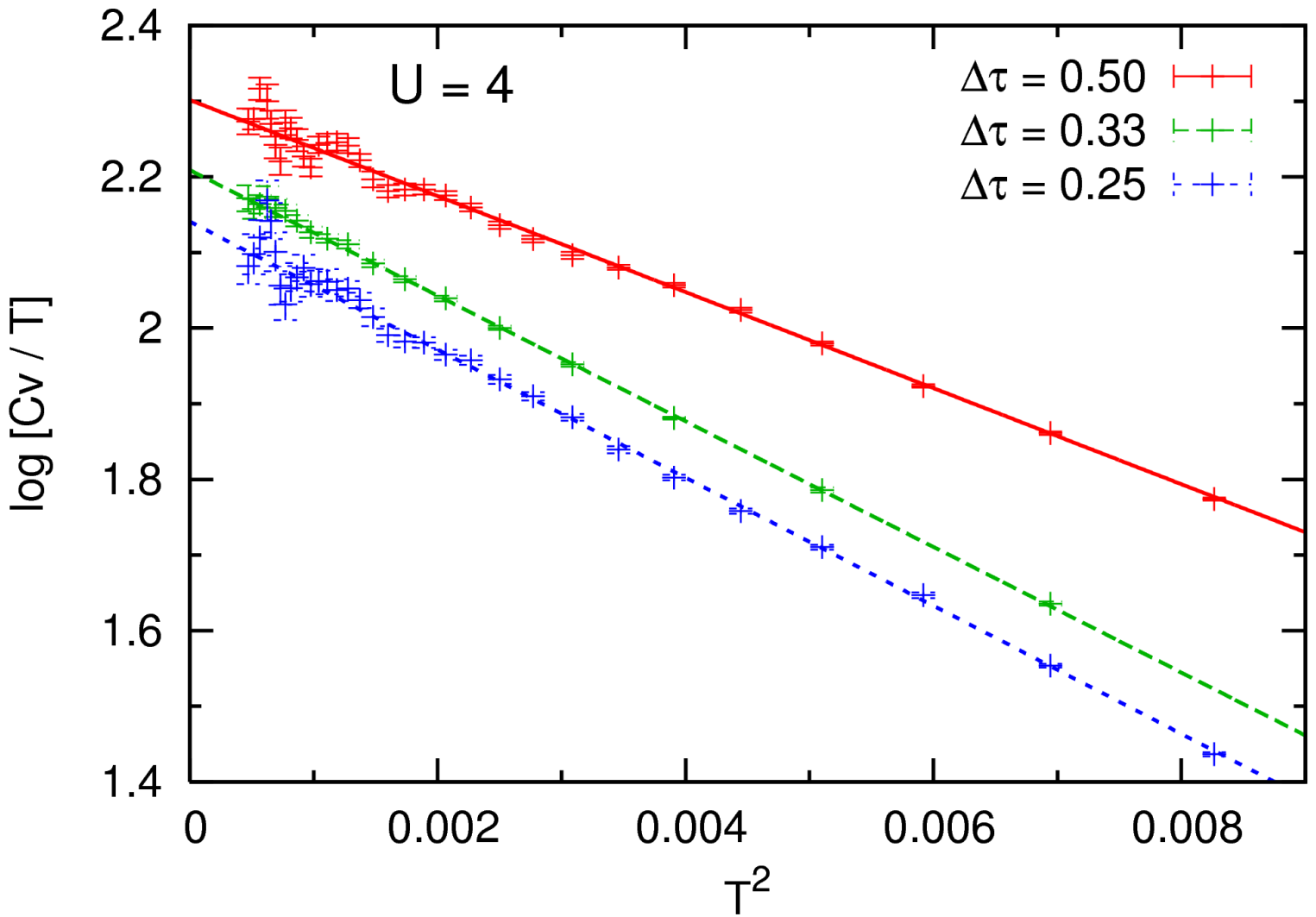

Now: more QMC sweeps + iterations, extended T range, smaller $\Delta\tau$ derivatives with error bars (via parabolic least-squares fits to 5-tupels)

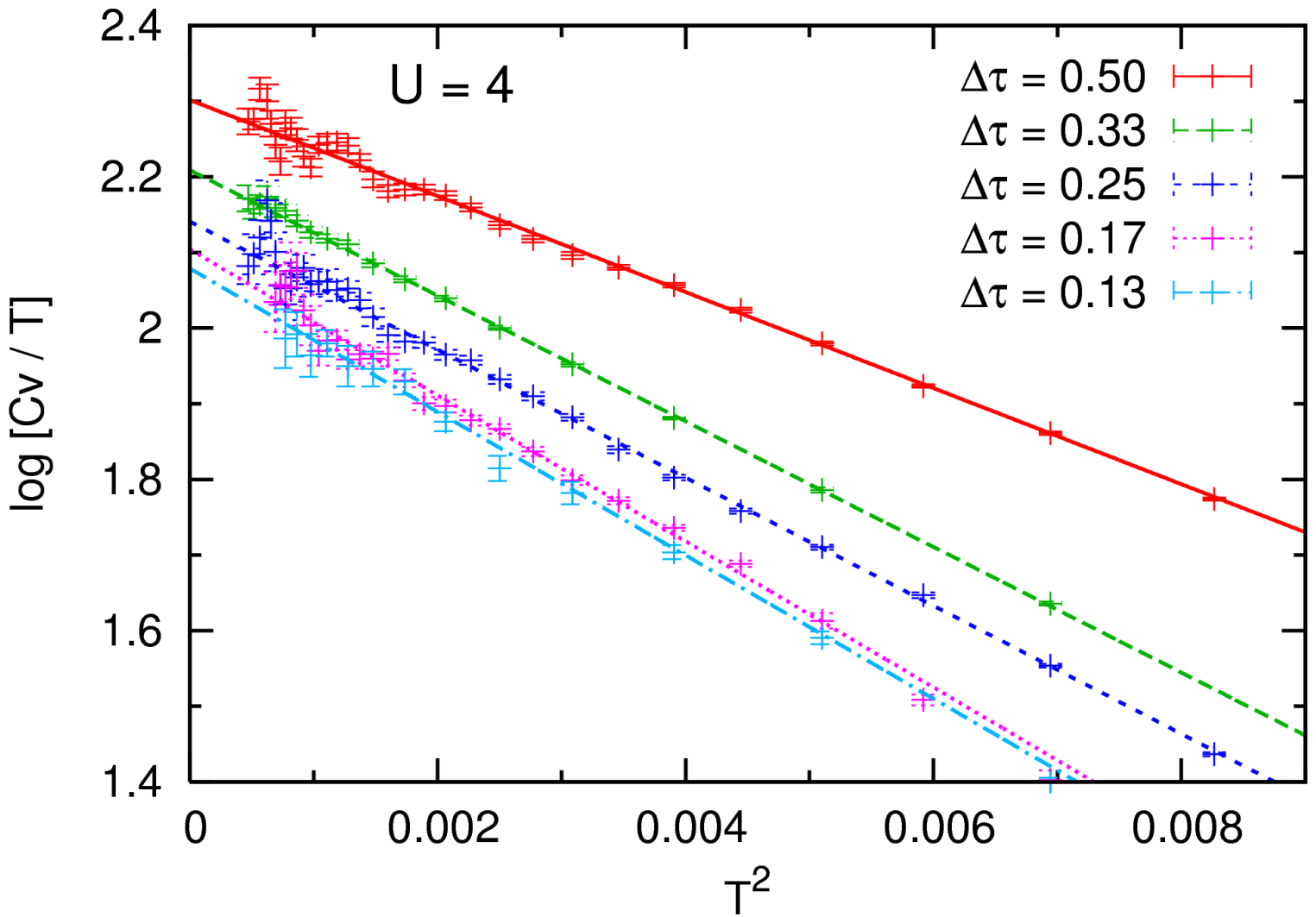

Now: more QMC sweeps + iterations, extended T range, smaller $\Delta\tau$ derivatives with error bars (via parabolic least-squares fits to 5-tupels)

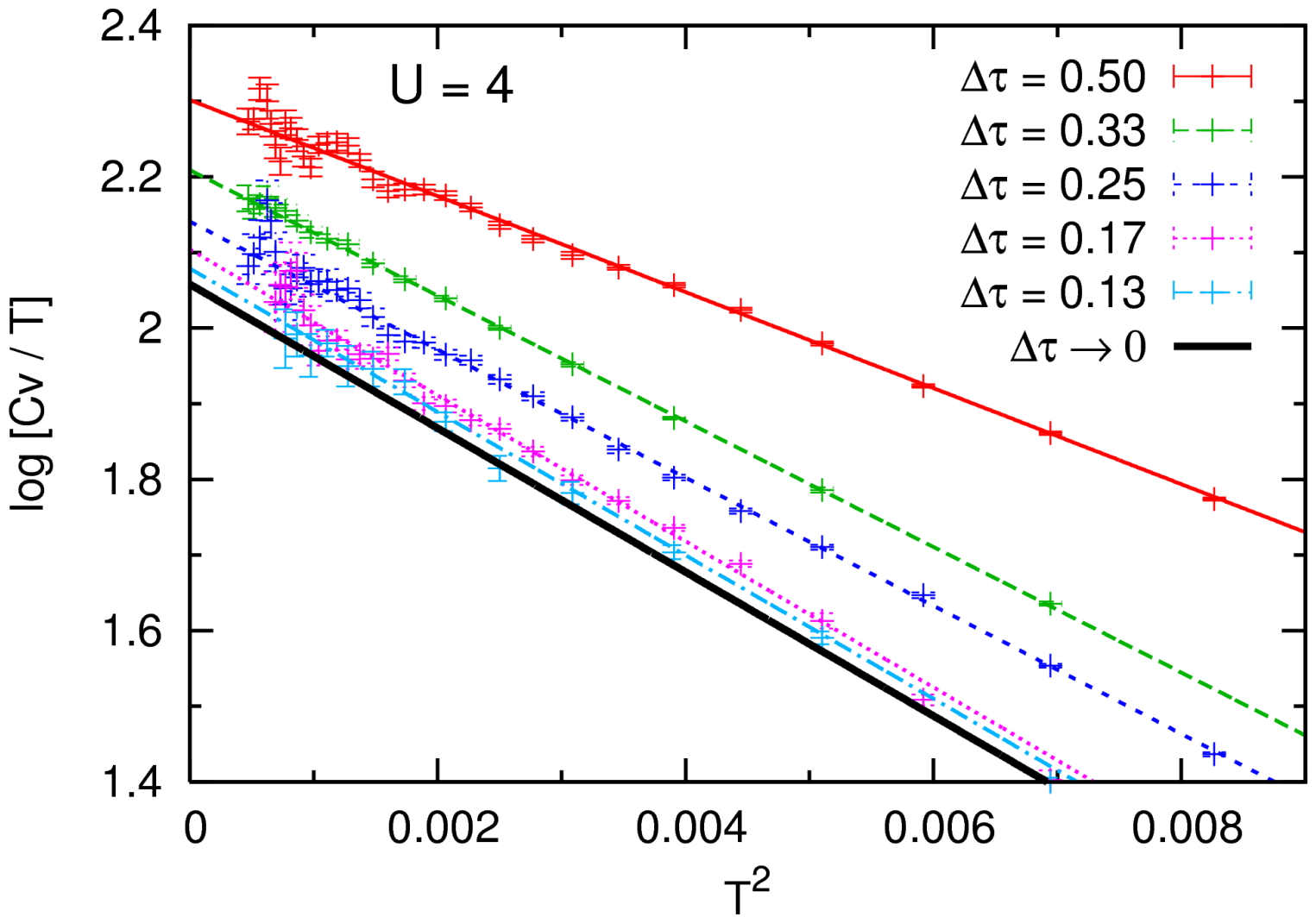

Parametric extrapolation $\Delta\tau \to 0$ is reliable

Independent check of γ via quasiparticle weight (from self-energy)

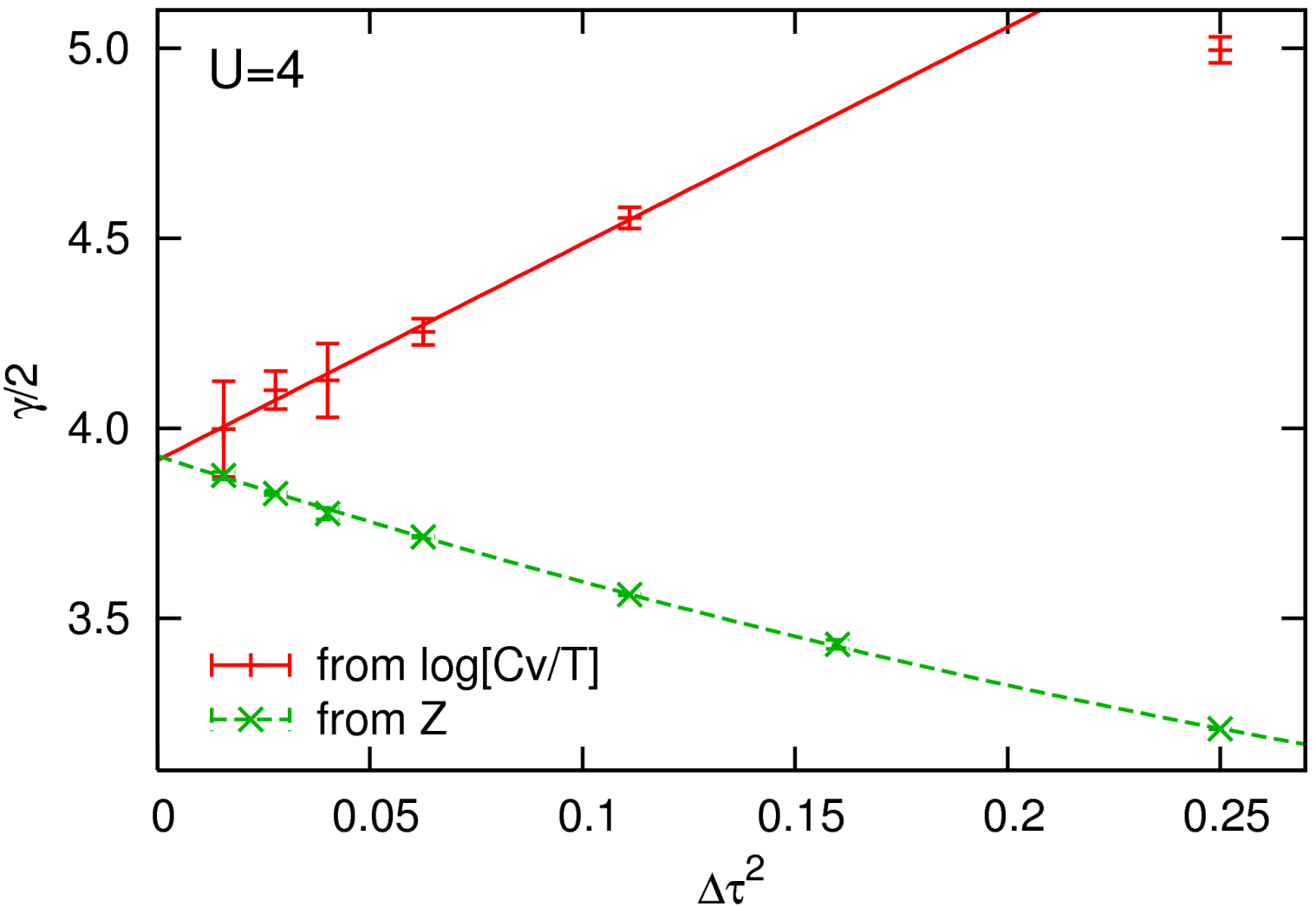

Perfect agreement (also with PRB **56**, 205120 (2007))

Now back to unscaled specific heat

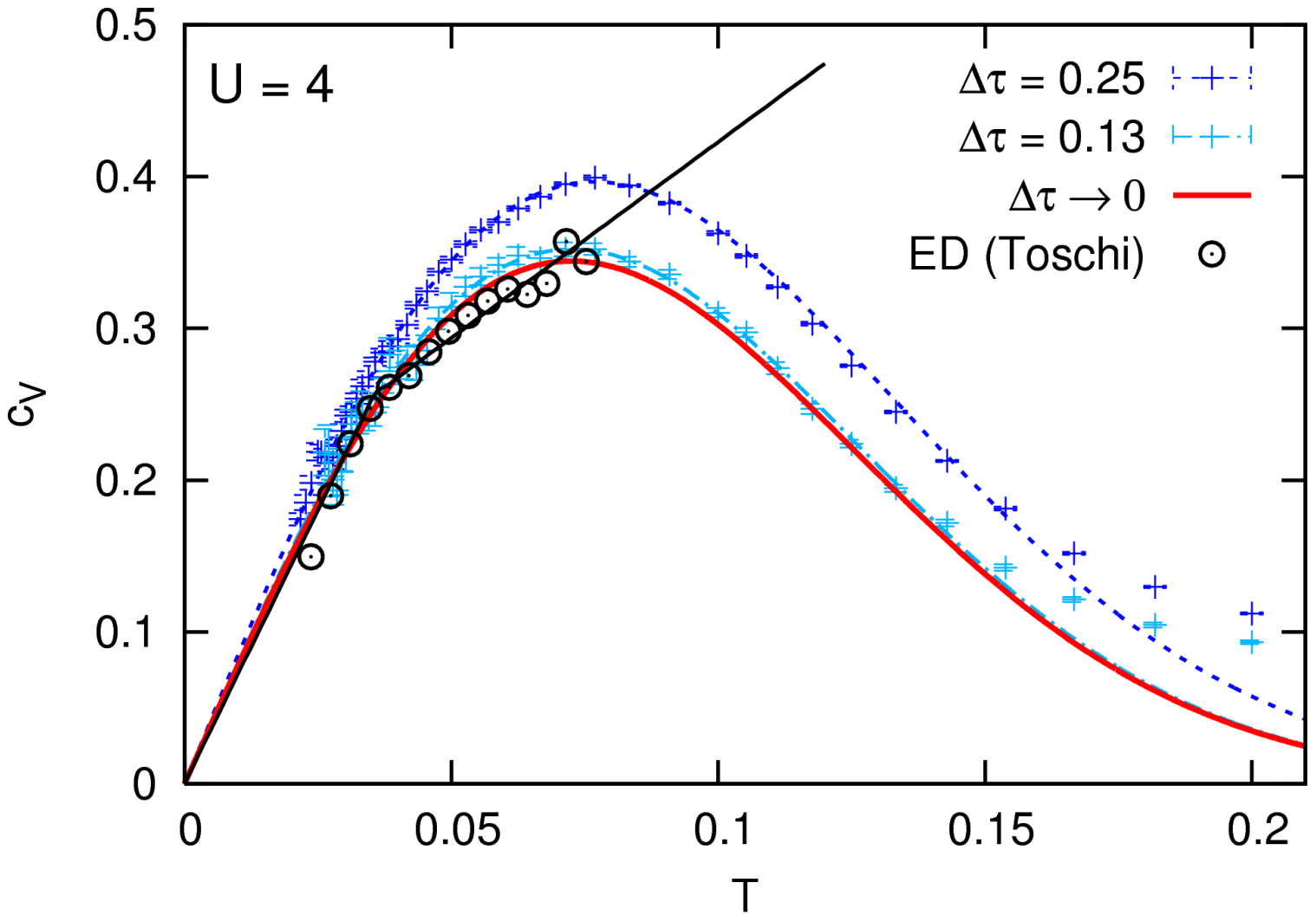

Exponential law valid far beyond fit range ($T \leq 0.084$)

ED raw data has reasonable accuracy, but fit lines are incorrect

Is entropy consistent? Yes!

$$S(T) = \int_0^T dT' \, \frac{c_V(T')}{T'} = \int_0^T dT' \, 7.83\, T' e^{-95.14 T'^2} \overset{T\to\infty}{\longrightarrow} 0.711 \approx 0.693 \approx \log(2)$$

Interpretation: free spins at $T \gtrsim 0.2$ (in subspace without double occupancies)

Is entropy consistent? Yes!

$$S(T) = \int_0^T dT' \, \frac{c_V(T')}{T'} = \int_0^T dT' \, 7.83\, T' e^{-95.14 T'^2} \overset{T\to\infty}{\longrightarrow} 0.711 \approx 0.693 \approx \log(2)$$

Interpretation: free spins at $T \gtrsim 0.2$ (in subspace without double occupancies)

Generalized Fermi liquid law for quasiparticle contribution to specific heat

$$c_V(T) = \frac{2\pi}{3Z} T \, \exp\left[-(T/T_0)^2 \right]; \quad T_0 = \frac{3\log(2)}{\pi^{3/2}} Z \qquad \text{(Bethe DOS)}$$

Single (low-frequency) qp weight $Z = \left. \frac{d\Sigma(\omega)}{d\omega} \right|_{\omega=0}$ governs c_V!

Prediction with no free parameters, to be tested at smaller/larger U.

Summary

New methods: unbiased Green functions from conventional HF-QMC
numerically exact multigrid HF-QMC algorithm

Applications: spectral weight transfer at Mott transition
breakdown of a Fermi liquid

Summary

New methods: unbiased Green functions from conventional HF-QMC
numerically exact multigrid HF-QMC algorithm

Applications: spectral weight transfer at Mott transition
breakdown of a Fermi liquid

Not shown: Orbital-selective Mott transitions (with C. Knecht, P. van Dongen)
Materials with high spin polarization (w. E. Jakobi, P. van Dongen)

Summary

New methods: unbiased Green functions from conventional HF-QMC
numerically exact multigrid HF-QMC algorithm

Applications: spectral weight transfer at Mott transition
breakdown of a Fermi liquid

Not shown: Orbital-selective Mott transitions (with C. Knecht, P. van Dongen)
Materials with high spin polarization (w. E. Jakobi, P. van Dongen)

Outlook

Wide application of new methods (with generalizations), DFG projects

Summary

New methods: unbiased Green functions from conventional HF-QMC
numerically exact multigrid HF-QMC algorithm

Applications: spectral weight transfer at Mott transition
breakdown of a Fermi liquid

Not shown: Orbital-selective Mott transitions (with C. Knecht, P. van Dongen)
Materials with high spin polarization (w. E. Jakobi, P. van Dongen)

Outlook

Wide application of new methods (with generalizations), DFG projects

Flavor-selective Mott transitions in ultracold quantum gases (SFB/TR 49)

Material-specific multiband calculations in context of LDA+DMFT

Fundamental model issues, e.g.: full thermodynamic information (1 band)

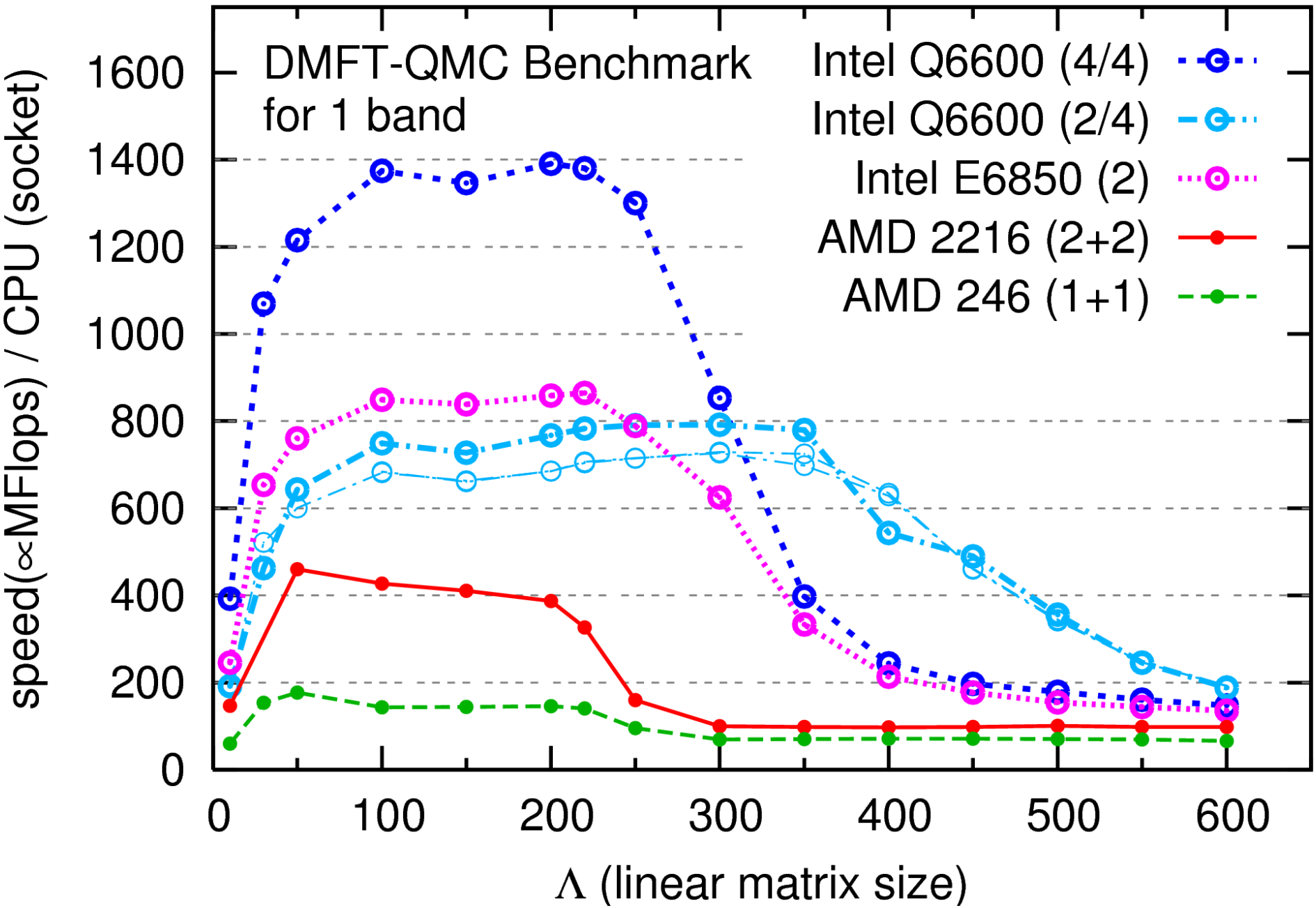
DMFT-QMC Benchmark
for 1 band
Intel Q6600 (4/4)
Intel Q6600 (2/4)
Intel E6850 (2)
AMD 2216 (2+2)
AMD 246 (1+1)
speed(∝MFlops) / CPU (socket)
Λ (linear matrix size)
0
200
400
600
800
1000
1200
1400
1600
0
100
200
300
400
500
600